Title

Characterization of Avalanche-Burst Invasion Percolation: A Case Study in Pseudo-Criticality and Multifracticity

Author

Ortez, Ronaldo

Publication Date

2023

Peer reviewed|Thesis/dissertation

Characterization of Avalanche-Burst Invasion Percolation: A Case Study in Pseudo-Criticality and Multifracticity

By

Ronaldo Antonio Ortez

Dissertation

Submitted in partial satisfaction of the requirements for the degree of

in

Physics

in the

Office of Graduate Studies

of the

University of California

Davis

Approved:

John Rundle, Chair

David Wittman

Richard Scalettar

Committee in Charge

2023

To my prime mover, whose love, wisdom, and strength sprouted my own practice, and whose dedication inured my commitment to the priestly duties beset on those striving to contribute to those doctrines born of universal truths.

Contents

List of Figures

List of Tables

Abstract

Characterization of Avalanche-Burst Invasion Percolation: A Case Study in Pseudo-Criticality and Multifracticity

Given the variety and large number of systems displaying scale invariant characteristics, it is becoming increasingly important to understand their fundamental and universal elements. Much work has attempted to apply second order phase transition mechanics due to the emergent scale invariance at the critical point. This symmetry produces much of the fractal characteristics that is shared among these systems. Percolation systems offer a simple and well developed framework that exhibit all the key features of a second order phase transition, and has been a fertile framework for exploring generalizing insights. A close variant is invasion percolation.

Invasion percolation is a model that was originally proposed to describe growing networks of fractures. Here, we first describe a loopless algorithm on random lattices, coupled with an avalanche-based model for bursts. The model reproduces the characteristic b-value seismicity and spatial distribution of bursts consistent with earthquakes resulting from hydraulic fracturing ("fracking"). We test models for both site invasion percolation (SIP) and bond invasion percolation (BIP) and characterize their density, cluster, and correlation scaling exponents D_f, τ, and ν respectively. These models have differences on the scale of site and bond lengths l, but since the networks are characterized by their large scale behavior, $l \ll L$, we find only small differences between their respective scaling exponents. Though these differences are likely too small for empirical data to differentiate between models, they remain significant enough to suggest that both models belong to different universality classes.

Because we likely cannot empirically distinguish differences associated with their underlying critical characteristics, we next aim to understand the particular manifestation of criticality in the avalanche invasion percolation (AIP) system. This is a SIP based model with additional growth mechanics described through distinct, sequentially connected bursts. Instead, we find that it is a hybrid critical system with the presence of

a critical Fisher type distribution, $n_s(\tau, \sigma)$, but lacks other essential features such as an order parameter and to a lesser degree hyperscaling. This suggests that we do not need a full phase transition description in order to observe scale invariant behavior. This was a positive result, since for many systems, notions of phases and critical points are both artificial and cumbersome. AIP also recasts dynamics as a slowly driven non-equilibrium proccss and provides a pathway for more suitable descriptions.

We extend our previous model, avalanche-burst invasion percolation (AIP) by introducing long-range correlations between sites described by fractional Brownian statistics. In our previous models with independent, random site strengths, we reproduced a unique set of power-laws consistent with some of the b-values observed during induced seismicity. We expand upon these models to produce a family of critical exponents which would be characterized by the local long-range correlations inherent to host sediment. Further, in previous correlated invasion percolation studies, fractal behavior was found in only a subset of the range of Hurst exponent, H. We find fractal behavior persists for the entire range of Hurst exponent. Additionally, we show how multiple cluster scaling power laws result from changing the generalized Hurst parameter controlling long-range site correlations, and give rise to a truly multifractal system. This emergent multifractal behavior plays a central role in allowing us to extend our model to better account for variations in the observed Gutenberg-Richter b-values of induced seismicity. Finally this provides a framework for generating scale invariant statistics without adhering to the scaling hypothesis which underlies the scale invariance of critical systems.

Chapter 1

Introduction

Though the field of complexity seemingly evades a formal definition, one might make an initial attempt to describe complexity through mathematical quantities like Lyapunov exponents. These exponents characterize the exponential separation associated with the temporal evolution of nearby phase space trajectories. The trajectories in phase space describe the system's temporal evolution, and a system's Lyapunov exponents do capture one of the characteristic features of complexity. This feature being: the observation that a small neighborhood of initial states does not lead to a small neighborhood of final states. Instead, the exponential amplification of deviations insures final states can grow to be arbitrarily distant, and in this way complex systems can often times be indistinguishable from random systems.

Complexity can also arise absent any formal description of differential dynamics governing the time evolution of the system. One might begin with a rather simple system (for example, a cellular automata system with a specified rule for nearest neighbor interactions) whose fundamental elements are well known, but their interactions are sufficiently numerous, that features of complexity become an emergent property of the system.

We also only mention that there exist entire fields characterized by more purposeful biological agents that have methods unto themselves. Briefly, this motivates the notion that the landscape of systems that fall underneath the complexity umbrella are both diverse and numerous. However, the most interesting aspect of this landscape is that we find the intersection of many seemingly disparate concepts. Illustrative, but non

exhaustive examples eliciting the different kinds of flavors are: The geometric connection between the mapping of coastlines and the random stochastic nature of market time series [1]; attempts to quantify a complexity measures through measures of various entropies and information [2]; the interesting connection between phase transitions and the statistical behavior of seismicity [3].

The last example is of particular interest and represents the particular flavor which defines the majority of the interest in this project. Typically, in the field of complexity, the phase space is so rich with trajectories that it is very difficult to develop any principles which might serve to constrain behavior. The goal of such attempts would be to identify suggestive characterizing and simplifying principles. This has lead some to speculate that in fact irreducibility is fundamental and must lie at the core of complex systems [4].

However, as is typically the aim of any good physical theory, the goal is to distill simplicity from complexity, and in fact there are many examples of this in complexity sciences where recursive feedback mechanisms with underlying simple interactions lead to the emergent complexity in outcomes. With these examples we find that complexity emerges from an underlying simple structure. The spirit of our pursuit is to find the simplifying structure that underlays the complex behavior of seismic systems. Of course, it could be that some iteration of Maxwell's demon lurks behind the dynamics, ensuring the system is described by both many interacting parts with very sophisticated interaction rules.

For our purposes we will focus one of the key insights which binds seismicity to complexity, and hinges around the presence of a particular kind of symmetry called scale invariance. This is particularly satisfying, since a physicist's primary strategy is to utilize symmetries to effectively constrain and simplify problems. As physicists sought to understand second order phase transitions, they found that many of the systems parameters naturally became described by many quantities bounded only by the system's size and exhibited a symmetry known as scale invariance. This type of transition (an example of being the Ising second order phase transition described below) was a radical departure from the dynamics that describe systems in their normal states of matter.

Similarly, it was shown that seismic systems are also described by quantities which are scale invariant. Given that scale invariance is the result of no natural length, that the system can be rescaled arbitrarily and the relations remain the same, suggested that their existed a common mechanisms between these two systems. The goal of this brief introduction is to provide the essential concepts that will be utilized to make comparisons between the two disparate phenomenon of criticality and seismicity.

1.1 Second-Order Phase Transitions

In thermodynamic systems the phases of different substances serve to define various equilibrium dynamics which can effectively describe much of the observed behavior. This leads to the powerful result that regular molecular and small-scale ($l << L_{sys}$) interactions lead to stable ensemble averaged macro ($l \sim L_{sys}$) quantities which effectively describe the state of the system. Phase transitions mark where these typically well-behaved quantities encounter abrupt non-equilibrium dynamics that alter the underlying interactions. The result is a system that emerges with different relations between the state variables. One typically uses a "state function" to describe the system's state, and for our purposes we will use either the Gibbs free energy or Helmholtz free energy state functions,

$$dF(T, V, N) \equiv -SdT - pdV + \mu dN \tag{1.1}$$

where the two are related by Legendre transforms,

$$G(T, P, N) = F(T, V, N) + PV \tag{1.2}$$

$$dG = -SdT + VdP + \mu dN \tag{1.3}$$

The choice of thermodynamic potential depends on the constraints of the system. For example, particles in a box allowed to exchange heat with the environment or are in contact with a heat bath allows one to externally control the system's temperature. Thus, temperature and volume become the natural variables of the system. Alternatively, if we seek to control the pressure of the system rather than the volume, such that the volume is the natural variable, then the Gibbs free energy potential is suitable. Transform-

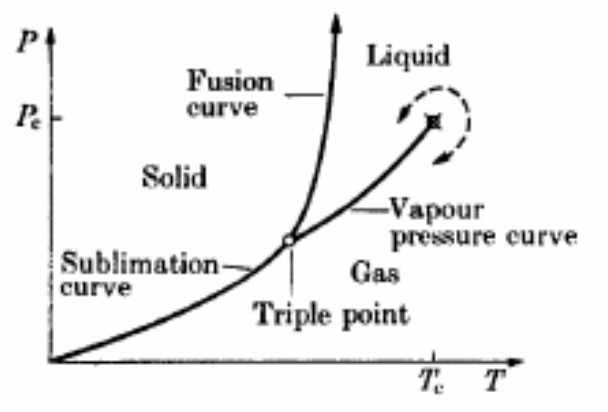

Figure 1.1. Illustrative PT phase diagram. The sublimation curve and the vapor pressure curve separate a system's state into distinct domains: solid, liquid, and gas. While in many cases the fusion curves continue indefinitely, the vapor pressure curve terminates at a critical point. [5]

ing between different state functions can be done formally with the respective Legendre transforms.

Because many of our examples are lattice-type models, it is convenient to instead encode the state functions, which are macroscopic descriptions, using the Hamiltonian formulation. Here, we begin by describing the energy of each element and its possible interactions, and then utilize all the machinery of statistical mechanics to determine the stable macroscopic quantities. This is a very powerful way of determining the behavior of $\sim 10^{16}$ elements from the simple energy interactions of each element. The Hamiltonian lattice formulation is given by,

$$F = -\frac{1}{\beta} log Z \tag{1.4}$$

where Z is the all important partition function, which is the sum over all system's energy microstates, and is given by

$$Z = \sum_i \exp^{-\beta H} \tag{1.5}$$

and β is the standard $1/k_B T$.

One of the key parameters derived from either thermodynamic potentials or the Hamiltonian statistical mechanics is the order parameter. The order parameter can be the density in liquid systems or the magnetization in magnetic systems, and is given by the first derivative of the thermodynamic potential. The order parameter undergoes a disconti-

nuity in a phase change, and is used to distinguish distinct equilibrium states known as phases from one another. The set of thermodynamic parameters (P,V,T,S,ρ, etc) collectively make a multidimensional phase space, and the selection of two of these variables makes a surface where we can show distinct domains corresponding to distinct states. The line in surface where the order parameter is discontinuous, generally represents regions of a phase change where the system transforms from one phase to the other on opposite sides of the boundary. An example is shown in Figure 1.1.

Since the order parameter is typically given by the first derivative of the thermodynamic potential, those transitions whose first derivative of the thermodynamic potential are discontinuous became known as first order phase transitions. It became apparent that there also existed cases where the first derivative is continuous but the second derivative is discontinuous. Because of this Ehrenfest suggested that depending on which derivative became discontinuous could universally categorize phase transition. This classification suggests a rather cohesive description between phase transition descriptions, but this classification perhaps belies the magnitude of difference between the subsequent phenomena being described.

For critical phenomena, we observe that the order parameter remains continuous, but the second derivative diverges. Thus, it is for this reason that critical phenomena describe second order phase transitions where quantities like compressibility and heat-capacity become discontinuous.

As a representative, concrete example, we first consider the lattice liquid-gas model, which nicely illustrates how many interesting features can arise from a relatively simple model. Here, we consider a grid of cells (shown in Figure 1.2) which can either be occupied or empty. We imagine gas particles moving about on this square grid, where the grid size roughly corresponds to the particle size. If the particle happens to be at the center of the cell, then that cell becomes occupied, otherwise the cell is left unoccupied. This ensures that two particles cannot occupy the same cell. We also allow an energy difference to distinguish occupied and unoccupied cells, which is controlled by the chemical potential, μ (though the main insights won't depend on this interaction). Next, we allow

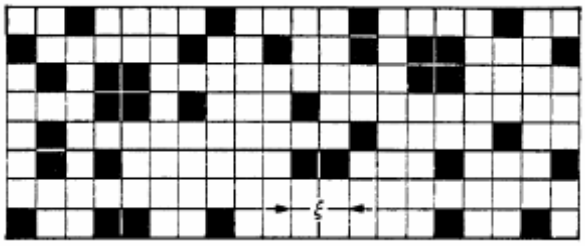

Figure 1.2. An example of the lattice gas model. Interaction rules: each dark cell indicates a particle occupying the center. Nearest neighbor occupied cells interact with energy $-j$. Multiple particles cannot occupy the same cell. [5]

interactions between nearest neighbor cells with interaction strength j in order to simulate an attractive potential for nearby particles. We forbid particles to occupy the same site. Except for the nearest neighbor interactions, we have no other kinds of interactions between the cells. Even given this simple setup, we have implemented a Lennard-Jones type of potential. The Hamiltonian is written as,

$$H = -j \sum_{l,m} s_l \cdot s_m - \mu \sum_l s_l \tag{1.6}$$

where $s_l = 0, 1$ if occupied or not. The partition function can subsequently be written as,

$$Z = \sum_{sites} e^{\beta j \sum_{l,m} s_l \cdot s_m + \beta \mu \sum_l s_l} \tag{1.7}$$

If we were proceeding analytically, we would need to sum over all microstates of the system in hopes of finding a closed form expression for the sum. Onsager [6] famously was the first to achieve an analytical solution, and whose tremendous effort awarded him a Nobel prize. Onsager solved a slightly different two-dimensional Ising model with external field B, but we can still make use of his efforts with a simple transformation.

The Hamiltonian for the 2D Ising model with external field can be written as,

$$H = -j/4 \sum_{l,m} \sigma_l \cdot \sigma_m - \mu \sum_l \sigma_l \tag{1.8}$$

The Hamiltonian of the two models are the same under the transformation,

$$\sigma_l = 2s_l - 1 \tag{1.9}$$

and by substituting magnetic field B with chemical potential μ. Further, we can now quote the well established Ising model results, beginning first with the order parameter.

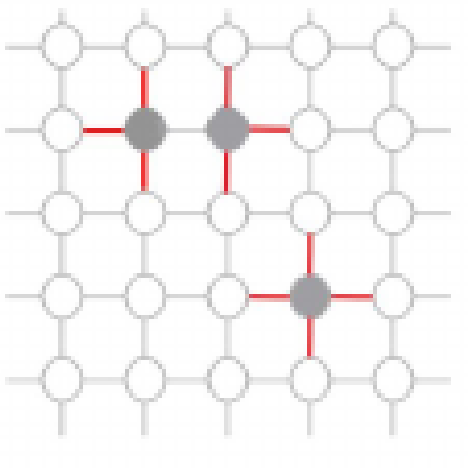

Figure 1.3. Ising Model. Each lattice site contains a spin can be up or down, (-1, 1). Nearest neighbor spins in the same state interact with energy $-J$ and is denoted by the presence of a bond. Energetically the spins will prefer to clump since an isolated spin flip must break 4 bonds, however, if the spin is a neighbor than only bonds are broken.

For the case of the liquid-gas transition, the order parameter is some function of the density. Using the results of the Ising model the order parameter is,

$$\rho = \frac{1}{N\beta}\frac{\partial logZ}{\partial \mu} = \frac{1}{N}\left(2\sum_{k}^{N_c}\langle s_k\rangle - N_c\right) \tag{1.10}$$

where here we can see that the density is determined as a function of the average number of occupied sites per cluster. A closer look shows the order parameter is the difference between two density terms, which is consistent with liquid-gas transitions where the order parameter is taken to be the difference between a fluctuating average density and a fixed density [7].

For most values of temperature, there exists a discontinuous change in the density, reflecting the different densities of the distinct gas and liquid states. For the Ising system, this represents the spontaneous macroscopic magnetization that emerges given any nonzero external magnetic field. Yet, there does exist a critical temperature, T_c, where this difference in density continuously goes to zero, and in this region it would suggest little difference in the density between the two states.

However, even though the order parameter, which is a function of the first derivative of the free energy, is continuous, higher order derivatives are discontinuous which point

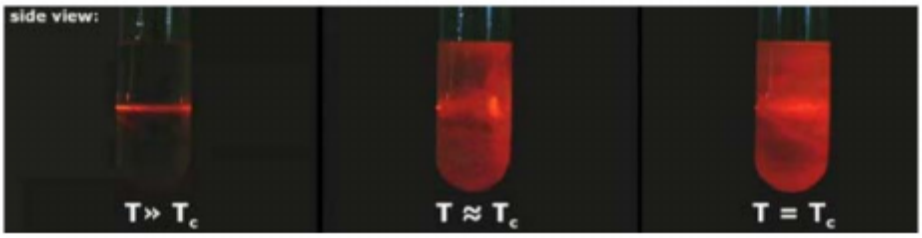

Figure 1.4. Shown here is one of the first observations of critical phenomena, critical opalescence. The liquid is shown at 3 different temperatures with a laser shining through it and becoming increasingly opaque. There is a critical temperature where the opacity is maximum, and this corresponds to mixed phase liquid or a super liquid where droplets of different sizes nucleate to produce the opalescence.

to singular behavior in other important quantities like heat capacity and compressibility,

$$\kappa_T = \frac{1}{N}\left(\frac{\partial^2 F}{\partial^2 \mu}\right)_{T,N} \tag{1.11}$$

$$C_v = -\frac{1}{\beta N}\left(\frac{\partial^2 F}{\partial^2 T}\right)_{V,N} \tag{1.12}$$

The divergence of compressibility κ_T is the result of fluctuations in the order parameter growing far larger then they would when in a particular state where their thermal averages remain well-behaved. This singular behavior in compressibility as a result of fluctuations in the density is the explanation for the phenomena of critical opalescence, one of the earliest known examples of second order phase transitions.

During Einstein's seminal work on Brownian motion and his studies in statistical physics, he attributed large fluctuations to be the result of critical opalescence [8]. Figure 1.4 shows the basic phenomena of critical opalescence. One can shine a laser through a liquid in its regular state with very little diffraction of the laser as it passes through the liquid. However, there exists a critical temperature, T_c, where as one approaches T_c the opacity very suddenly starts to change in a small region near T_c. At T_c the fluid becomes almost entirely opaque to the laser. This process has been traditionally described as the result of the liquid entering a mixed state where gas and liquid simultaneously exist, and droplets form over a very large range of sizes. These will act to scatter light strongly as the associated fluctuations in the scattering index also experience large fluctuations.

1.2 Thermodynamic Fluctuations and Critical Fluctuations

In order to properly understand critical fluctuations, we first contrast its behavior with that of fluctuations in the "thermodynamic limit". The thermodynamic limit is characterized by the stability of average values. This insight comes from an understanding of how fluctuations scale with system size. The way that this is typically understood is by looking at the variance of energy, which nicely characterize a systems fluctuations. We define it in the usual way,

$$\delta E^2 = \left\langle E^2 \right\rangle - \left\langle E \right\rangle^2 \tag{1.13}$$

where the average energy can either be determined from a distribution of energies (ex. Boltzmann) or directly from the partition function (ex. Eq.1.7), which computes the ensemble average

$$\langle E \rangle = -\frac{\partial}{\partial \beta} log Z \tag{1.14}$$

Similarly the variance can be conveniently written in terms of average energy,

$$\delta E^2 = -\frac{\partial}{\partial \beta} \langle E \rangle \tag{1.15}$$

This nicely provides the intuition that fluctuations are determined by how the energy changes given a change in temperature. This is essentially the definition of the heat capacity of a substance and heat capacity is known to be an extensive quantity which scales according to the mass of the substance. Thus, we find energy fluctuations $\delta E^2 \sim C \sim N$. Similarly, average energy is an extensive quantity leading to $\langle E \rangle \sim N$. The amplitude of fluctuations are given by the ratio,

$$\frac{\delta E}{\langle E \rangle} \sim \frac{1}{\sqrt{N}} \tag{1.16}$$

So, as the system size increases or as N increases, the magnitude of fluctuations goes to zero. This clearly shows that the thermodynamic limit leading to a stability of state variables does not apply to critical phenomena where the compressibility and heat capacity diverge.

This boundedness of thermodynamic state variables can better be understood by looking at the behavior of the correlation length. Properly defined, the correlation length characterizes the spatial extent of particle interactions. Typically, this is measured by the connected correlation function, which for spin systems can be intuitively written as,

$$C(i,j) = \langle (s_i - \langle s_i \rangle) \cdot (s_j - \langle s_j \rangle) \rangle \tag{1.17}$$

where the average is an ensemble average over all spins. This form shows we are interested in interactions different from average values. This ensures we don't consider contributions of external influences that might act to correlate spins beyond their actual interactions with one another. This would be the case, if for example, the system was put in the presence of an external magnetic field or the like. Formally, we are interested in characterizing the spatial extent of the random inherent system fluctuations. We can write the connected correlation function in a more familiar way as,

$$C(i,j) = \langle s_i s_j \rangle - \langle s_i \rangle \langle s_j \rangle \tag{1.18}$$

Because it will be useful to define a length characterizing the spatial extent of interactions, we write the correlation function in terms of distance r between sites. Thus, for any arbitrary spin selected to be at the origin, $r = 0$(and again, performing an ensemble average), we can write,

$$\begin{aligned} C(r) &= \langle (s(r) - \langle s \rangle)(s(0) - \langle s \rangle) \rangle \\ &= \langle s(r) \cdot s(0) \rangle - \langle s \rangle^2 \end{aligned} \tag{1.19}$$

In the Ising model, and in most cases the general behavior of the correlation function, $C(r)$ is characterized by a decaying exponential,

$$C(r) = C_0 e^{-r/\xi} \tag{1.20}$$

where the correlation length, ξ, is the decay constant. In the case of regular equilibrium fluctuations, we find $\xi \ll L_{sys}$ and the correlation function quickly decays to zero. This allows energy fluctuations to follow the equilibrium stability and their magnitude decreases according to $N^{-1/2}$. However, for what will come to characterize critical fluctuations, we

will find that $\xi \sim L_{sys}$ which consequently means $\xi \gg r$ and the exponential function goes to unity. This allows fluctuations to become arbitrarily large up to the scale of the system.

In fact in conjunction with the correlation length, the correlation function near the critical point was found to behave according to [7],

$$C(r) \sim \frac{1}{r^{d-2+\eta}} \tag{1.21}$$

where η typically takes on a small value for most systems. This tells us that rather than exponentially decaying, correlations decay with a polynomial and produce long range correlations.

The presence of long range correlations directly impacts the macroscopic behavior. To see this, we show how the system's susceptibility is determined directly from the correlation function. In order to give the correlation function a more obvious physically significant role, we note that we are interested in knowing the average correlation of all spins with an arbitrary spin in the system, and subsequently average over all spins to get some measure of average connectivity in the system. This means we would want to integrate over the entire volume, V and the total average correlation becomes,

$$C = \frac{1}{V} \int_V d^3r \; C(r) \tag{1.22}$$

A fundamental relationship between susceptibility and the average correlation gives [9],

$$\chi \sim \beta C \tag{1.23}$$

This allows us to directly attribute the divergence of the susceptibility as the result of the divergence of the correlation function, where again the correlation function is the spatial extent of fluctuations. For the correlation function to diverge means that fluctuations are allowed to grow arbitrarily large, which again is exactly the point of view argued previously.

This in large part motivates the Finite Size scaling hypothesis, which posits that the correlation length divergence is fundamentally the source of all divergences during a

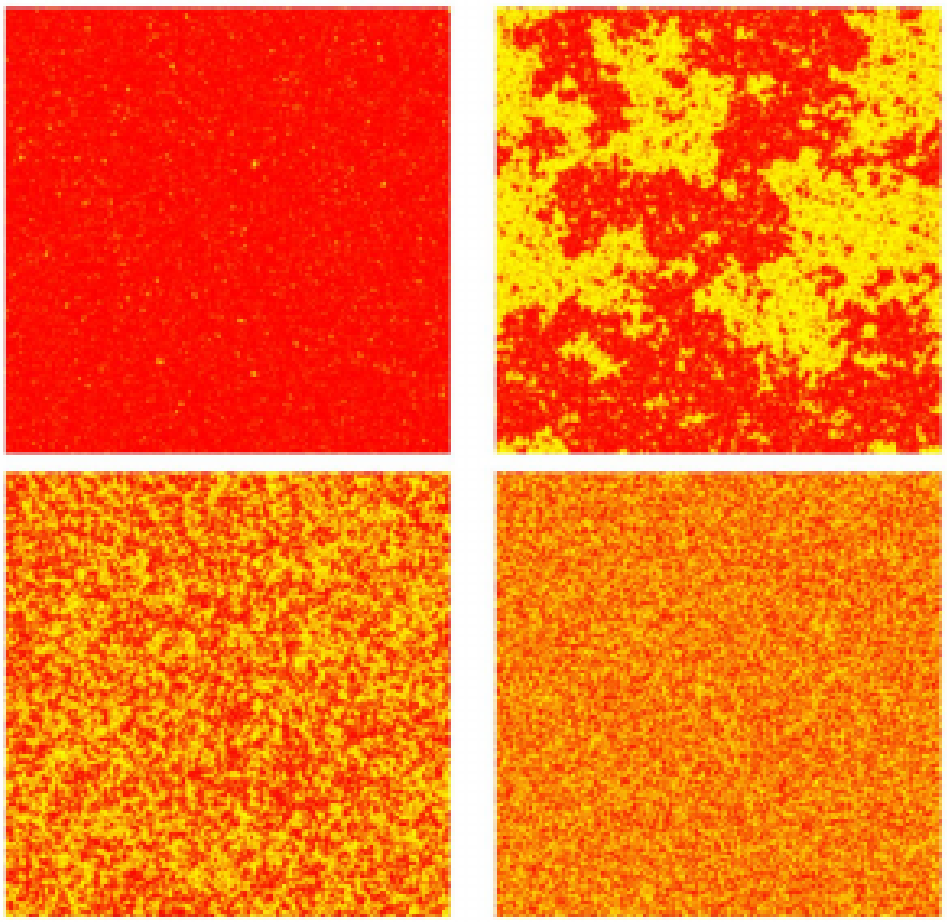

Figure 1.5. Here we show Monte Carlo simulation of Ising clusters for different T. (Top Left) $T \ll T_c$: Low temperature with spins in nearly the same state. (Top Right) $T \sim T_c$ Large clusters only begin to form near the critical temperature, T_c. (Bottom Left) $T > T_c$: At higher temperatures the cluster's sizes decrease in size. (Bottom Right) $T \gg T_c$: High temperatures limit where spin states are independent and random.

second order phase transition. Moreover, the divergence of the correlation length makes it more likely for the correlation length to be the only relevant length of the system. This is a radical departure from equilibrium dynamics which arose from stable states and their characteristic small-scale interactions, and where previously fluctuation magnitudes decreased by $N^{-1/2}$, now the correlation length extends to the size of the system ensuring that fluctuations can no longer be exponentially suppressed.

That the correlation length of random fluctuations becomes prominent on all scales of the system ensures that macroscopic properties will likewise become dominated by random fluctuations. This places the characterization of the correlation length at the center of any attempt to characterize a system's critical behavior. However, the finite size scaling hypothesis is mostly empirically driven as it is on an observational basis that we justify the functional behavior of the correlation length to be a power-law, characterized by its proximity to the critical point, T_c

$$\xi \sim |T - T_c|^{-\nu} \tag{1.24}$$

where ν is a critical exponent characterizing the divergence of the correlation length.

Because a single length dominates the system, this allows us to write many quantities in terms of this length. Consequently, these quantities must also follow power-laws, and therefore, relations between these quantities become relations between their respective exponents. For example, we can write

$$\frac{\gamma}{\nu} = 2 - \eta \tag{1.25}$$

by recalling that the correlation function is described by $C(r) \sim r^{-(d-2+\eta)}$. If ξ is the only relevant length than we can write $r = b\xi$. We can make use of the fluctuation dissipation theorem, giving rise to Eq.1.23, to establish relation, $\chi \sim \int_\xi d^d\xi \; C(\xi) \sim \xi^{-(-2+\eta))}$. Using Eq.1.24 we can write $\chi \sim |T - T_c|^{-\nu(2-\eta)} = |T - T_c|^{-\gamma}$ where the equality between exponents gives rise to Eq.1.25, and emphasizes that if the correlation function diverges so too must the susceptibility.

The divergence of the correlation length also brings about another interesting property, universality. Since the correlation function is a measure of average correlations of random

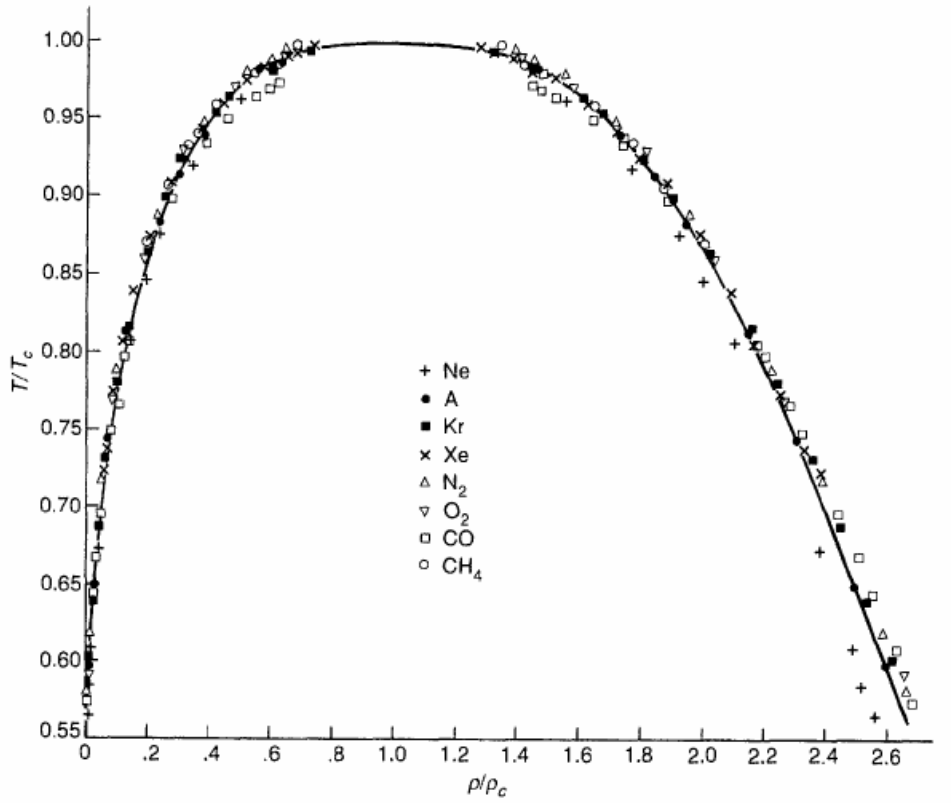

Figure 1.6. Coexistence curve of several different fluids [10]. That randomness dominates the behavior is what gives rise to the concept of universality in critical phenomena. This famous plot shows the behavior of the order parameter near the critical point for different molecules. Distinct inter-molecular dynamics of the various plotted fluids result in different equilibrium relations between their state variables (in this case, ρ and T) away from the critical point. When normalized by their respective critical values, we find that all the fluids lie along nearly the same curve! In fact, the critical exponents of the 2D Ising model and that of the gas-liquid systems are nearly the same.

order parameter fluctuations, and because this quantity fundamentally diverges, which is to say that these critical fluctuations are allowed to grow to dominate the behavior of the system, we find previously distinct systems with different inter-molecular interactions collapse to the same behavior near their critical points. This observation made famous by [10] shows how nitrogen, oxygen, carbon monoxide, and methane follow the same coexistence curve shown by Figure 1.6, reflecting that they are described by nearly the same critical exponent, characterizing the order parameter divergence, $\rho - \rho_c \sim |T - T_c|^\beta$.

The Finite Size Scaling Hypothesis elegantly explains why universality is the natural consequence of the emergent scale invariance, and proposes interesting questions about the sort of universality classes and what serves to define distinct classes. Here, we have an elegant example of distilling simplicity from complexity. We will pursue this generality even further in the next section.

1.3 From Ising to Percolation

The Ising Model can be generalized by considering more spin states available to each spin located at each lattice vertex. This generalization is characterized by variable s defining the number of available states. A careful analysis [11] into the various kinds of models one can map to depending on the value of s has led to very interesting results. For $s = 2$ we reproduce the well known Ising model. For $s = 0$, we reproduce the resistor network. More interestingly, s need not even be an integer as $s = 1/2$ leads to the dilute spin glass model. Our interest is in the $s = 1$ which maps to the percolation system. These generalizations are all classed under the name of the Potts model, who first described the critical points of the $s = 2, 3, 4$ variants.

The Potts model Hamiltonian is very similar to the Ising Hamiltonian and is given by,

$$H_p = -J \sum_{x,y} [\delta_{\sigma_x \sigma_y} - 1] - h_p \sum_x [\delta_{\sigma_{x1}} - 1] \tag{1.26}$$

here, kronecker delta, $\delta_{\sigma_x \sigma_y}$ is 1 if the spin at lattice positions x, y are in the same state and is 0 if they are not. The model usually assumes nearest neighbor interactions, so the

sum is over nearest neighbor pairs, (x, y). As is usual, the partition function is given by,

$$Z = \sum_{\{\sigma\}} \exp^{-\beta H_p} \tag{1.27}$$

where the sum is over all spin configurations, σ. While this choice of notation emphasizes the generality of the Potts Model by writing the same Hamiltonian, the consequence is that the spin state variable, s, also won't explicitly appear in the partition function either. Thus, when we compute the free energy state function in the usual way given by Eq1.4 there isn't any explicit dependence on s. This is detrimental for our purposes because we would like to distinguish behavior as a function of s.

In what is now known as the Fortuin-Kasteleyn (FK) representation [12], a far more powerful framework is established to study the behavior of the Potts model, and succeeds in characterizing behavior in the limits of different spin states, s. Additionally, emphasis on s allows in some sense a generalization of the study of phase transitions as it is believed that high s systems lead to discontinuous phase transitions, while low s models lead to continuous transitions. For our purposes, one of the key insights comes in rewriting the partition function such that the dependence of spin states, s, is made more explicit. For simplicity, we will consider the case in which there is no external field so $h_p = 0$. In this case the partition function is written as,

$$Z_P = \sum_{\{\sigma\}} \exp^{\beta J(\sum_{l,m}[\delta_{\sigma_l \sigma_m} - 1])} \tag{1.28}$$

We note that the sum, $\sum_{l,m}[\delta_{\sigma_l \sigma_m} - 1]$, has nonzero terms for nearest neighbors that are in different states. We could alternatively define a bond to correspond between these nearest neighbor pairs that are anti-aligned, and perform the sum over the bonds instead. Bonds are similarly referred to as edges which establish the connection between two sites. It will be convenient to think about summing over edges rather lattice sites. For convenience we define another Kronecker delta for each edge connecting two spins, and define a bond to exist when both spins are in the same state.

$$\delta_e(\sigma_x, \sigma_y) = \frac{1}{s}[1 + (s-1)\sigma_x \sigma_y] \tag{1.29}$$

where s is the number states available to each spin. This allows us to write the Potts partition function, Z_P as,

$$\begin{aligned} Z_P &= \sum_{\{\sigma\}} \left\{ \exp \beta J \sum_{\{nn\}} [(\delta_e(\sigma) - 1)] \right\} \\ &= \sum_{\{\sigma\}} \left\{ \prod_{\{nn\}} \exp \left[\beta J (\delta_e(\sigma) - 1)\right] \right\} \end{aligned} \tag{1.30}$$

where the sum in the exponential is over the allowed nearest neighbor interactions. For example, in the Ising model on a square lattice, there are 4 nn interactions per spin site σ as shown in Figure 1.3.

As a specific example of the combinitorics of the FK mapping, we consider $s = 2$, corresponding to the 2 spin state Ising model: here, $\delta_e(\sigma_x, \sigma_y) = \frac{1}{2}[1 + \sigma_x \sigma_y]$, where $\sigma_i = +1, -1$. For every bond the exponential term in Eq 1.30 we will generate either $e^{-\beta J}$ or 1. Thus we can rewrite the exponential using,

$$e^{\beta J(\delta_e(\sigma)-1)} = 1 - p + p\delta_e(\sigma) \tag{1.31}$$

where we define p as,

$$p = 1 - e^{-\beta J} \tag{1.32}$$

Thus far, the notion of a bond serves to define the interaction between two sites in the same state which effectively lowers the energy of the system. If we were to instead sum over every potential interaction between sites (edge), and define things such that $\omega(e) = 1$ if a bond exists at edge e and $\omega(e) = 0$ if there is no bond, then we get the following relation,

$$1 - p + p\delta(\sigma) = \sum_{\omega(e)} [(1-p)\delta_{\omega(e),0} + p\delta_{\omega(e),1}\delta_e(\sigma)] \tag{1.33}$$

We can easily recover the expression on the left of the equality by performing the sum of $\omega(e)$ over values 0 and 1, each contributing the first and second terms respectively. Additionally, this has the nice interpretation that each edge contributes $(1 - p)$ for being closed (no connecting bond) and p for being open (connecting bond) and a $\delta_e(\sigma)$ factor

which depends on values of the spins. We are now in a position to sum over edges, but rather than just summing over the nearest neighbor, $\{nn\}$ for each spin, σ, we will some over the entire set of edges, e.

Plugging in this relation in addition to relation 1.31 into Eq.1.30 gives,

$$Z_P = \sum_{\{\sigma\}} \left\{ \prod_{\{nn\}} \sum_{\omega(e)} [(1-p)\delta_{\omega(e),0} + p\delta_{\omega(e),1}\delta_e(\sigma)] \right\} \tag{1.34}$$

Because of the nature of the delta functions in each term, the $\sum_{\omega(e)}$ and $\prod_{\{nn\}}$ are interchangeable. . Thus, we can write,

$$\begin{aligned} Z_P &= \sum_{\{\sigma\}} \left\{ \sum_{\omega(e)} \prod_{\{e\}} [(1-p)\delta_{\omega(e),0} + p\delta_{\omega(e),1}\delta_e(\sigma)] \right\} \\ &= \sum_{\{\omega\}} (1-p)^{N-n_b} p^{n_b} \left(\sum_{\{\sigma\}} \prod_e \delta_e(\sigma)^{n_b} \right) \\ &= \sum_{\{\omega\}} (1-p)^{N-n_b} p^{n_b} s^{m(\omega)} \end{aligned} \tag{1.35}$$

where N is the total number of edges. n_b is the total number of open bonds and $m(w)$ is the total number of connected clusters for each edge state $\omega = 0, 1$.

More formally the mapping between the two partition functions Z_P and Z_RC can be written as [13],

$$\begin{aligned} Z_P &= \sum_{\{\sigma\}} \left\{ \prod_{\{e\}} \exp\left[\beta(\delta_e(\sigma) - 1)\right] \right\} \\ &= \sum_{\{\omega\}} \left\{ \prod_{\{e\}} p^{\omega(e)} (1-p)^{1-\omega(e)} \right\} s^{m(\omega)} \\ &= e^{\beta JN} Z_{RC} \end{aligned} \tag{1.36}$$

where the exponential factor is the proportionality constant for the interaction energy for a total of N spins. This mapping can be better understood by the following equivalence between FK's random cluster model [12] and the 2D Ising Model: we can start with a lattice of spins, each of which is already assigned to be in one of two states $s = \{-1, 1\}$. For every spin we check its nearest neighbors, and if a nearest neighbor is in the same state

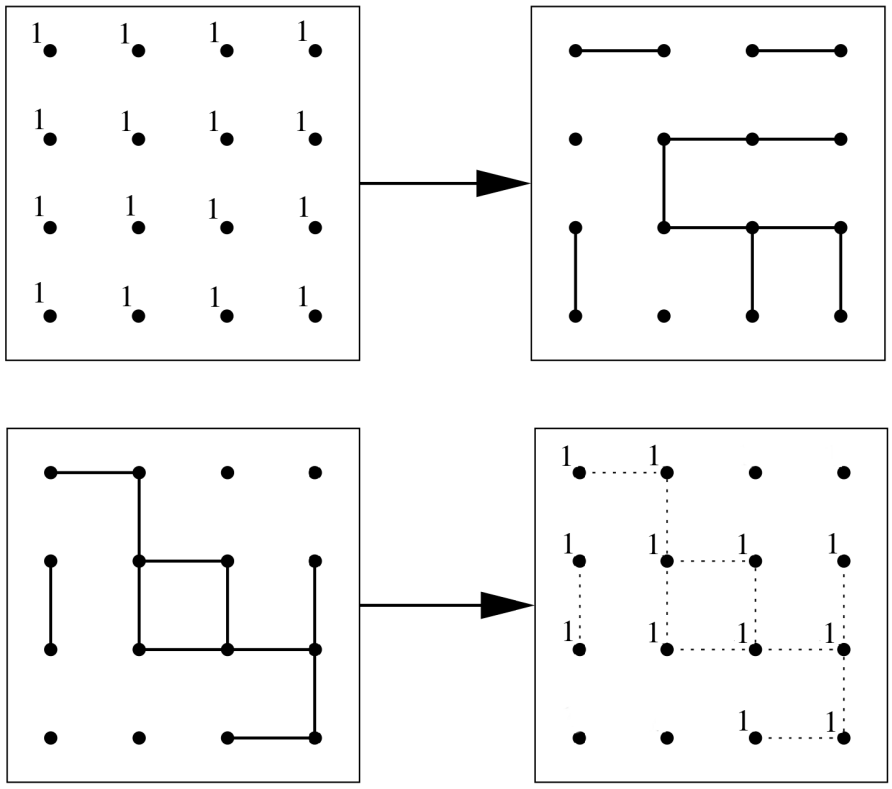

Figure 1.7. FK, $s = 1$, mapping example. (top) We begin by randomly laying down edges (bonds) connecting two sites with probability p. Clusters are the collection of connected edges (bonds). (bottom) Alternatively, we start with some random collection of clusters which can be made to correspond with a probability p to the occupation probability for sites to be in state $s = 1$.

we draw a bond with probability p connecting the two sites. A cluster of spins is defined as a set of spins connected by bonds. Alternatively, we can start with an arrangement of open and closed edges on the entire lattice. Similarly a cluster is defined as the sequence of connected open edges. If an edge connects to no other edge than its a cluster of size 1. Finally, for each connected cluster we randomly (uniformly) assign all vertices to be in one of the two s states.

The random cluster model is essentially a generalized bond percolation model where connected clusters are distinguished. However, if all connected clusters are identical we recover the bond percolation model.

The mapping is made concrete by the variable p connecting the two models. Further, as it was shown by Onsager [6] that the 2D Ising model exhibited critical behavior at

critical temperature T_c. This suggest that there exists a critical value, p_c, corresponding to the probability of the existence of a bond joining two sites,

$$p_c = 1 - e^{-\beta_c J} \tag{1.37}$$

Because percolation models are characterized by emergent macroscopic connectivity, it is intriguing that the critical behavior can be understood more simply by how this connectivity emerges near the critical point.

Again, the advantage of the random cluster model is that its partition function explicitly depends on the number of spin states, s. This is advantageous since this allows us to form relevant expressions in terms of derivatives of the partition function just as was done in section 1.1. For the Potts model, the free energy per spin is given as,

$$f(\beta, s) = -\frac{1}{N\beta} ln(Z) \tag{1.38}$$

Using the random cluster partition function $Z_R C$ as a substitute, we can compute the derivative of $f(\beta, s)$ as,

$$\frac{df}{ds} = -\frac{Z_{RC}^{-1}}{N\beta} \frac{dZ_{RC}}{ds} \tag{1.39}$$

As was mentioned previously, we can recover bond percolation from the Potts model in the limit $s = 1$. This is important because we can produce the generating function for bond percolation by computing $\frac{df}{ds}|_{s=1}$. We can now straightforwardly compute the derivative of Z_{RC},

$$\begin{aligned} \frac{dZ_{RC}}{ds}\Big|_{s=1} &= \sum_{\{\omega\}} m(\omega) \left\{ \prod_{\{e\}} p^{\omega(e)} (1-p)^{1-\omega(e)} \right\} \\ &= \sum_{\{\omega=1\}} m(\omega)\ p^{n_b} (1-p)^t \\ &= \langle m \rangle \end{aligned} \tag{1.40}$$

where in the second relation we used the fact that because $s = 1$, then likewise $\omega = 1$, which reflects the fact that all edges are sampled with a probability p of being open. Consequently, the product only over the edges contributing p, of which there are n_b instances (number of open edges), leads to the factor p^{n_b} for occupied and $(1-p)^t$ for

unoccupied. When we sum over all realizations of lattices and possible edge configurations, the result is that the derivative of the free energy in the cluster model describes the average number of clusters per site containing m sites. This is very similar to the lattice-animal calculation done by authors [14, 15] which calculates this quantity, and for percolation this corresponds to the cluster distribution, n_s [16]. The FK mapping establishes that because the generating function acts as the order parameter of the Potts model, one can similarly construct it for bond percolation [17].

In the previous section we showed how fluctuations in the order parameter coupled to a diverging correlation length lead to the scale invariant behavior characterizing critical phenomena. With this mapping to percolation we can see that the essential bits of critical behavior is reduced to the emergence of long range connectivity. The two point correlation function of the Potts model gets mapped to a quantity describing two point connectivity. Formally, these two measures can be related as [13],

$$\tau_{\beta,s}(x,y) = (1 - s^{-1})\phi_{p,s}(x \leftrightarrow y) \tag{1.41}$$

where $\tau_{\beta,s}$ is the two point correlation function and $\phi_{p,s}$ is defined as the two point connectivity function describing a path between lattice sites (x, y). That is, it describes the likelihood of a connected path existing between two sites. That this quantity should diverge provides us with the key insight: the long range order which emerges near the critical point of the Potts model corresponds to the existence of an infinite cluster in the percolation model.

1.4 Fisher Criticality and the Cluster Approach

From the complexity and diversity of generalized second order phase transitions, we have taken a trajectory which seeks to distill only the essential pieces required to properly describe critical phenomena. In the previous section, we arrived at the generating function, which in the $s = 1$ limit of the random cluster model, describes the average number of clusters per lattice site. This is precisely the percolation limit. Further, from this quantity we can derive many of the other essential quantities of the respective system (ex. percolating cluster probability, cluster counts, average cluster size or order parameter,

heat capacity, and susceptibility respectively). However, in describing the criticality of percolation, we leave behind much of the generalizing machinery inherent to the Potts and Random Cluster model. Instead, we follow the nomenclature of [16], but we have the added intuition that motivates the central importance of the the generating function (or as is typically more simply referred to as the number distribution n_s in percolation) to this class of critical systems.

From the Random Cluster model we can understand that the critical transition is described by the emergence of long range connectivity which in percolation takes the central role as the emergence of a percolating cluster (also referred to as sample spanning cluster (SSC) or incipient infinite cluster (IIF) in various texts). Though well motivated thus far, a focus on criticality characterization via a cluster description did not arise exclusively from percolation. This approach received an impetus by the older problem of attempting to describe condensation from a gas to a liquid, and is described by classic nucleation theory which attempted to remedy the shortcomings of the Van der Waals equation of state. The Van der Waals unfortunately failed to describe the proper behavior near the critical point (predicting a quadratic dependence for the coexistence curve shown in Figure 1.6 which exactly fits a cubic function represented as a solid line). Rather than specifying particle interactions, Nucleation theory attempts to describe the free energy of droplets and the metastable states where condensation droplets could grow to very large sizes. In trying to characterize the size distribution of these non-interacting droplets, Fisher famously showed how one could simply describe the distribution with a form [18],

$$n_s\left(T\right) = s^{-\tau} f\left[\left(T - T_c\right) s^{\sigma}\right] \tag{1.42}$$

which was to be characterized by 2 critical exponents, τ and σ. It is convention to define $z = (T - T_c)s^{\sigma}$ such that at the critical point where $z = 0$ we get $f(0) = 1$, leaving behind power-law behavior $s^{-\tau}$. Away from the critical point and supposing that $z \ll 1$ we can represent $f[z] = e^{-s/s_\xi(p)}$ where $s_\xi(p) = |p - p_c|^{-1/\sigma}$, revealing that s_ξ behaves as the characteristic cluster size where clusters larger than s become exponentially suppressed. Fisher's scaling form elegantly solves a number of issues as we'll see when defining the order parameter, and also, correctly reproduces the analytically derivable scaling of percolation

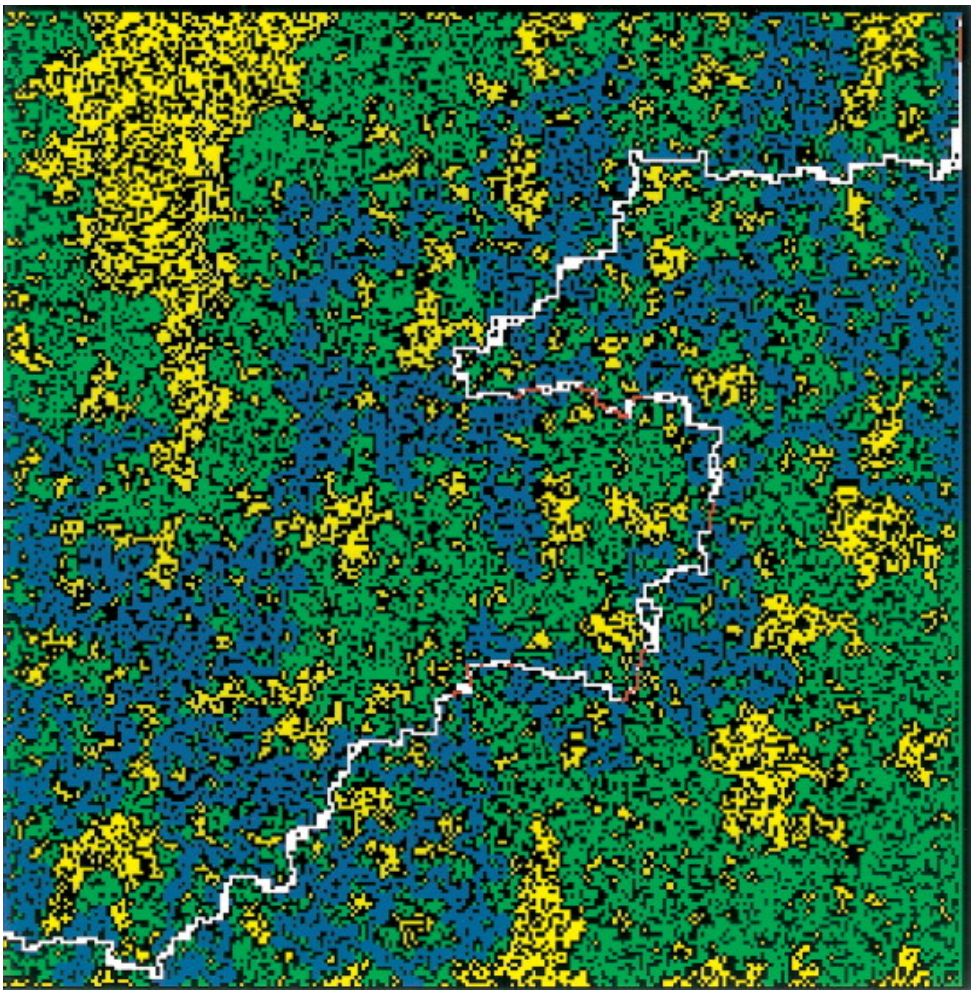

Figure 1.8. Percolation clusters near the critical point [19]. The yellow clusters represent the finite clusters. The blue cluster is the sample spanning or infinite cluster. The green sites are the unoccupied sites. The white path is the shortest occupied distance between the two endpoints.

in 1D. Having established that the Ising transition could likewise be understood through connected clusters, a similar scaling behavior was found for Ising droplet clusters and by extension percolation clusters. Though we have established direct mapping to bond percolation it can also be extended to its more famous twin, site percolation, which likewise captures the essential features of criticality. In site percolation, we define a cluster to be the sequence of connected nearest neighbor sites. Each site is sampled with occupation probability p for being occupied or empty. Phases are defined by the existence (or lack) of a sample spanning cluster which spans the entire lattice from end to end. (In the limit of an infinite lattice, the sample spanning cluster becomes an the infinite cluster)

A cluster approach to critical behavior allows one to reproduce the essential features of critical behavior as is reported in [20]:

> (i) the size of the clusters must diverge at the Ising critical points, (ii) the linear dimension of the clusters must diverge with the same exponent as the correlation length, and (iii) the mean cluster size must diverge with the same exponent as the susceptibility.

As we will see, establishing that Eq.1.42 describes the clustering of a system is an efficient method for establishing the existence of critical behavior, and as such, means that the starting point is typically an observation that the systems clusters (however they may be defined) follow Eq.1.42. Therefore much of what follows can be applied to the whatever elements are doing the clustering with slight minor differences (universality classes etc.) distinguishing systems. For example, one could derive site and bond percolation from suitable Random cluster limits, but we will not continue to delve into those subtleties, though these continue to be intriguing problems.

Having now established the significance and intuition behind the cluster number distribution n_s (or generating function), we will now show how percolation's important quantities can be derived from it. First, we begin with the order parameter, which is the probability that an arbitrary site belongs to an infinite cluster or SSC. For percolation, the critical occupation probability, p_c, indicates when it is likely to generate an SSC in the lattice, and the cluster distribution, n_s, defines the scaling of all finite clusters. Note for $p < p_c$, all sites are likely to belong to one of the finite clusters in cluster distribution n_s and consequently $p = \sum_s s n_s$. That is, p should reflect the total fraction of occupied sites. If P represents the probability of an SSC (or the fraction of sites belonging to it) then a site will either belong with probability p to a finite cluster, or to an infinite cluster. We can represent P as the difference, $p - p_c$, and also define $\epsilon = p_c - p$. Now summing

over all sites gives,

$$\begin{aligned} P(p) = p_c - p &= \int_L ds\ [n_s(p_c) - n_s(p)]s \\ &\propto \int_L ds\ s^{1-\tau}\left(f[0] - f\left[\epsilon s^{\sigma}\right]\right) \\ &\propto \int_0^{\infty} \left(dz\ \epsilon^{-1/\sigma} z^{1/\sigma - 1}\right) \epsilon^{-\frac{(1-\tau)}{\sigma}} z^{\frac{1-\tau}{\sigma}}\left(f[0] - f[z]\right) \\ &\propto \epsilon^{\frac{\tau-2}{\sigma}} \int_0^{\infty} dz\ z^{\frac{2-\tau}{\sigma}-1}\left(f[0] - f[z]\right) \\ &\propto \epsilon^{\frac{\tau-2}{\sigma}} \int_0^{\infty} dz\ z^{\beta}\frac{df}{dz} \\ &\propto \epsilon^{\frac{\tau-2}{\sigma}}\Gamma(\beta - 1) \\ &\propto \epsilon^{\frac{\tau-2}{\sigma}} \propto |p_c - p|^{(\tau-2)/\sigma} \\ &= |p_c - p|^{\beta} \end{aligned} \tag{1.43}$$

where in the third line we used $z = \epsilon s^{\sigma}$ and subsequently make use of $ds = \frac{\epsilon^{-1/\sigma}}{\sigma} z^{1/\sigma - 1} dz$. Also, $f[z] \sim e^{-z}$ and we made use of the fact that $\Gamma(\beta - 1)$ is a multiplicative constant. Care is needed when evaluating the integral for general p. If $p < p_c$ as we assumed here then the integral should evaluate to zero reflecting that it is highly unlikely for a percolating cluster to exist except near the critical point.

Near the critical point the order parameter remains continuous but still follows a power law determined by cluster distribution exponents, τ and σ. It is customary to assign the order parameter its own exponent, β, but Eq.1.43 establishes the relation between β and the cluster distribution exponents, τ and σ.

$$\beta = \frac{\tau - 2}{\sigma} \tag{1.44}$$

The order parameter is responsible for signaling the system change change as it undergoes a phase transition, therefore we attempt to elicit a slightly more physically significant description. It is instructive to see how the order parameter, $P(p)$ is related to a more intuitive and insightful site density parameter. We can begin again with the relation, $P + \int ds\ sn_s = p$, which states that an occupied site is likely to belong either to a finite cluster belonging to n_s or to an infinite cluster with probability P, and p is occupation probability or since sites are uniformly sampled with probability p it represents the

fraction of occupied sites. we can rewrite this as,

$$\begin{aligned} p = \frac{occupied\ sites}{total\ sites} &\sim \frac{L^{D_f}}{L^d} \\ &= L^{D_f - d} \\ &= \rho_L \end{aligned} \tag{1.45}$$

where we have made use of the percolation canonical mass scaling relation defining fractal exponent D_f by $M \sim L^{D_f}$. We note that p behaves as the total lattice site density described by ρ_L. If we similarly define finite cluster site density with term $\rho_{FC} = \int ds\, sn_s$, then at the critical point where $P \to 0$ this means $\rho_{FC} \to \rho_L$. This reflects an essential feature of droplets or clusters during the critical transition . In particular, at any given moment the liquid water has density fluctuations which produce holes inside the raindrop just like holes in Swiss cheese. Only if we average over these holes we get a homogeneous density, for both raindrops and Swiss cheese.

In the previous sections we sought to describe the onset of a critical transition by the sudden dominance of unbounded order parameter fluctuations. Here we will see how order parameter fluctuations are manifest in the cluster approach.

As it began to became clear that large connected clusters were the direct result of critical transition, early authors attempted to provide rigorous relat. In [21], Coniglio and Russo rigorously established the general inequality characterizing the connectivity of what would become the percolation problem,

$$(1-p)(p_{ij} + p_{ij}^{\infty}) - p(t_{ij} + t_{ij}^{\infty}) \geq g_{ij} \tag{1.46}$$

where we have the following definition of variables:

p is the occupation probability of each site.

p_{ij} is finite connectivity function ($\langle s_i s_j \rangle$ term in Eq1.18) describing the probability that two sites, i, j belong to the same finite cluster.

p_{ij}^{∞} is the infinite connectivity function describing the probability two sites belong to the infinite cluster.

$t_{ij}(t_{ij}^{\infty})$ is the perimeter function describing the probability that site i belongs to a finite (infinite) cluster and j to its perimeter.

g_{ij} is the general pair connectivity defined in by Eq.1.18

The perimeter of a cluster is defined as the set of unoccupied sites surrounding a connected occupied cluster. Because for large cluster sizes the perimeter scales in proportion to number of sites it has the same scaling as p_{ij}. For this reason, we will work with a simpler relation that relies only on the occupied sites.

Note that we can break the general connectivity function into two parts,

$$g_{ij} = p_{ij} + p_{ij}^{\infty} \tag{1.47}$$

That is for a connected site, either the site will be long to a connected finite cluster or a connected infinite cluster.

Now what we would like to do is write Eq.1.47 to be explicitly dependent on order parameter fluctuations, which we can write as follows,

$$\begin{aligned} \Delta P_{\infty}^2 = \sum_i (p_{ij}^{\infty} - P_{\infty})^2 &= \sum_i \left\langle p_{ij}^{\infty} \right\rangle - \left\langle p_i^{\infty} \right\rangle \left\langle p_j^{\infty} \right\rangle \\ &= \sum_i \left\langle p_{ij}^{\infty} \right\rangle - P_{\infty}^2 \end{aligned} \tag{1.48}$$

Plugging this into Eq.1.47 gives,

$$p_{ij} + p_{ij}^{\infty} - P_{\infty}^2 = g_{ij} \tag{1.49}$$

Next summing over i and performing an ensemble average gives,

$$\langle S \rangle + \Delta P_{\infty}^2 = \chi \tag{1.50}$$

where we have made use of the relation $\sum_i p_{ij} = \langle S \rangle$ [16] where $\langle S \rangle$ is the average finite cluster size, and $\sum_i g_{ij} \sim \chi$ is the dissipation fluctuation relation given by Eq.1.23.

At this point it is worth making a few observations regarding Eq.1.50. First, the divergence of the susceptibility has two contributions, one from average cluster size and the other resulting from order parameter fluctuations. For $p < p_c$ where $P_{\infty} = 0$, the susceptibility is characterized by mean cluster size since its also the case that order parameter fluctuations are nearly zero, $\Delta P_{\infty}^2 \sim 0$. However, near the critical point both terms contribute and are coincidentally of the same order of magnitude so neither dominate. Further, it was shown by [22] that both terms diverge with the same exponent.

Because of this fact, we can characterize the divergence of the susceptibility by looking at the divergence of the mean cluster size, $\langle S \rangle$, alone.

We can once again rely on the burst size distribution function, n_s, to determine the scaling exponent of the susceptibility. The probability of a cluster of size s is $p(s) = sn_s$, therefore mean cluster size is given as,

$$\begin{aligned} \langle S(p) \rangle &= \frac{\int_L ds\ s^2 n_s(p)}{\int_L s n_s(p)} \\ &\sim |p - p_c|^{-\gamma} \end{aligned} \tag{1.51}$$

where the denominator we have normalized by total number sites. For $p \to p_c$ we get lower power-law relation.

We recognize that the divergence of the susceptibility is determined as a function of the second moment of the cluster distribution. This is satisfying as usually the second moment of a distribution characterizes the variance or rather fluctuations of the distribution. We can perform a calculation similar to that done with the order parameter to determine the relation between cluster distribution exponents, τ and σ. This leads to the following relation,

$$\gamma = \frac{3 - \tau}{\sigma} \tag{1.52}$$

We note that the order parameter, P, is a function of the first moment of the cluster distribution. This is not merely a coincidence. In fact we can similarly compute the zeroth moment, which corresponds to the total number of finite clusters, $N_{FC} = \int ds\ n_s$. We can perform a similar calculation as was done with $P(p)$ to derive a relation between the first moment, which for its association with its dual Ising quantity (heat capacity) gets exponent $2 - \alpha$, in order to derive relation between cluster distribution exponents and the first moment.

$$2 - \alpha = \frac{\tau - 1}{\sigma} \tag{1.53}$$

The major advantage of cluster approach is that we can characterize many of the important quantities as moments of the distribution, $M_k = \int_s s^k n_s$. That is, by characterizing the cluster size distribution, we can effectively characterize much the critical behavior.

1.5 Correlation Length and Hyperscaling

What remains is the characterization of the correlation length, ξ. This is related to the two point connectivity function presented in the previous section. Recall that the correlation function generally follows Eq1.20 where ξ is the correlation length defining the spatial extent of correlations. In percolation, the correlation length defines the spatial extent in which two occupied sites are likely to belong to the same cluster. In this regard, it is convenient to introduce the radius of gyration of a cluster, which essentially amounts to the second moment of the center of mass and is given by,

$$R_s^2 = \int_s ds \frac{|r_i - r_{cm}|^2}{s} \tag{1.54}$$

where r_i is the position of the i-th site in the cluster, and we normalize by the total number of sites belonging to th cluster, s. Once can show that the average distance between two sites is given simply by $2R_s^2$. Therefore, using the cluster size distribution we can determine the average distance of two sites belonging to the same cluster as,

$$\xi^2(p) = \frac{2\int_s ds\ R_s^2 s^2 n_s(p)}{\langle S(p) \rangle} \tag{1.55}$$

As one might expect and given the finite scaling hypothesis, near the critical point the correlation length diverges with with exponent, ν,

$$\xi(p \approx p_c) \sim |p - p_c|^{-\nu} \tag{1.56}$$

and Eq3.9 allows us to work out the relation between cluster distribution exponents and ν. To this end, we will need to make note of one other relation. Near the critical point, we find a power-law relation between average radius of gyration, R_s, and cluster size, s. This relation is similar to the canonical fractal dimension, $M \sim L^{D_f}$. In percolation as a result of hyperscaling these two exponents are the same, and this very important property

will be discussed shortly. Generally, we have $s \sim R_s^{D_s}$. Plugging this into Eq.3.9, gives,

$$\begin{aligned}\xi^2(p) &= \frac{2\int_s ds\ s^{2/D_s} s^2 n_s(p)}{\langle S(p)\rangle} \\ &= \frac{2\int_s ds\ s^{2/D_s+2-\tau} f[z]}{\langle S(p)\rangle} \\ &\propto \frac{\epsilon^{\frac{-2/D_s-3+\tau}{\sigma}}}{\epsilon^{\frac{3-\tau}{\sigma}}} \\ &= \epsilon^{\frac{-2}{D_s\sigma}} = \epsilon^{-2\nu}\end{aligned} \tag{1.57}$$

where as before we used that integration leads to a constant, and near the critical point we are interested in the divergence of the correlation length and the associated scaling exponent. In the last line the power-law behavior characterizing the divergence of the correlation length is given by $\xi \sim \epsilon^{-\nu}$. This leads to the following relation,

$$\nu = \frac{1}{D_s\sigma} \tag{1.58}$$

As expected, because we used the Hausdorff scaling exponent in order to determine ν, which means in addition to the 2 cluster distribution exponents, we also need D_s which brings the count to 3 exponents in order to describe the essential elements of the critical behavior of percolation.

Now that we have developed the essential quantities we can elucidate one of the key additional features in percolation. To that end, a particularly insightful quantity is the average number of cluster contained in a correlation volume. We define this quantity as $\langle N\rangle_\xi$, and use the zeroth moment of the cluster distribution which corresponds to the number of clusters,

$$\begin{aligned}\langle N(p)\rangle_\xi &= \xi^d(p) N_0(p) \\ \langle N(p \approx p_c)\rangle_\xi &\sim \epsilon^{-d\nu+2-\alpha}\end{aligned} \tag{1.59}$$

We find that near the critical point the number of clusters in the correlation volume scales according to exponent $a = -d\nu+2-\alpha$. To see how this exponent behaves, we consider the 2D example where $\tau = 187/91$, $\sigma = 36/91$, and $D_s = 91/48$. Using our scaling relations, we can deduce $\nu = 4/3$ and $\alpha = -2/3$, and we find $a = -2(4/3) + 6/3 - (-2/3) = 0$. This is an interesting result which suggests near the critical point the number of clusters

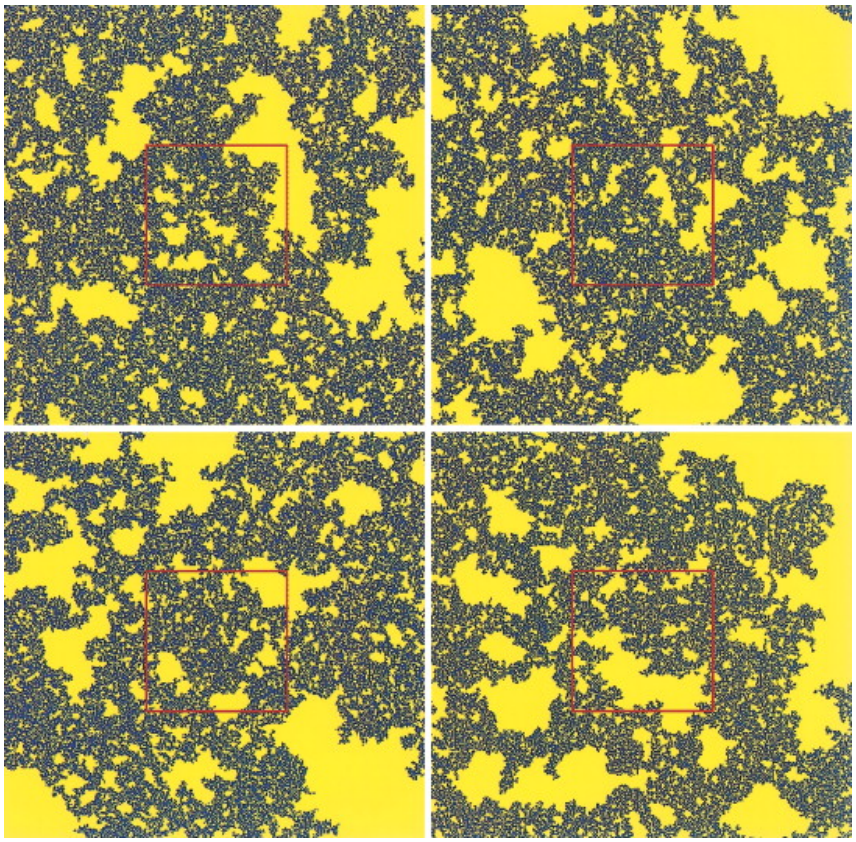

Figure 1.9. Percolation Scale invariance [19]. The only relevant length to the system is the correlation length, so if we imagine rescaling our system by some factor, so long as that factor is smaller than the correlation length (suppose we have a lattice of infinite size such that the correlation length is also infinite in size) then it becomes difficult to know which version is the scaled version of which. This is equivalent to saying the mass of the clusters follows a power law with arbitrary length L which will always be preserved if we perform a scaling operation

in a correlation volume remains constant, and its been shown that for $d < 6$ this result remains true and leads to the following hyperscaling relation,

$$d\nu = 2 - \alpha \tag{1.60}$$

Hyperscaling relations are loosely defined by relations relating other exponents to the dimension of the system. However, the above relation tells us that as the correlation length increases the number of clusters will increase so as to keep the number of clusters in a correlation volume constant. If this were not the case and clusters could outgrow their volume, then it would suggest that either the correlation length is larger than it should be or there are multiple correlation lengths competing for dominance in different regimes. More generally, this hyperscaling relation tells us that the density of spins making up

large clusters near the critical point should be the same as the density of clusters. This is why we can determine the Hausdorff dimension from the scaling of the cluster distribution near the critical point, which (using Eq.1.60) allows us to deduce,

$$D_s = \frac{d}{\tau - 1} \tag{1.61}$$

Note that, here, there is no dependence on the other cluster distribution exponent, σ, which characterizes the exponential cutoff off cluster sizes. Rather, this tells us about the clusters very near the critical point and how they assume the density of the sites corresponding to the entire lattice.

1.6 The Approach

Having laid out the essential framework describing the critical features of percolation. We are now in a better position to establish the connection between criticality and seismicity. We interpret the fractal properties of seismic systems as likely the result of some kind of critical fluctuations. The existence of scale invariant magnitude frequency distributions, event epicenter distributions, and temporal aftershock statistics strongly suggest this. However, rather than the full apparatus of second order phase transitions which describe the transition of states of matter, Fischer showed that much of critical features can be extracted from a scale invariant burst distribution characterized by two exponents, τ, σ. This distribution also carries with it the notion of a correlation length defining the cutoff cluster size, s_ξ. The existence of these distributions need not be connected to a phase transition. As an example with the droplet nucleation model, a potentially very long-lived metastable state characterized by the growth of critical droplets is proposed that effectively distances the behavior near the critical point from a being temporally bound to period where the system is transitioning states. Therefore, the existence of a scale invariant distribution will suffice to extract many of the essential features. The cluster distribution defines a generating form which we can derive many of the systems fractal properties.

Though physically, since we aren't attempting to motivate a phase transition, this framework lends itself to a statistical description of scale invariant events. In particular,

rather than looking for a description detailing the transition between two phases, we instead pursue descriptions of distinct universality classes. Phase transitions seem to be a subclass of all models capable of forming distinct universality classes. It represents one where there exists only a single correlation length scale that brings with it additional nice properties like hyperscaling. Since we intend to map our models onto seismicity which doesn't seem to have natural analogues of distinct phases, we propose an avalanche-burst invasion percolation (AIP) model that lifts some of these restrictions, namely critical order parameter fluctuations and hyperscaling. However, with a critical Fisher type distribution it satisfies the broader fractal properties characterstic to many complex systems and seismicity in particular. Thus, in the class of models consistent with observation, we need not limit ourselves to those described by second order phase transitions.

With this shift, the task becomes thinking about the underlying nature of fluctuations and how those scale up to determine the macroscopic properties of the system. With our AIP model, we model inherent randomness from a uniform distribution, and define a growth mechanism that allows fluctuations to spread across the lattice following a principle of least resistance growth algorithm. Further, we implement a definition of distinct bursts which allows us to produce a burst distribution that is also scale invariant.

The notion of a cutoff clusters size serves to naturally define a correlation length for clusters, such that clusters larger than the cutoff cluster size will become exponentially suppressed. The avalanche mechanism ensures that this length diverges according to the power law near the critical point, and properly becomes scale invariant only near a critical value. Thus, we still retain some of the criticality features with the existence of a critical control parameter, and this serves to define critical and subcritical cluster growth regimes.

Finally, we aim to characterize the site density within our burst clusters, and the density of burst themselves within the lattice. One of the interesting insights is that these two quantities need not be the same and suggests the existence of multiple correlation lengths in the problem. Despite this, it still is possible to produce a critical Fisher distribution, and suggest that multiple correlation lengths can exist without stifling scale invariance. With the characterization of exponents, τ, σ, ν, D_f, and D_s, we can define

destinct universality class of our model and match them with those observed in seismic systems.

References

[1] B. B. Mandelbrot, "A multifractal walk down wall street," *Scientific American*, vol. 280, no. 2, pp. 70–73, 1999.

[2] M. Gell-Mann and S. Lloyd, "Information measures, effective complexity, and total information," *Complexity*, vol. 2, no. 1, pp. 44–52, 1996.

[3] D. Sornette, "Discrete-scale invariance and complex dimensions," *Physics reports*, vol. 297, no. 5, pp. 239–270, 1998.

[4] N. Israeli and N. Goldenfeld, "Computational irreducibility and the predictability of complex physical systems," *Physical review letters*, vol. 92, no. 7, p. 074105, 2004.

[5] H. E. Stanley, *Phase transitions and critical phenomena*, vol. 7. Clarendon Press, Oxford, 1971.

[6] L. Onsager, "Crystal statistics. i. a two-dimensional model with an order-disorder transition," *Physical Review*, vol. 65, no. 3-4, p. 117, 1944.

[7] J. J. Binney, N. J. Dowrick, A. J. Fisher, and M. E. Newman, *The theory of critical phenomena: an introduction to the renormalization group*. Oxford University Press, 1992.

[8] E. R. Gopal, "Critical opalescence," *Resonance*, vol. 5, no. 4, pp. 37–45, 2000.

[9] S.-K. Ma, *Modern theory of critical phenomena*. Routledge, 2018.

[10] E. A. Guggenheim, "The principle of corresponding states," *The Journal of Chemical Physics*, vol. 13, no. 7, pp. 253–261, 1945.

[11] F.-Y. Wu, "The Potts model," *Reviews of modern physics*, vol. 54, no. 1, p. 235, 1982.

[12] C. M. Fortuin and P. W. Kasteleyn, "On the random-cluster model: I. introduction and relation to other models," *Physica*, vol. 57, no. 4, pp. 536–564, 1972.

[13] G. R. Grimmett, *The random-cluster model*, vol. 333. Springer Science & Business Media, 2006.

[14] A. B. Harris and T. C. Lubensky, "Connection between percolation and lattice animals," *Physical Review B*, vol. 23, no. 8, p. 3591, 1981.

[15] A. B. Harris and T. C. Lubensky, "Generalized percolation," *Physical Review B*, vol. 24, no. 5, p. 2656, 1981.

[16] D. Stauffer and A. Aharony, *Introduction to Percolation Theory.(2nd edn), 1992*. London, Taylor and Francis., 1994.

[17] M. J. Stephen, "Site-cluster distributions and equation of state for the bond percolation model," *Physical Review B*, vol. 15, no. 12, p. 5674, 1977.

[18] M. E. Fisher, "The theory of condensation and the critical point," *Physics Physique Fizika*, vol. 3, no. 5, p. 255, 1967.

[19] H. E. Stanley, J. S. Andrade Jr, S. Havlin, H. A. Makse, and B. Suki, "Percolation phenomena: a broad-brush introduction with some recent applications to porous media, liquid water, and city growth," *Physica A: Statistical Mechanics and its Applications*, vol. 266, no. 1-4, pp. 5–16, 1999.

[20] A. Coniglio and W. Klein, "Clusters and Ising critical droplets: a renormalisation group approach," *Journal of Physics A: Mathematical and General*, vol. 13, no. 8, p. 2775, 1980.

[21] A. Coniglio, "Cluster size and shape in random and correlated percolation," *Journal of Physics A: Mathematical and General*, vol. 12, no. 4, p. 545, 1979.

[22] A. Coniglio and D. Stauffer, "Fluctuations of the infinite network in percolation theory," *Lettere al Nuovo Cimento*, vol. 28, no. 2, pp. 33–38, 1980.

Chapter 2

Universality Class for Loopless Invasion Percolation Models and a Percolation Avalanche Burst Model for Hydraulic Fracturing

Summary

Invasion percolation is a model that was originally proposed to describe growing networks of fractures. Here we describe a loopless algorithm on random lattices, coupled with an avalanche-based model for bursts. The model reproduces the characteristic b-value seismicity and spatial distribution of bursts consistent with earthquakes resulting from hydraulic fracturing ("fracking"). We test models for both site invasion percolation (SIP) and bond invasion percolation (BIP). These have differences on the scale of site and bond lengths l. But since the networks are characterized by their large scale behavior, $l \ll L$, we find small differences between scaling exponents: D_f, D_{min}, and ν. Though data may not differentiate between models, our results suggest that both models belong to different universality classes.

2.1 Introduction

Invasion percolation ("IP") was proposed by [1] as a model for the displacement of one fluid in a porous medium by another "invading" fluid. It has since been applied to a variety of other dynamical processes including drainage [2], magnetic depinning of domain walls [3], contact line motion [4], and propagation of crack fronts [5].

Though all these examples have radically different small-scale behavior, their large scale statistics reveal the universality of how the inherent randomness of each system grows to dominate their respective critical phases. Hydraulic fracturing (HF) is a similar process. During HF, low-viscosity, high pressure fluid is pumped into porous rock which produces a network of fractures within the deep, thin reservoirs. Previous studies have made attempts to characterize this fracture network for purposes of efficient gas extraction [6, 7].

More recently, studies have shown significant increased seismicity in regions previously seismically inactive [8, 9]. They attribute HF as the likely culprit. This is not altogether surprising since fracking is somewhat analogous to steam production via geothermal pumping. Here, steam is generated by injecting fluid into the geothermal fields. In doing so, the fluid injected into basin sediments interacts with the ambient stress fields to nucleate earthquakes [10] in a similar way.

A key feature of IP is that networks grow according to random percolation (RP) near the critical point. Critical systems are described by a family of critical exponents which characterize all aspects of the system. These power-laws arise from a system having no characteristic length scale and therefore becomes symmetric under scale transformations. We observe that in classical, tectonic seismicity essentially all of the statistical properties are described by a power-law: magnitude frequency distribution (G-R magnitude scale) [11], temporal aftershock clustering (Omori aftershock law) [12], and the two-point correlation distribution [13]. In hydraulic fracturing and geothermal injection, studies show power-laws describing both the magnitude-frequency distribution and two-point correlation function [14], therefore, we believe much of the observed seismicity is well described as a system near a critical point.

Previous authors have noted the self-similar and invariant properties present in rock fractures [10], and since naturally occurring porous structures are well described by a lattice of sites connected by bonds [15], we choose to model the pumping of high pressure, low viscosity fluid into the sediment as a modified invasion percolation (IP) process. Here single phase liquid invades sediment by propagating through bonds adjoining sites in a 2D NxN square lattice. The result is a percolation network that is self-similar and scale invariant. Aki initially proposed using the fractal dimension, D_f, of a network to determine the power-law Gutenber-Richter b parameter that characterizes the associated seismicity arising from the fracture network. [16]

The observed magnitude-frequency distribution of induced seismic events differs from those localized in tectonic fault environments having Gutenberg-Richter b-value near 1 [17]. Instead, a range of b-values (1.2-1.5) have been observed [18]. Rather than the traditional fault slip mechanisms hosted in regions tectonically active, this kind of induced seismicity can occur in regions absent major fault structures. This suggest different universality classes describe tectonic and induced seismicity. These differences in part correspond to a different fracture mechanism for induced seismicity which is better described as the rapid re-opening of the pre-existing fracture network and the disturbance of the local stress field. [6] If the newly fractured network mostly follows preexisting natural fractures which themselves were the result of high pressure oil and gas escaping and fracturing the reservoir, then we hypothesize HF as fundamentally a drainage process. Therefore, a network grown by IP should be appropriate.

Table 2.1 shows the landscape of percolation models we discuss in this paper and where our model fits. When percolation was introduced it was intended to simulate the quasistatic movement of fluid through a porous matrix driven by capillary forces. Such a model is better suited to describe the static properties of a medium. In our case, the fluid is driven by large pressure gradients generated by the HF process, and we therefore advocate going beyond static network measures like the fractal dimension (and those similar to Aki) and implementing burst dynamics into our IP algorithms to describe induced microseismicity. In addition hydrodynamic considerations suggest

Percolation Models			
Percolation	RP	Quasi-static network growth ideal for describing medium properties. Natural clusters. No dynamic burst cluster growth.	
	IP	L	Critical single phase injection with no defending fluid (or highly compressible). Critical burst growth and cluster formulation for the invading fluid.
		NT	Critical nontrapping multiphase fluid propagation with natural clusters for incompressible defending fluid. No burst or clustering for invading fluid.
		Reg	Critical network growth for multiphase injection with clustering for compressible defending fluid. No burst or clustering for invading fluid.

Table 2.1. A comparison of percolation models considered in this paper. Random percolation (RP) and invasion percolation (IP) are both percolation models which generate percolating clusters. We consider variants of IP. Loopless (L) invasion percolation model coupled with the avalanche burst mechanics is the model we propose in this paper. We distinguish it from the regular variant [1] and the nontrapping (NT) variant [7] since the clusters in those models are clusters of the defending fluid. Our LIP model considers clusters and bursts of invading fluid. All IP models have bond or site variants corresponding to whether the random weights are bond strengths or site sizes.

a loopless network is appropriate. [19] Therefore, we adopt a similar loopless bond IP network as in [20] (except here we also compare with site IP), but grow the network using our own avalanche-burst model (discussed in section IV). With these added dynamics to the percolation network, we are able to produce power-law burst-frequency distributions which have scaling exponent, $\tau = 1.53$, larger than 1, and falls in the range observed in induced seismicity.

In percolation models which represent porous sediment by a lattice of sites adjoined by bonds, the precise interactions at the fluid boundaries is a function of the pore size

and the capillary throat diameter. We therefore consider 2 loopless invasion percolation models (LIP) corresponding to the two limits: if the throat sizes are smaller than all the pores, then the fluid will tend to become trapped in the larger pores. In this limit, the pore sizes govern the motion of the invading fluid. In our simulations we would need to assign strengths to pores representing the pore size and such a model would be site invasion percolation (SIP).

In the other limit where the throat sizes dominates the flow of fluid, (for example throat sizes are small compared to pore size restricting flow) we would instead assign strengths to the bonds/throats representing the bond size and such a model would be bond invasion percolation (BIP). Initially, we imagined fracking as being necessarily a drainage process since the invader would have most difficulty with the smallest constrictions, thereby making BIP the appropriate choice. However since the algorithms are characterized using their global properties, we may be insensitive to the details down to the bond site scale.

This then becomes a question of whether SIP and BIP share the same universality class. The literature seems to conflict on the this point. It was originally argued that SIP and BIP belong to the same universality class [21] but later it was argued that important differences arise between the two [19, 22]. Here, we perform a careful study of the two, illustrating the differences on the small scale, and we find that on the largest of scales, there remains a significant difference in fractal dimension D_f, though other scaling exponents remain similar. These results suggest the two processes belong to different universality classes.

Being able to distinguish between these two processes serves to illustrate the kind of sensitivity we can expect with this approach as each corresponds to different small scale processes. Ultimately, our choice to model HF as critical phenomena necessarily restricts the phenomenology we consider. From the theory of critical behavior, the critical point is a region of phase space where the typical small scale physics which governs much of the potential behavior becomes dominated by the inherent random fluctuations which are allowed to grow to all scales of the system. [23] In this paper we investigate which model

of randomness is appropriate for the inherent randomness of HF, and by which method the randomness grows to all scales.

To Summarize Our Results: Because the appropriate model for randomness in HF is unclear, we begin by comparing the simplest motivated models: loopless site invasion percolation (LSIP) and loopless bond invasion percolation (LBIP). We are interested in determining if there are significant differences in the critical exponents of these two models. If differences do exist, then we may be able to gain insight into the details of fluid displacement on the pore/bond scale since each process has different mechanism for fluid displacement. We find that on the scale of lattice spacing there are significant differences in networks between LSIP and LBIP. However, as the scale approaches that of a very large lattice (10^4x10^4 for example), their difference in scaling exponents D_f, D_{min}, and τ is still significant but becomes smaller. Because both models still produce sufficiently similar networks and our constraining data are limited, neither is preferred for modeling the fracture networks produced during hydraulic fracturing. Still, the small differences between the two models are significant enough to suggest they are described by different universality classes, and a sufficiently careful characterization of observed critical exponents could shed light into a more appropriate detailed small scale model.

2.2 Simulation Algorithm

The invasion begins at the center with a seed site and grows through the lattice following a principle of least resistance until reaching the lattice boundary. Since this is not a multiphase flow problem (we treat the defending gas as highly compressible) we don't concern ourselves with complications like trapping. Further, since our model is loopless, we will never have any trapped regions in the traditional sense. We first describe how we simulate SIP, which essentially amounts to maintaining two lists: the first is a list of filled sites, S_f and second is a list of nearest neighbor sites to all filled sites, S_{nn}.

1) The invasion begins at the center of the lattice with a seed site corresponding to the injection site. 2) The seed site's 4 nearest neighbors are added to the list of available sites, S_{nn}. This list will be updated serving as the list of "invadable" sites during each

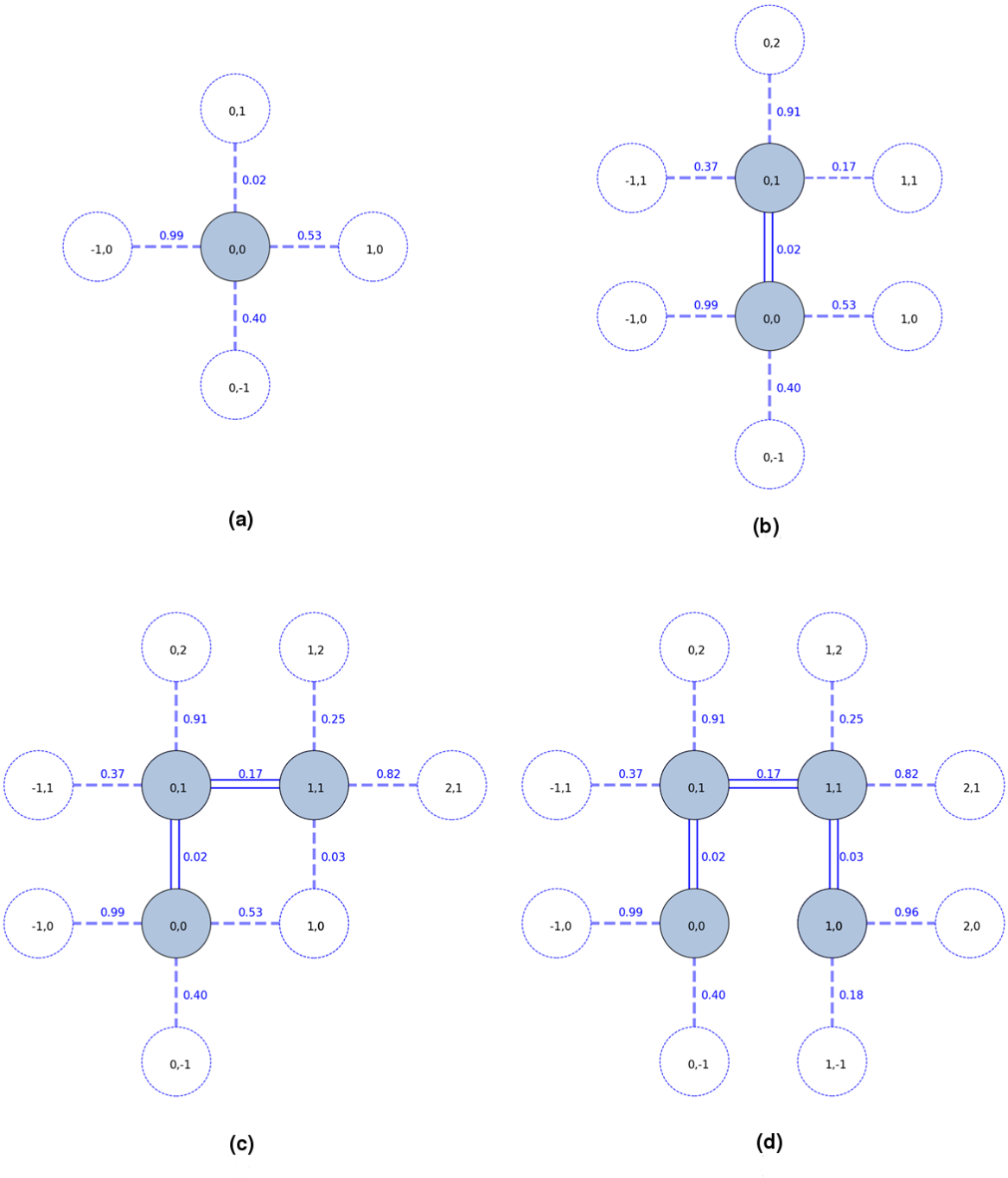

Figure 2.1. Bond Invasion Percolation algorithm illustration. a) A seed site is chosen in the center of the square lattice. The 4 nearest neighbors are added to the percolation front with random strengths between (0,1) assigned to the bonds adjoining available sites b) The bond with the smallest value is broken and the adjoining site is filled and added to the cluster. New values are assigned to the bonds adjoining nearest neighbors to the freshly invaded site c) Weakest bond again breaks adding the filled site to the cluster and assigning bond strengths connecting new nearest neighbors d) Loopless condition is enforced by removing all unbroken bonds joining two filled sites. Bond joining (0,0) and (1,0) is removed in this example.

iteration. 3) At each iteration, all new elements to S_{nn} are assigned a number from a random uniform distribution between (0,1) representing the site's strength. The list of "invadable" sites along with its strength is called the percolation front. 4) The site with the lowest strength in the percolation front is invaded and added to the list of filled sites, S_f. 5) The invaded site is removed from the percolation front ensuring it cannot be invaded multiple times. 6) The new nearest neighbor sites to the freshly filled site is added to the list of available sites, S_{nn}. 7) Repeat 3-6 until reaching the lattice boundary or until reaching the desired number of invaded sites.

Most of the computation time comes in searching the percolation front at each iteration for the weakest site. Considering that each iteration changes the percolation front at most by 3 values, as the percolation front grows the amount of change at each iteration is small, therefore searching the list each iteration becomes highly inefficient. Instead we maintain an ordered list which is simply updated with the new available sites at each iteration in their respective order. One then only needs to pick the first element of the list at each iteration. Even though we are assigning strengths to the sites we can still infer the path taken from site to site. This inferred network is similar to that created by assigning strengths to all bonds.

However, there is a key difference. Since this algorithm never advances by going from an occupied site to another occupied site, the inferred bond network will always be loopless. This is a desirable feature for us, since pressure gradients drive the fluid from filled sites to empty sites. If two neighboring sites are filled, no pressure gradient between them exists, so the bond between the sites should never be allowed to break. The bond network inferred by SIP naturally implements this physical condition.

Next, in order to simulate BIP we need only make a minor tweak to the SIP algorithm. Figure 2.1 shows an example of how BIP might proceed. If we instead assign the strengths to the sites, we see that we can largely preserve a one-to-one correspondence between a site being invaded and the bond that must have broken. However, if we look at Fig.2.1c), we see that there should be two bonds which can break and cause site (1,0) to be invaded. These bonds correspond to bonds $(0,0) \rightarrow (1,0)$ and $(1,1) \rightarrow (1,0)$ with strength 0.53

and 0.03 respectively. In SIP, since each site is only allowed to have a single value, there will only ever be one opportunity for site (1,0) to break.

To perform BIP we can still assign values to sites, but sites must be allowed to take on multiple values. Since the numbers were assigned randomly, we can randomly choose which bond broke. By doing this we can preserve one-to-one correspondence between a site being invaded and the associated bond which broke. Further, because the cluster can only grow by invading an unfilled site, we don't need to implement additional logic to ensure loops in the bond network don't arise. The bond in joining sites (0,0) and (1,0) in Fig.2.1d) will never be allowed because those sites are already filled.

Fig.2.2 shows clusters generated by the two algorithms (LSIP, LBIP) at different scales. Because the networks produced are loopless, we can apply to our clusters much of the rich theory associated with trees. This is also a convenient and insightful way to store the percolation clusters because it in many ways reflects the self-similar structure of the percolation cluster. We implement a recursive algorithm to create a tree data structure that reproduces the connectedness of the sites in our percolation clusters. Not only is this a natural way to represent our clusters but it allows one to quickly traverse the various paths through the cluster, which is key since traditional path finding algorithms can be more computationally expensive than creating the entire cluster. With a tree structure and a recursive path finding algorithm we can efficiently extract the path characterization to further characterize the network of our algorithms.

We also utilize the tree structure in defining and characterizing our avalanche burst model. We discuss this in more detail in section IV, but quickly, our burst model defines a burst to be all connected sites which sequentially break below some threshold strength. Since we can produce different burst statistics by changing the threshold while using the same tree, we can more efficiently characterize the effects of our burst model. By changing the burst threshold we merely change how the root tree is broken down into sets of subtrees where each subtree represents a burst. This takes less time than creating a cluster grown by bursts with a particular threshold each time to generate burst statistics for a different thresholds.

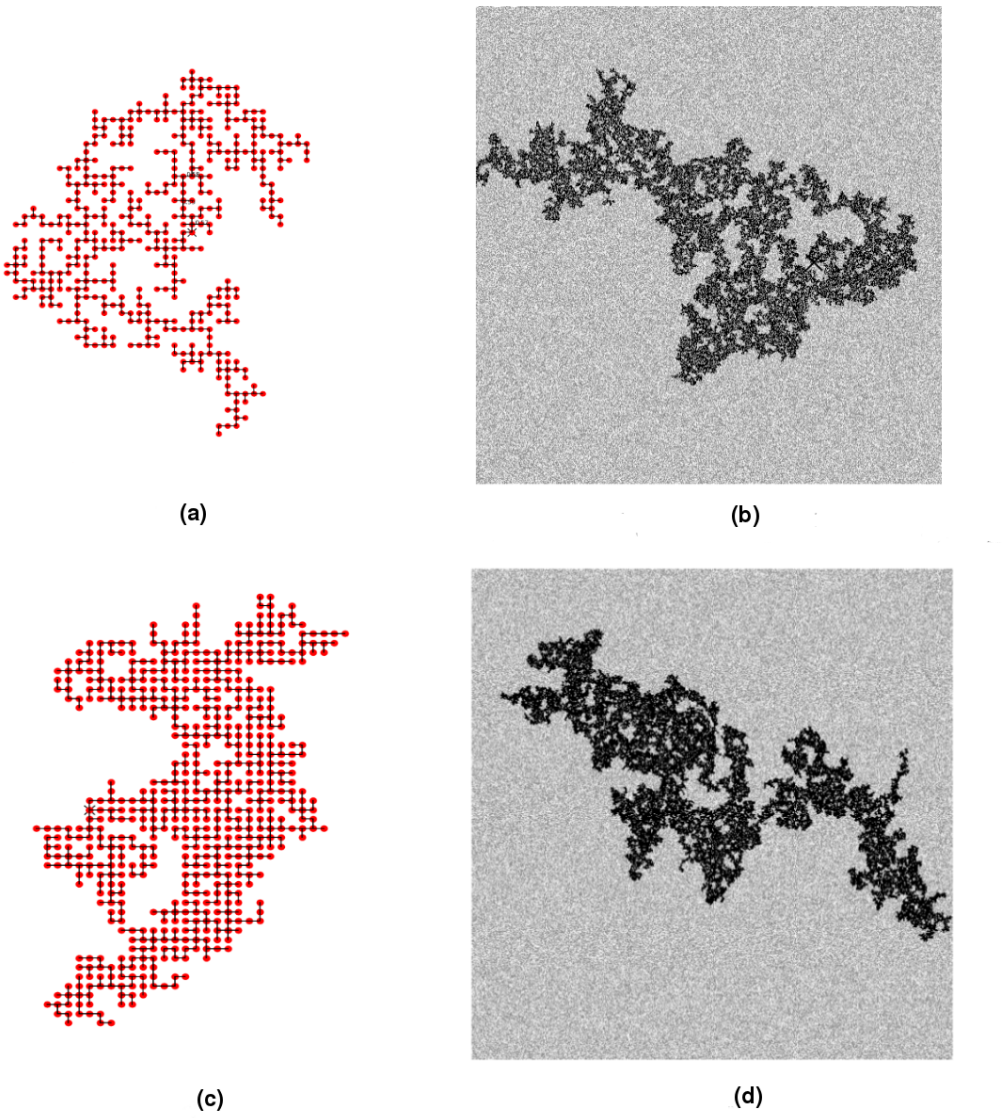

Figure 2.2. Examples of LSIP (top) and LBIP (bottom) at different scales. On the left is an example of a lattice size of $\sim$ 50x50 and the right is 2000x2000. LBIP seems to be much more compact on smaller scales, but this difference becomes less noticeable at larger scales.

2.3 Network Characterization

Following traditional percolation theory we characterize networks through various scaling relations. Initially, It was argued that the scaling relations would be insensitive to whether or not one simulated bond or site percolation [15], and thus they would fall under the same universality class. More recent work has called this into question [19].

In this work, we highlight the difference between BIP and SIP and the changes one must make to SIP to reproduce BIP. In effect, it supports the more recent work finding differences in the scaling relations between the two and suggests they should belong to different universality classes. From Fig.2.2 we can see a clear difference in site occupation density between LSIP and LBIP. self-similarity and scale-invariance suggests these difference should exist on all scales (ignoring finite size effects). Still, the significance of universality classes is somewhat undermined because even if they did belong to the same universality classes, the universality would be broken depending on whether or not an IP model is trapping or non-trapping. Much of the literature focuses on two phase dynamics (the displacement of one fluid by another) which makes the trapping variety more appropriate. We focus on the invasion of a fluid into an empty lattice, so we opt for the less common non-trapping variety.

The first and perhaps most important scaling relation is the fractal dimension of the network. If the number of filled sites represents the mass of a cluster then its mass should scale according to the following relation:

$$M\left(L\right) \sim L^{D_f} \tag{2.1}$$

Where D_f is called the fractional or fractal dimension. There are multiple techniques for determining the fractal dimension of the sample spanning cluster (SSC). The standard approach in the literature relies on counting the number of sites within circles of increasing radii with a fixed center [24]. Norris et. al. [20] relied on a similar technique, but rather than randomly choosing the center of the set of circles to be random sites within the SSC, they chose the injection site to be the center and averaged the counts over many clusters (1000) with fixed mass (number of sites, m=100 million sites). These results are possibly

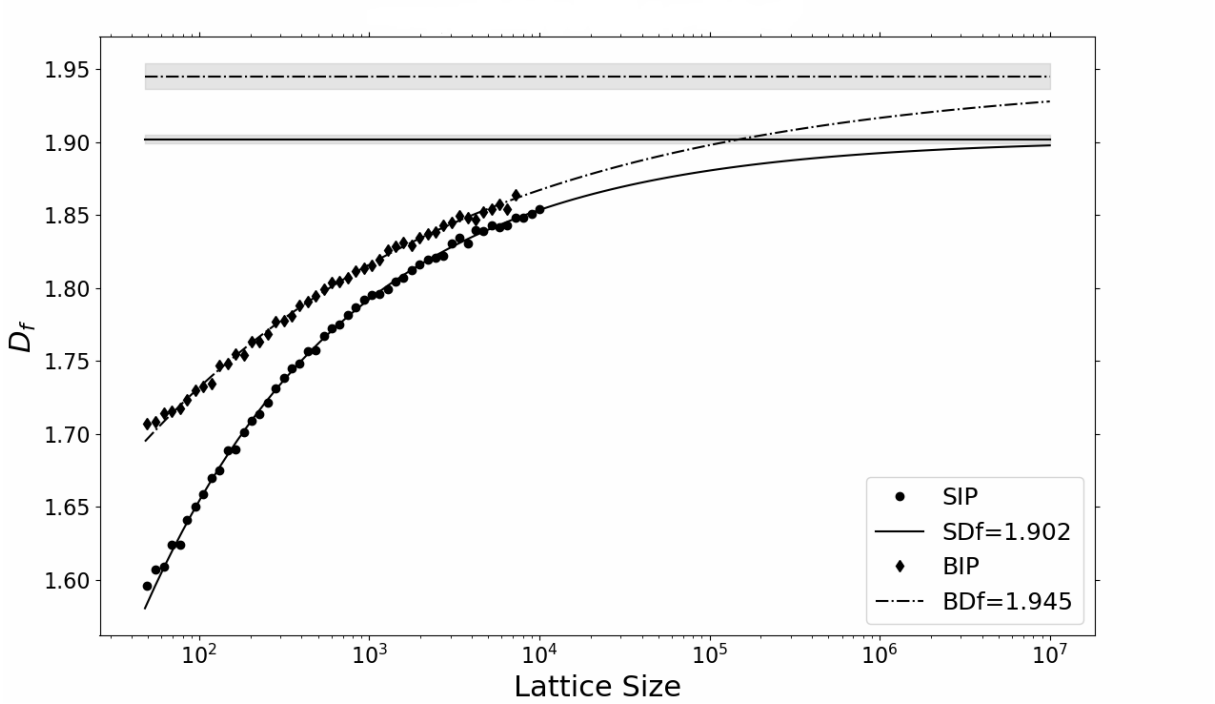

Figure 2.3. The behavior of the local fractal dimension $D_f(M)$ as defined by Eq.2.2 for LSIP (solid) and LBIP (dashdot). We compute an ensemble average $< D_f(M) >$ for lattices in the range [50,10^4] and fit the results to an exponential function via minimization of least squares. We determine the asymptote of each curve from the fit and the gray region around the asymptotes indicates the error in asymptopte fit parameter.

somewhat problematic because they do not properly factor in finite size effects. Moreover, the fractal dimension should not depend on the choice of the center (which is why [24] argued for taking an average over many choices). [25, 26] used a similar technique, but instead defined a local fractal dimension, $D_f\,(M)$ which follows from Eq.4.22

$$D_f\,(M) \equiv \frac{d\log M}{d\log L} \tag{2.2}$$

and estimate how this function approaches the asymptotic value in the infinite limit.

Since periodic boundary conditions are not implemented, and because both previous work [20] and our models take the center to be sole injection point, the fractal dimensions of the clusters are more affected by finite size issues. The effect is especially pronounced if one percolates the cluster within a lattice of fixed size rather than percolating clusters up to a set mass.

With these considerations, we used a box counting technique (more commonly used

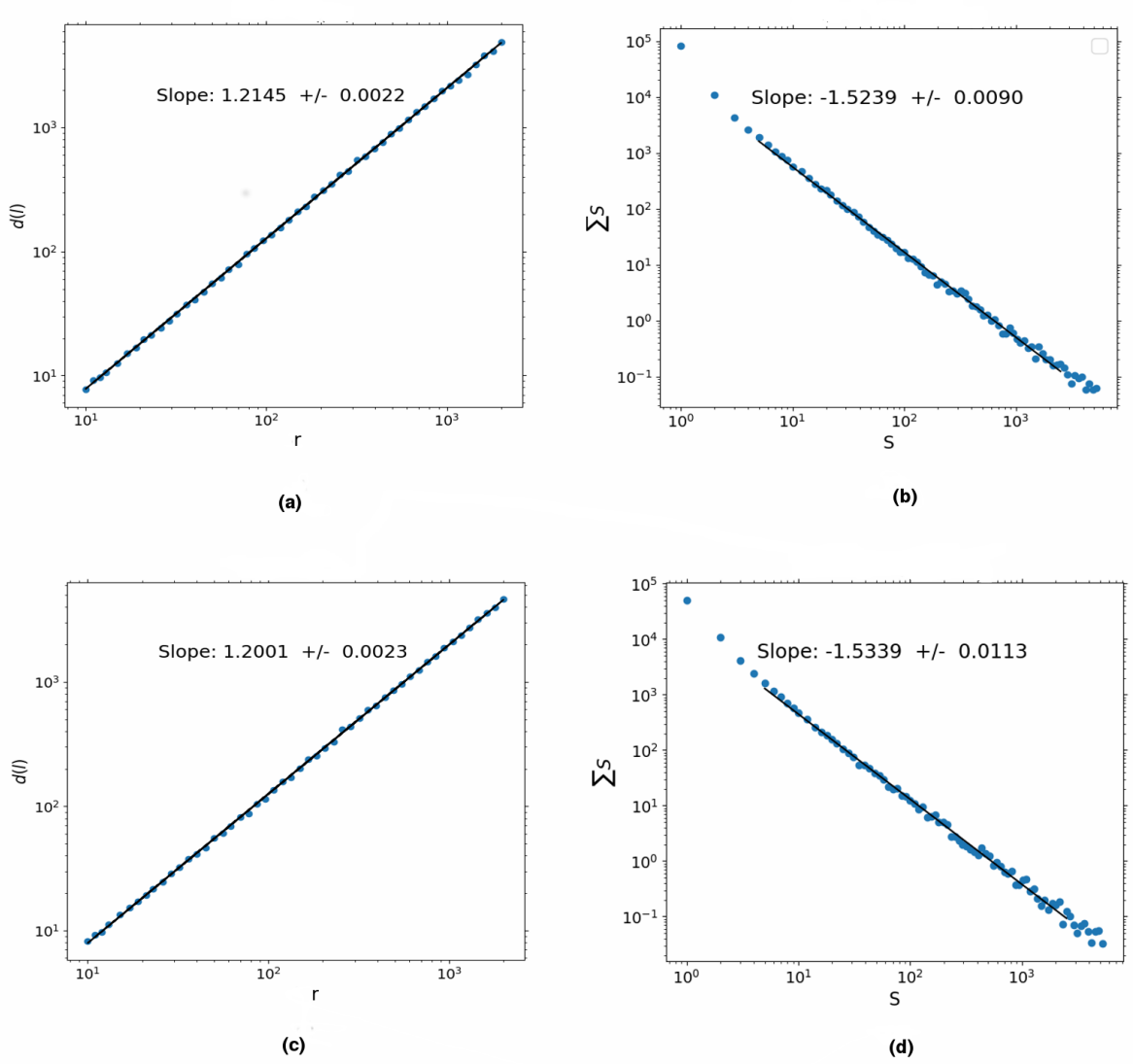

Figure 2.4. D_{min} and τ characterization for LSIP and LBIP. Plots a) and c) are a log-log plot of an ensemble average of the path distance between sites, $d(l)$, where the lattice spacing between sites is l. We averaged over 100 samples for each L in the range [10,2000]. Plots b) and d) show the burst magnitude-frequency scaling for LSIP and LBIP respectively. For each, we generated $\approx 120,000$ bursts which ranged from size 1 to $\sim 4 \times 10^3$. We binned the counts of each burst size (blue dots) using log sized bins in order to extend the fit data range. The fits were all done via minimization of least squares.

in fractal dimension studies) to determine the mass scaling, and generated clusters with fixed mass rather than fixed lattice size. Moreover, rather than a simple linear fit, we use the approach of [25, 26] to determine how the local fractal dimension approaches its asymptotic limit. Finite size scaling theory argues that at criticality the correlation length of the system becomes infinite. This means there is only one fundamental length scale to

the system. Since the mass scales with L according to some power law, the mass itself should also follow a power law. This leads to the following assertion:

$$|D - D_f(M)| \equiv M^{\omega} \tag{2.3}$$

Where local fractal dimension, $D_f \rightarrow D_f(M)$ in the infinite mass limit. If we plug Eq.4.22 into Eq.2.2 we get the following differential equation (approach asymptotic value from below):

$$\frac{d\log M}{d\log L} = -CA^{-\omega}L^{-\omega D_f} + D_f \tag{2.4}$$

The solution of which is found to be of the form:

$$\log M = \frac{c0}{\omega Df}L^{-\omega D_f} + D_f \log L + c1 \tag{2.5}$$

where $c0, c1$ are constants. If we perform a log-log plot then the first term is the non-linear correction. This can be compared to what is done in [25] which writes the scaling along with the smallest correction term:

$$\begin{aligned} \log M &= \log A + D_f \log L + \log\left(1 + aL^{-\omega}\right) \\ &\approx \log A + D_f \log L + aL^{-\omega} \end{aligned} \tag{2.6}$$

Thus, rather than fitting to a line in a log-log plot one fits to Eq.2.5 or Eq.2.6 (gave comparable results) and simultaneously finds the best D_f, ω. We found this technique to produce marginal success, but still found evidence of finite size effects. Instead, we chose to directly reproduce Eq.2.3 by extracting the local fractal dimension for lattices in a range of sizes $[50, 10^4]$ and fitting the asymptote directly. The results are shown in Figure 2.3 and Table 2.2.

In order to determine whether SIP and BIP share the same universality class, one must determine at least two of the scaling parameters. From these, all others can be determined. A common measure is the percolation backbone which is closely related to the transport properties of a sample-spanning cluster. The backbone is defined to be the subset of the cluster which has all dangling ends removed (ends not in contact with the lattice boundary). It serves as a measure of conductivity, since it is the set of paths

through the lattice if one begins on one boundary side and ends at another. The backbone is characterized by the path distance, D, of the connected sites composing the backbone, and the lattice size L which hosts the cluster according to:

$$D\left(L\right) \sim L^{D_{bb}} \tag{2.7}$$

A closely related quantity is how the distance between two arbitrary lattice points scale in terms of lattice site spacing l. This follows another power law:

$$M\left(l\right) \sim l^{D_l} \tag{2.8}$$

Where $M(l)$ is the number of sites within lattice spacing l and D_l is the chemical dimension [27]. With backbone studies one must be more careful with how boundary conditions are imposed (periodic etc.). Thus it is preferable to use D_l which is largely independent of such effects. Further, what we are really interested in is characterizing the compactness of a cluster which describes the types of paths connecting sites. We can relate the Pythagorean distance r and l as:

$$l \sim r^{D_{min}} \tag{2.9}$$

Therefore if d is the path distance from the origin to the boundary of lattice size L, then $L = nl$ and by Eq.2.9 we can write:

$$d \sim r^{D_{min}} \tag{2.10}$$

Where D_{min} is the fractal dimension of the shortest path. A peculiar effect is how diffusion slows near criticality because the sizes of the holes in the cluster become scale invariant, thus allowing holes of all sizes to form. The paths are then forced to become more circuitous. Because the (IP) process is always critical, we expect the path length to follow Eq.2.10.

To determine the path length described by Eq.2.10, we make use of the loopless condition which allows us to reorganize the cluster of connected sites into a tree. We show an example of the shortest path for LSIP in Fig.2.5. Since there only exists a single path

between two points this path trivially represents the shortest path between two points, we use recursive search routines to find paths between sites much more efficiently. We create an ensemble of clusters with lattice size L in range [10, 2000] and calculate the path length from the origin to the boundary. The results are shown in Fig.2.4 where we find $D_{min} = 1.215 \pm 0.002$ and $D_{min} = 1.200 \pm 0.002$ for LSIP and LBIP respectively.

The loopless condition simplifies the paths within our clusters since there can only be one. Absent recursive methods, path search algorithms can take more time finding paths between sites than creating the original cluster. Also, this simplification creates paths with other applications like the paths which resembles domain walls in the strong disorder limit of spin glass systems [28]. The paths also resemble Prim's algorithm for finding the shortest spanning tree of a weighted random graph. It represents the minimum energy tree spanning all vertices [29].

2.4 Burst Characterization

Physically, we think of a burst in our model as a rapid accumulation of filled sites which corresponds to a formation of sub-lattice regions having different permeability or conductivity from which the sub-lattice originates. In fracking, these would be the regions where the stress field rapidly changes and hosts the observed microseismicity. Our burst model must then follow a power law, and we also expect to reproduce similar spatial distribution of burst centers to the epicenters of earthquakes from fracking.

IP was intended to simulate the quasistatic displacement of one fluid by another through capillary forces. The networks produced simulate long time expectations of systems eventually able to achieve equilibrium. Though at each iteration a site is invaded or a bond breaks, the network characteristics are loosely coupled to these details (as we see SIP and BIP sharing nearly identical network characteristics). While there doesn't seem to be inherent time dynamics in IP models, different attempts have been made to understand or uncover inherent time dynamics Furuberg et al. [30].

These authors examined the dynamics that arise when a time step corresponds to the invasion of a single site. They found $r \sim t^{1/D}$, which we expect since here t is also the

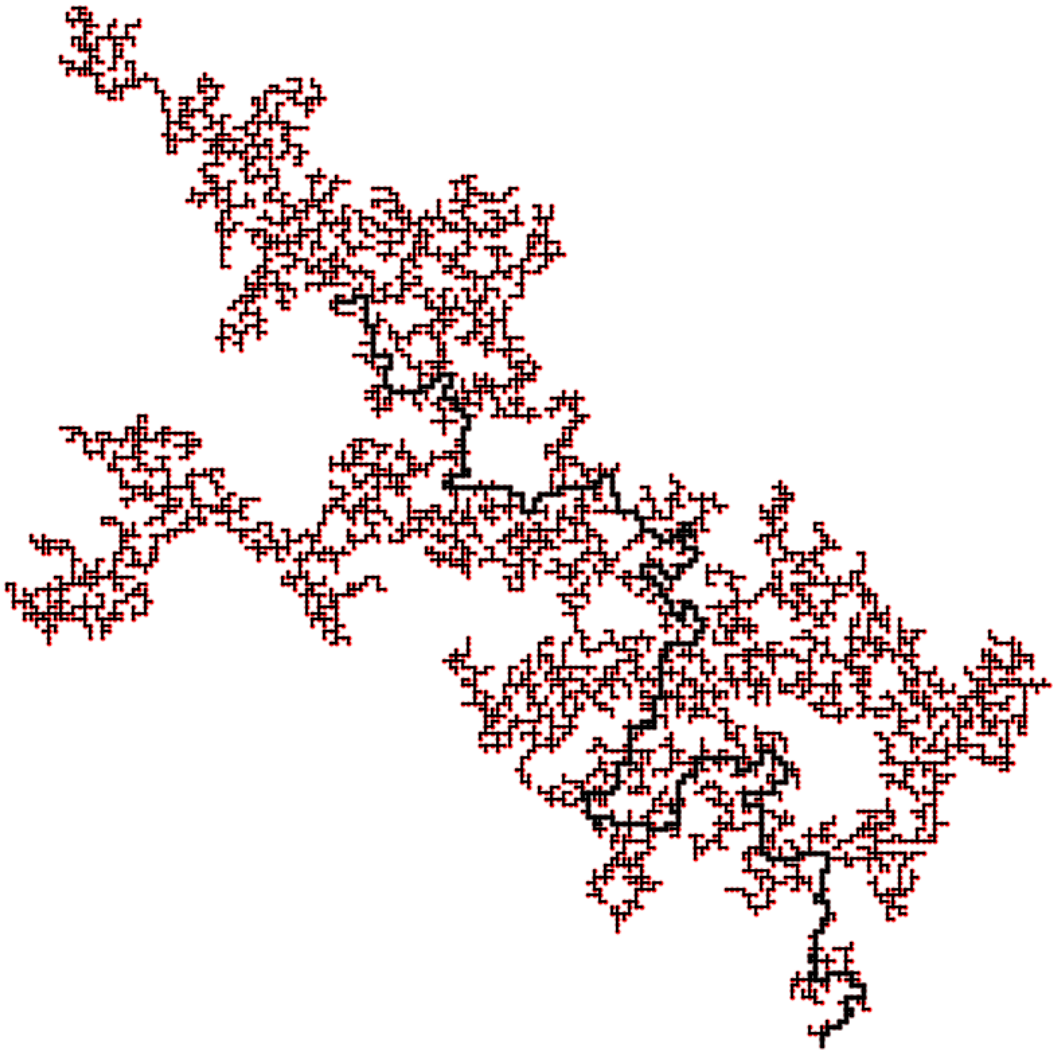

Figure 2.5. An example of a typical path (darkened line segment) produced by the LSIP algorithm. We use a recursive algorithm to find the path from the injection site to the end of cluster. The end of the cluster is defined to be the site of the lattice boundary.

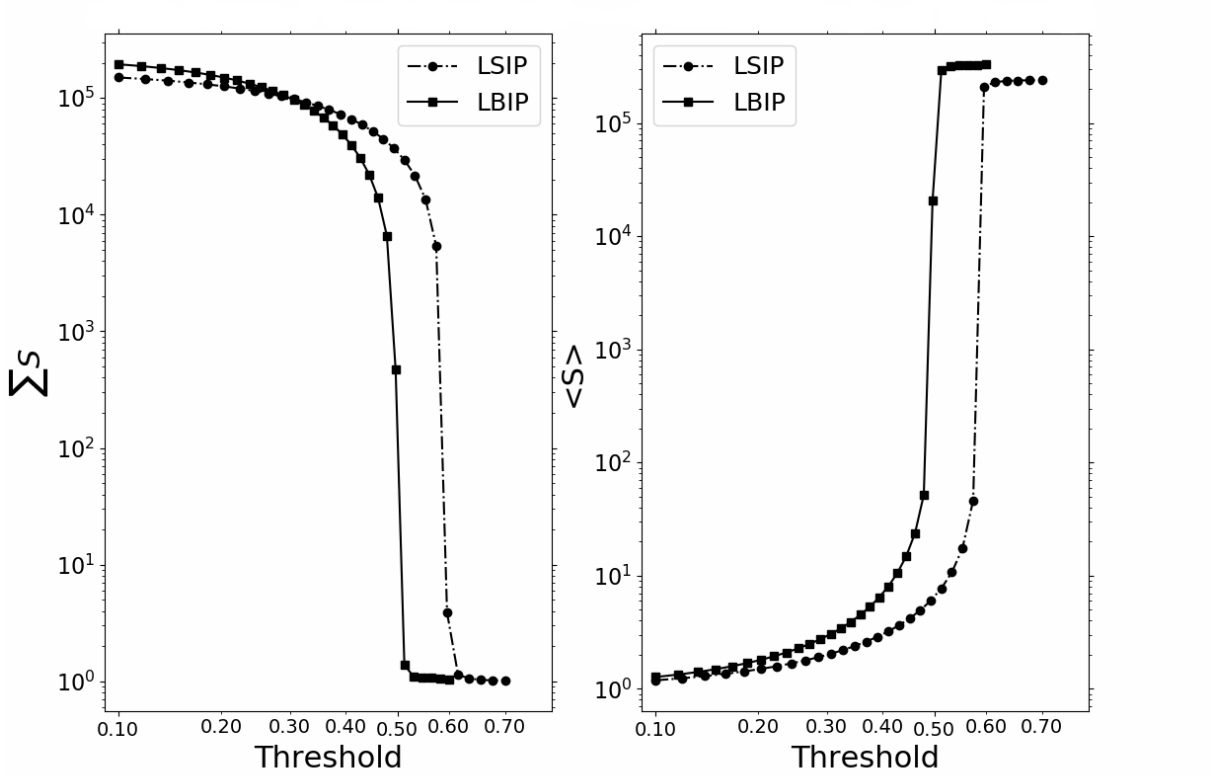

Figure 2.6. Critical behavior of LSIP and LBIP. Utilizing our notion of a burst, there exists a particular threshold where the average size of a burst, $< S >$, behaves critically for LSIP and LBIP. This value corresponds to the critical occupation probabilities, p_{crit} for BIP and SIP which are known to be 0.5 and ~ 0.592 respectively. The left plot shows how the number of bursts decreases to 1 if the threshold, $T > p_{crit}$. Similarly, the right plot shows how the average burst size, $< S >$, grows to include all sites if the threshold $T > p_{crit}$. If the threshold $T \sim p_{crit}$, then our burst magnitude frequency distribution will follow a power-law with b-value ~ 1.54.

number of invaded sites or has the equivalent interpretation as being the mass (number of invaded sites) for a cluster with size r. Here D is the fractal dimension of the SSC and in the limit where the fractal dimension ~ 2 (an SSC completely filling all sites of a lattice) we recover the results of distance traveled in a diffusion process.

If paths can only traverse filled sites, a lower fractal dimension will mean a more sparsely filled lattice which will limit potential trajectories on the lattice. The result is that we recover the path length of a random walk on typical percolation cluster. The authors took this relation to mean that at time t, most of the region within r is likely already invaded, and it is unlikely to have growth at distances larger than r. Their notion of a burst was that in time t, growth can be found to be in some distance r. Yet, it seems

	D_f	D_{min}	τ
LSIP (This Paper)	1.902 ± 0.003	$1.215 \pm .002$	$1.524 \pm .009$
LBIP (This Paper)	1.945 ± 0.009	$1.200 \pm .002$	$1.534 \pm .011$
RP [25]	$91/48 \approx 1.896$	1.13 ± 0.004	$187/91 \approx 2.05$
NTSIP [31]	1.8959 ± 0.0001	1.1307 ± 0.0004	-
TBIP (square lattice) [31]	1.822 ± 0.008	1.214 ± 0.002	-
DLA [32]	1.69 ± 0.24	1.0 ± 0.02	-

Table 2.2. A comparison of scaling exponents for loopless site invasion percolation (LSIP), loopless bond invasion percolation (LBIP), random percolation (RP), loopless random percolation (LRP), non-trapping site invasion percolation (NTSIP), trapping bond invasion percolation (TBIP), and diffusion limited aggregation (DLA)

this is merely restatement of the behavior of a random walk on a percolation cluster and does not introduce any true burst dynamics.

Much of the dynamics associated with IP has to do with the transport exponents which are mostly governed by the kinds of paths which can form through the percolating cluster. However, RP does follow a cluster size scaling law described by the Fisher exponent, τ:

$$n_s(p) = s^{-\tau} f\left[(p - p_c)\, s^{\sigma}\right] \tag{2.11}$$

where for $(p \to p_c)$, the cluster size,$n_s(p) \sim s^{-\tau}$. So, there is credence to the idea that a network can grow in bursts if IP grows its SSC by different realizations of these RP clusters.

The growth algorithm for IP is different from RP since IP will always grow indefinitely, and further exhibits a kind of self-organized criticality, since the cluster will grow by a self-organized selection of bonds strengths less than the critical probability. [33] defined a notion of a burst resulting in a power law similar to that of RP when $(p \to p_c)$. The authors showed that if we consider the sequence of broken bonds to be a signal $x(t)$ (where $x(t)$ is the bond strength broken at time t), then over some signal length $x(t+s)$, there will be a sequence of bonds broken. For all t' in range $t < t' < t$, the bond strengths broken, $x(t')$, will be $x(t) < x(t') < x(t+s)$.

The number of bonds broken in time range $(t + s)$ can be made to follow a power law if the threshold strength of $x(t)$ is chosen to be near the critical probability as was also shown by authors in [20]. That is, IP clusters will grow by a self-organized selection of bonds strengths less than the critical probability, but if the threshold is chosen to be near the critical probability, the SSC will grow in iterations of clusters similar to those of RP though with a different value for the Fisher exponent. In particular, from Figure 2.6 we see that if the threshold, $T \sim p_{crit}$, then the average burst size exhibits critical behavior. Choosing our threshold to be in this range will result in a burst-size frequency distribution that is scale invariant and reproduces a power-law.

In addition to this choice of burst threshold, we demand that our bursts be spatially connected in addition to sequentially (previous studies only demanded sequentially connected bonds/sites [20, 33]). Our bursts should only be allowed to grow from the local percolation front of a burst rather than the global percolation front from the entire cluster. Since our networks are necessarily loopless, we can utilize the tree structure to define sequentially and spatially connected bursts in a very natural way.

Again, the critical aspect of a burst is that it should fill up a certain portion of a lattice until it exhausts all the easiest bonds. Once a strong bond is forced to break, a new region of weak bonds should become available, allowing a quick succession of bonds to break. The successive breaking of weaker bonds below a threshold defines a burst. Again, because a percolation cluster has no intrinsic time dynamics, we are free to retroactively say how the tree grew and that it in fact grew in bursts.

Figure 2.7 shows how a cluster can be divided into different colored subtrees where each subtree is made to corresponds to a burst. The tree structure advantage is that one can define a burst to be its own subtree which connects at only 1 point to the original tree. The process of determining bursts becomes a process of cutting a single tree cluster into a collection of subtrees, all of which are connected to each other through only 1 node (i.e., a similar connectedness criteria as before).

To define a burst we then traverse the tree from the origin until we exhaust all bonds less than the threshold strength; we cut the tree at this point, and define this cut point

to be the root node of the subsequent tree. The process continues again traversing all the nodes weaker than the threshold strength. A similar mechanism is used to explain the opening of bronchial airways in lungs [34]. We note that generalized avalanche models on trees also follow power-laws [35].

2.5 Results

Detailed studies of fluid injection into a porous medium on the pore scale reveals very complex behavior. This is largely the result of porous medium morphology being itself highly disordered and random [36]. Therefore a statistical characterization seems appropriate and it is this characterization these (invasion) percolation models aim to reproduce. Within percolation theory we can model fluid displacement as two different processes. The process by which a fluid is drawn into a network of pores is imbibition, whereas a non-wetting fluid forced into porous volume is drainage. We model these as SIP and BIP respectively, and it is our primary interest to determine if HF is better described by one of these processes. In doing so, we might gain insight into the appropriate physics at the individual pore scale. Otherwise, it demonstrates our sensitivity to the dynamics at different scales.

Since the scaling exponents which characterize the universality class are the same as those used to constrain our model via observed microseimicity, a closely related question is whether SIP and BIP share the same universality class. While we find small differences between the two models which does suggest unique universality classes, the differences are sufficiently small to suggest that we don't have sensitivity in data to distinguish between the two. Table 2.2 shows our values along with their observed error.

There seem to be many conflicting values for the scaling exponents in the literature. We believe a major reason for this is inadequate treatment of finite size effects. Even large lattices with large SSC's with 10^7 sites can have significant finite size effects (as seen in Figure 2.3 where a lattice size of 10^4 has $\sim 10^7$ sites). We find evidence that in the limit of infinite lattice size, the fractal dimension of SIP approaches the expected value of RP.

For BIP, which seems to be more compact than SIP at all lengths scales approaches

a value of $D_f = 1.945 \pm .009$. This value is different from SIP, which has value $D_f = 1.902 \pm .003$. Figure 2.3 very clearly shows how the "local" fractal dimension can change as a result of the lattice size.

We find that because LBIP is more compact, there is a small difference in the value of D_{min} as described by Eq.2.10. The fractional dimension D_{min} was found to be, $D_{min} = 1.215 \pm .002$ and $D_{min} = 1.200 \pm .002$ for LSIP and LBIP respectively. Results from the literature for D_{min} are: 1.2138 [20], 1.2 ± 0.02 [29], 1.22 ± 0.01 [28], 1.23 ± 0.02 [37], and 1.214 ± 0.001 [38]. Regular percolation gives $D_{min} = 1.13$ and a random walk has $D = 1.19$.

Using our model of bursts near criticality and our simulated fracture network we can produce a representation of the expected microseismicity within a region. We compare to the magnitude-frequency distribution correlated with fracking microseismicity to test our models. We find that despite small differences in their other scaling exponents, our models produce the same magnitude-frequency distribution with their respective errors ($\tau = 1.5240.009$, $\tau = 1.530.01$ for LSIP and LBIP respectively).

However, these values are compatible with those observed during induced seismicity and are significantly different from the b-value of typical tectonic earthquakes. In order to account for the variability of b-values associated with induced microseisimicity we find that for thresholds $T < p_c$, we can produce burst statistics which prefer smaller earthquakes, suggesting that induced microseismicity may not be characterized by critical phenomena unlike tectonic seismicity which is known to be critical [17].

In order to maintain generality we emphasized maintaining model simplicity. Further, because we believe most of the observed HF seismicity is the result of critical phenomena, only a subset of system behavior becomes relevant. This subset being the nature of the inherent randomness and how it grows to all scales of the system. Our statistical approach means we avoided introducing much of the local environment conditions which have a large affect on individual realizations of induced miscroseismicity. Most notably the spatial distribution of the epicenters of earthquakes seem to depend on the local stress field and fracture network. This produces seismicity which uniquely clusters in

some regions and is rather isotropic in others.

This study shows that this approach can reasonably reproduce HF seismicity's essential statistics, and serves to illustrate the sensitivity to small scale physics one can hope for with such an approach.

Our models produce isotropic spatial distribution of bursts and can therefore only account for some of the observed features. It is known that pore sizes within rocks are not independent and random but rather exhibit correlations. Since we are insensitive to distinctions between pore/bond dynamics, by introducing correlations in pore sizes, we should be able to more accurately describe fracture networks and better account for the variations of induced microseismicity. This will be the subject of future work.

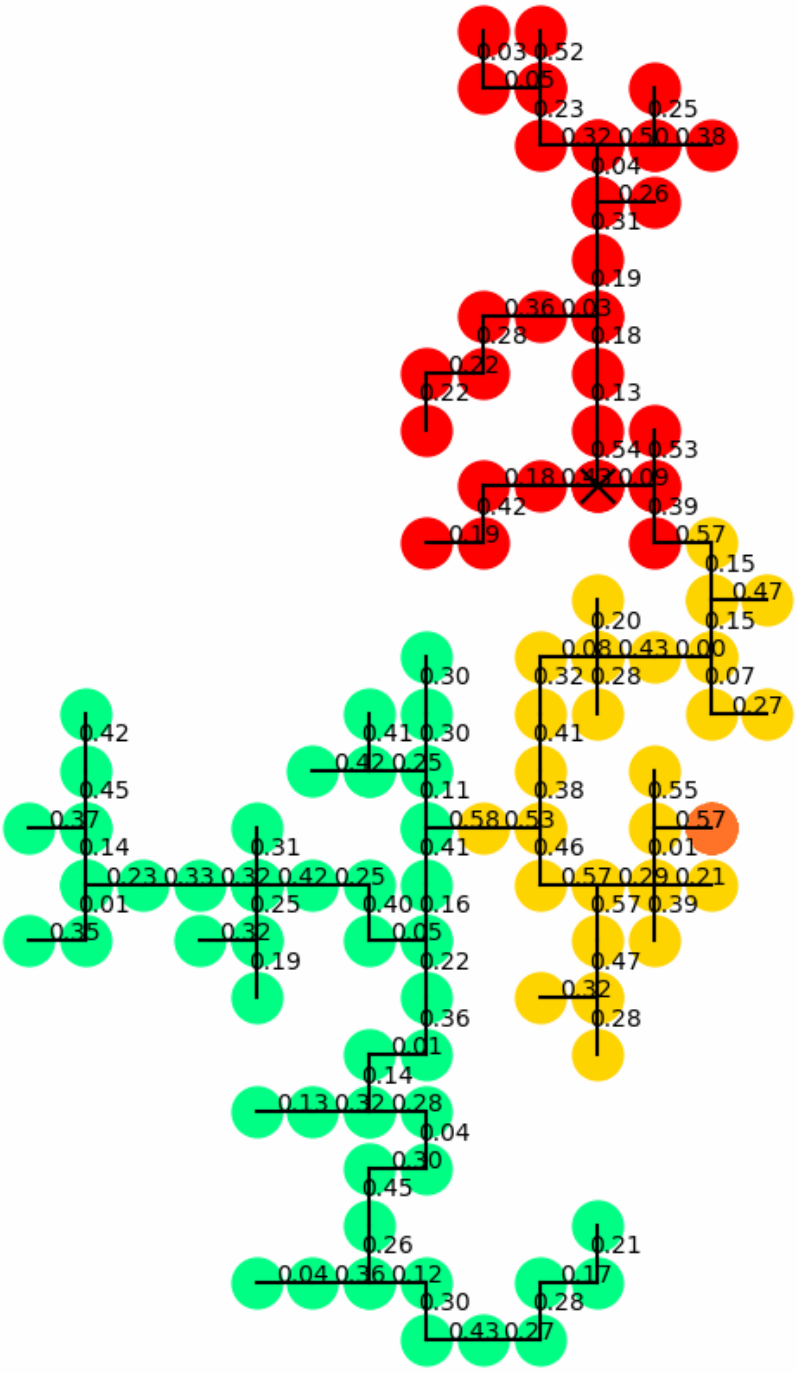

Figure 2.7. Avalanche tree burst example for SIP with a burst threshold set to be $T = 0.57$ near $p_c = 0.59$. Each burst is shown by a different color, where the injection site is marked by 'x' in the red burst and migrated to the yellow, blue, and green. The bond strengths are shown to illustrate all the sequence of connected bonds with strength less than T belong to the same burst.

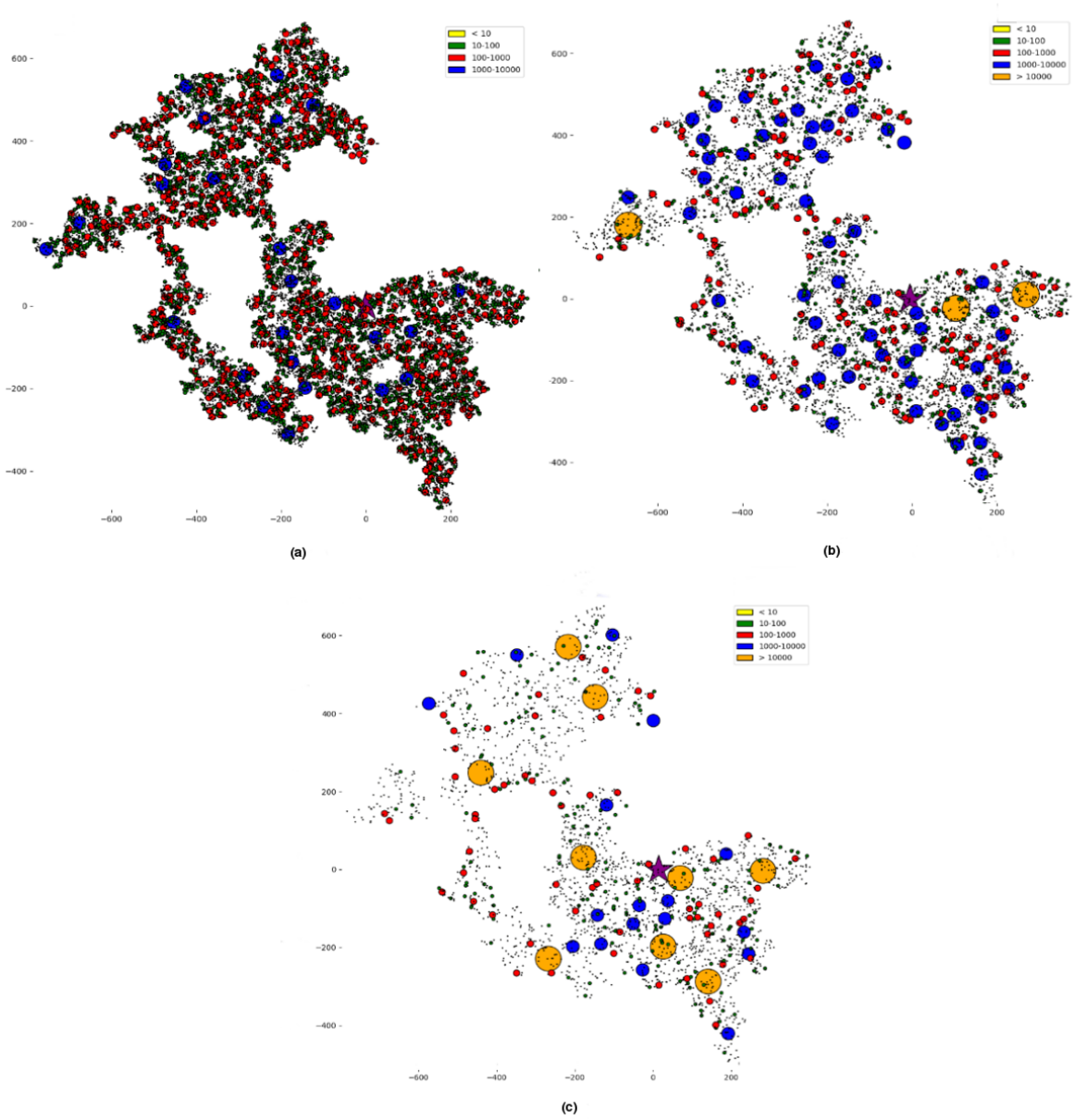

Figure 2.8. An example of a SSC containing 300,000 bonds broken into its separate bursts according to the burst threshold. The bursts are shown where each burst is drawn as a circle with size proportional to the number of broken bonds and the bursts' locations are determined by the bursts' center of masses. The plots (a),(b), and (c) are a comparison of how the burst size distribution changes as the burst threshold changes ($T = [0.45, 0.48, 0.49]$) respectively and approaches the critical probability, $p_{crit} = 0.5$. The sizes of the bursts tend to a power law distribution as the threshold tends to the critical probability. The purple star indicates the injection site of the entire cluster.

References

[1] D. Wilkinson and J. F. Willemsen, "Invasion percolation: a new form of percolation theory," *Journal of Physics A: Mathematical and General*, vol. 16, no. 14, p. 3365, 1983.

[2] C. P. Stark, "An invasion percolation model of drainage network evolution," *Nature*, vol. 352, no. 6334, p. 423, 1991.

[3] J. T. Clemmer and M. O. Robbins, "Anisotropic avalanches and critical depinning of three-dimensional magnetic domain walls," *Phys. Rev. E*, vol. 100, p. 042121, Oct 2019.

[4] J. P. Stokes, A. P. Kushnick, and M. O. Robbins, "Interface dynamics in porous media: A random-field description," *Phys. Rev. Lett.*, vol. 60, pp. 1386–1389, Apr 1988.

[5] K. J. Måløy, S. Santucci, J. Schmittbuhl, and R. Toussaint, "Local waiting time fluctuations along a randomly pinned crack front," *Phys. Rev. Lett.*, vol. 96, p. 045501, Jan 2006.

[6] S. Maxwell, "Microseismic hydraulic fracture imaging: The path toward optimizing shale gas production," *The Leading Edge*, vol. 30, no. 3, pp. 340–346, 2011.

[7] F. Ebrahimi, "Invasion percolation: A computational algorithm for complex phenomena," *Computing in Science & Engineering*, vol. 12, no. 2, pp. 84–93, 2010.

[8] M. M. Scuderi and C. Collettini, "The role of fluid pressure in induced vs. triggered seismicity: Insights from rock deformation experiments on carbonates," *Scientific reports*, vol. 6, p. 24852, 2016.

[9] M. Scuderi, C. Collettini, and C. Marone, "Frictional stability and earthquake triggering during fluid pressure stimulation of an experimental fault," *Earth and Planetary Science Letters*, vol. 477, pp. 84–96, 2017.

[10] M. Sahimi, M. C. Robertson, and C. G. Sammis, "Fractal distribution of earthquake hypocenters and its relation to fault patterns and percolation," *Physical review letters*, vol. 70, no. 14, p. 2186, 1993.

[11] J. B. Rundle, "Derivation of the complete Gutenberg-Richter magnitude-frequency relation using the principle of scale invariance," *Journal of Geophysical Research: Solid Earth*, vol. 94, no. B9, pp. 12337–12342, 1989.

[12] B. E. Shaw, "Generalized Omori law for aftershocks and foreshocks from a simple dynamics," *Geophysical research letters*, vol. 20, no. 10, pp. 907–910, 1993.

[13] Y. Y. Kagan, "Earthquake spatial distribution: the correlation dimension," *Geophysical Journal International*, vol. 168, no. 3, pp. 1175–1194, 2007.

[14] J. Henderson, D. Barton, and G. Foulger, "Fractal clustering of induced seismicity in the geysers geothermal area, california," *Geophysical Journal International*, vol. 139, no. 2, pp. 317–324, 1999.

[15] R. Chandler, J. Koplik, K. Lerman, and J. F. Willemsen, "Capillary displacement and percolation in porous media," *Journal of Fluid Mechanics*, vol. 119, pp. 249–267, 1982.

[16] K. Aki, "A probabilistic synthesis of precursory phenomena," *Earthquake prediction: an international review*, vol. 4, pp. 566–574, 1981.

[17] J. B. Rundle, R. Ortez, J. Kønigslieb, and D. L. Turcotte, "Constrained invasion percolation model: Growth via leath bursts and the origin of seismic b-value," *Physical Review Letters*, vol. 124, no. 6, p. 068501, 2020.

[18] M. Luginbuhl, J. B. Rundle, A. Hawkins, and D. L. Turcotte, "Nowcasting earthquakes: A comparison of induced earthquakes in Oklahoma and at The Geysers, California," *Pure and Applied Geophysics*, vol. 175, no. 1, pp. 49–65, 2018.

[19] M. Sahimi, M. Hashemi, and J. Ghassemzadeh, "Site-bond invasion percolation with fluid trapping," *Physica A: Statistical Mechanics and its Applications*, vol. 260, no. 3-4, pp. 231–243, 1998.

[20] J. Q. Norris, D. L. Turcotte, and J. B. Rundle, "Loopless nontrapping invasion-percolation model for fracking," *Physical Review E*, vol. 89, no. 2, p. 022119, 2014.

[21] A. KANTZAS and I. CHATZIS, "Network simulation of relative permeability curves using a bond correlated-site percolation model of pore structure," *Chemical engineering communications*, vol. 69, no. 1, pp. 191–214, 1988.

[22] M. Porto, S. Havlin, S. Schwarzer, and A. Bunde, "Optimal path in strong disorder and shortest path in invasion percolation with trapping," *Physical review letters*, vol. 79, no. 21, p. 4060, 1997.

[23] H. E. Stanley, *Introduction to phase transition and critical phenomena*. Oxford University Press, 1971.

[24] S. Havlin and A. Bunde, *Fractals in science*. Springer-Verlag, 1994.

[25] D. Stauffer and A. Aharony, *Introduction to Percolation Theory.(2nd edn), 1992*. London, Taylor and Francis., 1994.

[26] M. A. Knackstedt, M. Sahimi, and A. P. Sheppard, "Invasion percolation with long-range correlations: First-order phase transition and nonuniversal scaling properties," *Physical Review E*, vol. 61, no. 5, p. 4920, 2000.

[27] S. Havlin and R. Nossal, "Topological properties of percolation clusters," *Journal of Physics A: Mathematical and General*, vol. 17, no. 8, p. L427, 1984.

[28] M. Cieplak, A. Maritan, and J. R. Banavar, "Optimal paths and domain walls in the strong disorder limit," *Physical review letters*, vol. 72, no. 15, p. 2320, 1994.

[29] A.-L. Barabási, "Invasion percolation and global optimization," *Physical review letters*, vol. 76, no. 20, p. 3750, 1996.

[30] L. Furuberg, J. Feder, A. Aharony, and T. Jøssang, "Dynamics of invasion percolation," *Physical review letters*, vol. 61, no. 18, p. 2117, 1988.

[31] M. A. Knackstedt, M. Sahimi, and A. P. Sheppard, "Nonuniversality of invasion percolation in two-dimensional systems," *Physical Review E*, vol. 65, no. 3, p. 035101, 2002.

[32] P. Meakin, I. Majid, S. Havlin, and H. E. Stanley, "Topological properties of diffusion limited aggregation and cluster-cluster aggregation," *Journal of Physics A: Mathematical and General*, vol. 17, no. 18, p. L975, 1984.

[33] S. Roux and E. Guyon, "Temporal development of invasion percolation," *Journal of Physics A: Mathematical and General*, vol. 22, no. 17, p. 3693, 1989.

[34] B. Suki, A. Barabasi, Z. Hantos, F. Petak, and H. Stanley, "Avalanches and power-law behaviour in lung inflation," *Nature*, vol. 368, pp. 615–618, 1994.

[35] L. P. Kadanoff, S. R. Nagel, L. Wu, and S.-m. Zhou, "Scaling and universality in avalanches," *Physical Review A*, vol. 39, no. 12, p. 6524, 1989.

[36] M. Sahimi, *Flow and transport in porous media and fractured rock: from classical methods to modern approaches*. John Wiley & Sons, 2011.

[37] J. Mastorakos and P. Argyrakis, "Transport on the percolation backbone," *Physical Review E*, vol. 48, no. 6, p. 4847, 1993.

[38] A. P. Sheppard, M. A. Knackstedt, W. V. Pinczewski, and M. Sahimi, "Invasion percolation: new algorithms and universality classes," *Journal of Physics A: Mathematical and General*, vol. 32, no. 49, p. L521, 1999.

Chapter 3

Critical Description of the Avalanche Burst Invasion Percolation Model

Summary

Given the large variety and number of systems displaying scale invariant characteristics, it is becoming increasingly important to understand their fundamental and universal elements. Much work has attempted to apply second order phase transition mechanics due to the emergent scale invariance at the critical point. However, for many systems notions of phases and critical points are both artificial and cumbersome. We characterize the critical features of the avalanche burst invasion percolation (AIP) model since it exists as hybrid critical system (of which many self-organized critical systems may fall under). We find behavior strongly representative of critical systems, namely, from the presence of a critical Fisher type distribution, $n_s(\tau, \sigma)$, but we find other essential features absent such as an order parameter and to a lesser degree hyperscaling. This suggests that we do not need a full phase transition description in order to observe scale invariant behavior, and provides a pathway for more suitable descriptions.

3.1 Introduction

With the advent of complexity sciences there has been a steady discovery of systems which display behavior characterized by power-law (fractional) statistics. Such systems fall broadly under the umbrella of fractal, chaos, and critical theory with many interest-

ing links spanning these systems. As a cornerstone example, many authors have noted in classical, tectonic seismicity, essentially all of the statistical properties are described by a power-law relations: magnitude frequency distribution (G-R magnitude scale) [1], temporal aftershock clustering (Omori aftershock law) [2], and the two-point correlation distribution [3]. Similarly, induced seismicity also follows these statistical measures where in hydraulic fracturing [4] and geothermal injection [5] studies show power-laws describing both the magnitude-frequency distribution and two-point correlation function. Coupled with fractal fault and fracture properties, seismicity offers a plethora of tantalizing critical characteristics.

One of the key insights from the study of critical theory and second order phase transitions is that systems described by power-laws manifest a particular symmetry known as scale invariance. Scale invariance suggests that there is no fundamental scale associated with the system. In many cases, this is observed to correspond to a self-similarity across many different length scales, and an essential question is how these properties might arise naturally and in all their varied forms. In second order phase transitions, scale-invariance emerges when behavior becomes dominated by the inherent random fluctuations which are allowed to grow to all scales of the system [6]. This boundary between the order, dictated by the small scale physics governing the properties of distinct phases, and the emergence of critical fluctuations, is precisely described by critical theory. Fundamentally, this transition is stated as the finite scaling hypothesis which posits that the divergence of the systems correlation length is the mechanism by which realizations of critical fluctuations are allowed to grow to any accessible scale [7].

As a consequence, notions of universality emerged to form distinct universality classes. Universality classes, which describe power-law statistics shared by many distinct systems, arise because much of the small-scale physics which dominates behavior leading to the distinct phases fails to renormalize to all scales, leaving only the scaling of inherent fluctuations to dominate the observable properties. These insights applied to complex systems nurtured a general approach and led to a tremendous amount of work in the last 50 years.

It is with this perspective we formulate the approach which can address whether

seismicity, and in particular induced seismicity, is appropriately described as a critical transition. Because many distinct systems were found to share universality classes, notions of universality classes and isomorphisms between different critical systems found strong foundations. In particular, it was found that the thermal second order phase transition of the 2D Ising model could be mapped to the much simpler percolation problem [8–11]. Percolation theory, being the simplest example of a fully featured critical theory, provided the basis for understanding the essential elements which served to define distinct universality classes. As variations to percolation served to define distinct universality classes, authors naturally sought to find the corresponding physical systems matching the behavior.

Perhaps equally important, much of critical behavior can be neatly represented by the critical clusters describing the system's emergent connectivity near the critical point. This can be nicely represented by Fisher's formulation of cluster size distribution [12] parameterized by two exponents, σ, τ

$$n_s(T) = s^{-\tau} f\left[(T - T_c)\, s^{\sigma}\right] \tag{3.1}$$

The existence and characterization of such a quantity is a good starting point in describing the critical behavior that exists in a system.

Wilkinson proposed IP as a more dynamic variant to RP aimed at describing the invasion of fluid within a sediment guided by the path corresponding to that of least resistance through the sediment [13]. This model deviates fundamentally from RP, since it only describes a growth mechanism that "self-organizes" to produce a scale invariant cluster. Many aspects of IP have been studied, including various fractal dimensions [14, 15], its cluster characteristics [16], and the effects of long-range correlations [17], and its dynamics in correlated porous media [18].

The central aim of this paper is an attempt to understand how critical theory manifests itself in IP (and since IP is a prime example of self-organized criticality (SOC), perhaps SOC at large). IP is in most cases naturally taken to be a critical theory, since it produces an infinite cluster that is fully self-similar and is suitably characterized by an array of fractal functions. However, without a proper description of a cluster distribution, it

becomes difficult to rightly place IP with critical system landscape borne from the study of percolation systems.

Additionally, central to any critical theory must be the study of critical fluctuations and their scaling behavior. Therefore, in addition to the description of the cluster distribution, one must also define some notion of distinct order parameter fluctuations to IP and seek to understand their scaling behavior.

In hopes of establishing a natural notion of cluster distribution suitable to IP, authors have, for example, used the Leath algorithm to simulate independent realizations of SSC clusters to extract a Fisher like τ exponent for IP [19]. A distribution of independent cluster realizations provides limited insights into critical behavior of percolation. Briefly, such descriptions are not properly described by Fisher's relation, Eq.3.1, since it leads only to a τ exponent and not a σ as well. Here, we pursue a more interesting notion presented as an avalanche burst scheme described in a previous paper [20], which we define as avalanche-burst invasion percolation (AIP).

We introduced the notion of a connected burst defined as the sequential invasion of sites/bonds below some threshold strength, and found that there existed a critical threshold value which produced a scale invariant burst distribution leading to a description of τ. This burst threshold effectively serves as a control parameter which produces scale invariant bursts near its critical value and sub-critical bursts away from it. As a result, we observe the existence of a cutoff cluster characterizing the σ dependence.

Thus, the addition of burst dynamics allows one to simulate the burst nature of high pressure gradients induced seismicity, and provide a cluster distribution consistent with Fisher's description given by Eq.3.4. With this approach the key questions then become: which model of randomness is appropriate for the induced seismicity, and by which method do the fluctuations grow to all scales? Following the typical procedure of trying to find an appropriate critical model with similar fractional statistics, we proceed in identifying the family of power-laws with characteristic critical exponents to which AIP belongs.

3.2 Boundary Conditions

In a previous study, we characterized some of the essential network properties of our AIP model [20]. In this study, we utilized free edge boundary (FEB) conditions along both growth axes, and achieved the infinite lattice limit by extrapolating the finite size scaling (FSS) of the exponents to the infinite limit. This is important because the exponents defining particular universality classes are taken to be in the infinite lattice size limit. Additionally, other authors found that not only did hyperscaling and FSS break down above the critical dimension but universality did too, and concluded that the finite-size behavior seemed to depend strongly on boundary conditions. In particular, free boundaries appeared to deliver different results from periodic boundaries[21]. Preserving FEB conditions requires extrapolating to the infinite lattice limit, and becomes cumbersome to perform for every exponent (and more so for some quantities than for others).

Alternatively, because scale invariance is more manifest with periodic boundary (PBC) conditions, it reduces finite size corrections required to obtain infinite size limits for many of the system's scaling exponents [22]. For this reason and because we sought to characterize many more of the scaling exponents (critical exponents in particular) we chose to implement periodic boundary conditions similar to [23] in this study.

One of the primary challenges with implementing PBC conditions is coming up with a suitable stop condition. Most implementations of IP preserve some free edge to trigger a stop condition and make the others periodic [13, 16, 24, 25], but we chose to implement fully periodic boundaries following an implementation similar to [26]. Since we do not have a free edge to serve as a cutoff, we had to determine a suitable stopping condition otherwise the network would become maximally compact.

The infinite lattice limit is one where the power-law scaling exponent is expected to hold on all scales of the system, and because IP is isotropic, we expect the network to be manifestly self-similar. Thus, we manufactured the stop condition towards this end by tracking cluster growth from the initial central seed towards and around a boundary. Once the cluster reaches a boundary, we create artificial labels differentiating cluster growth along opposite boundaries. For example, if the central cluster first reached the

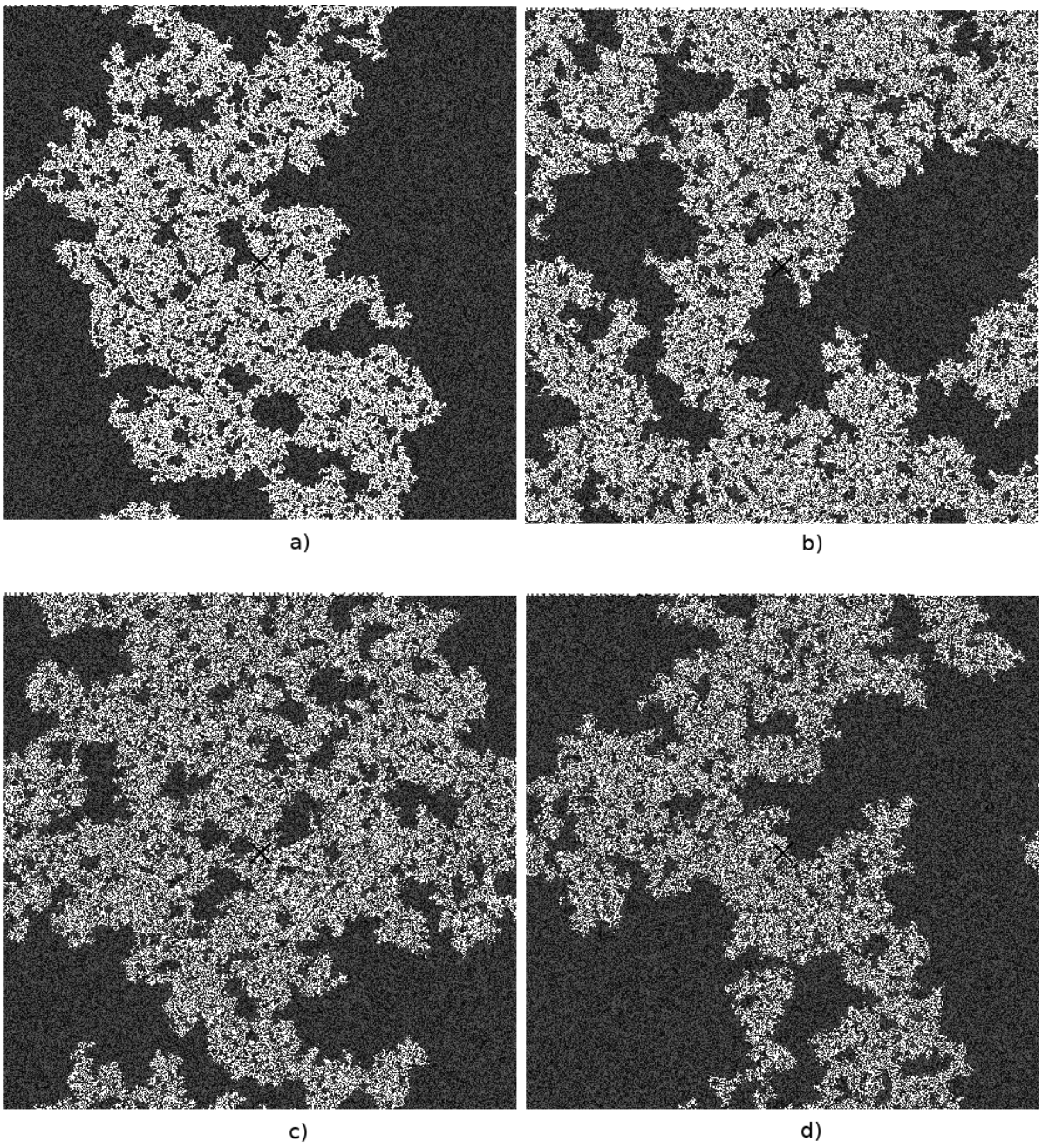

Figure 3.1. SIP algorithm with periodic boundary conditions (PBC)with four different lattice sizes corresponding to: a)500x500 b)1000x1000 c)5000x5000 d)10000x10000.

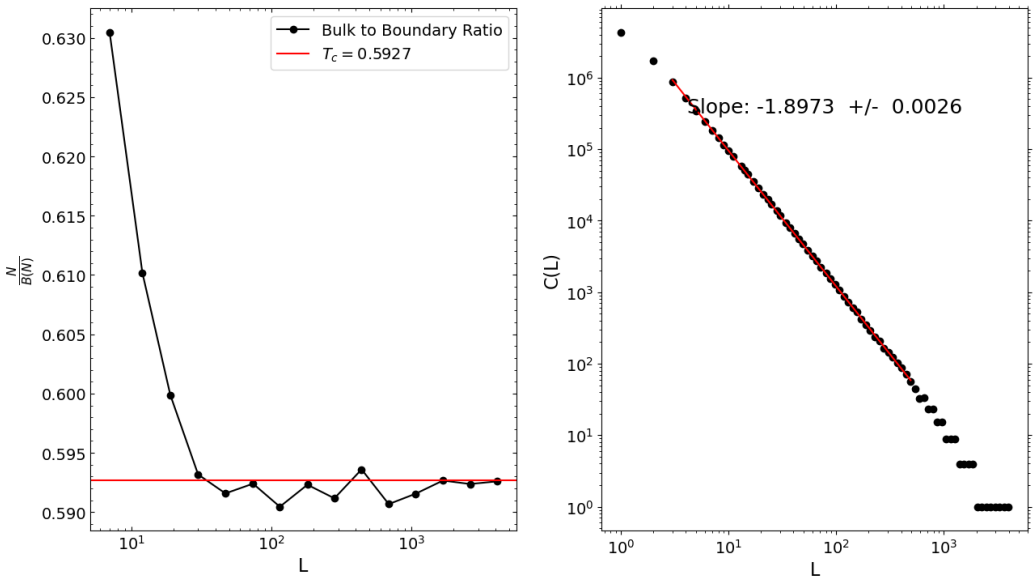

Figure 3.2. SIP algorithm with periodic boundary conditions (PBC). (Left) We show the bulk to boundary ratio of the invaded cluster as a function lattice size. This macroscopic geometric measure quickly approaches its critical value as lattice size increases. (Right) We compute fractal scaling exponent, D_f, using the boxing counting technique for clusters grown in a 4096x4096 lattice.

left boundary, then it now belongs to the left boundary cluster and is distinguished from sites growing from the right lattice boundary; these sites belong to the right boundary cluster. A stop condition is met when opposite boundary clusters share a perimeter site. The central cluster can belong to multiple boundary clusters and therefore activate multiple opposite boundary clusters which could trigger the stop condition. This is of course only possible so long as opposite boundary clusters' perimeters remain distinct. This stop condition nicely preserves self-similarity on all scales up to the lattice size. See Figure 3.1 for cluster examples where the lattice size is very difficult to decipher simply by inspection.

We can also refer to quantitative measures by observing the existence of scale symmetry relation $M \sim L^{D_f}$ where D_f is the typical percolation mass scaling exponent, $D_f \approx 1.89$. In the right plot of Figure 3.2, we compute D_f using the box counting technique on an ensemble of 100 lattices with size $4096x4096$. With this technique, the box count should scale with L according to $C(L) \sim L^{-D_f}$. We find $D_f = 1.897 \pm 0.003$ which

is very close to the expected infinite lattice limit.

In the next section we introduce the notion of the bulk to boundary ratio which is a geometric property indicative of a critical cluster. We can also compute the bulk to boundary ratio for clusters grown in different lattice sizes. We find the bulk to boundary ratio quickly settles down to that which is characteristic of a critical cluster. This is shown as the left plot of Figure 3.2. This ensures that our PBC implementation does not alter the geometry of a critical cluster by prematurely stopping cluster growth.

3.3 Critical Threshold

One of the most important features of percolation is its relation to critical phenomena [27]. Before discussing the critical cluster distribution directly, it is first worth discussing the control parameter and its critical value. In RP the site occupation probability, p, serves as the control parameter for RP's second order phase transition. This phase transition is described by the emergence of global connectedness where the many isolated clusters existing in regime $p < p_c$ conglomerate into a single lattice spanning cluster for $p \sim p_c$. To better elicit the connection between RP and IP, it is instructive to understand how RP's critical point manifests itself in IP.

We begin by looking at the distribution of site strengths of the invaded cluster. In IP all lattice sites are randomly assigned values from a uniform distribution in the range [0,1], but when looking at the distribution of the strengths of invaded sites, we find the selection of strengths to be a regular subset of assigned strengths. In particular, in the limit where the number of invaded sites, N, becomes infinite, the invaded strength distribution is described by a step function:

$$\lim_{N\to\infty} p(r) = \begin{cases} k & 0 \geq r \geq r_{max} \\ 0 & r > r_{max} \end{cases}$$

where a random strength, r, has constant probability k of being invaded up to some strength, r_{max}. These are related according to $1/k = r_{max}$, and its been shown that $r_{max} = p_c$ where p_c is RP's critical occupation probability [28].

Without a threshold, a cluster grown by IP (random) will grow indefinitely, and repro-

duce many of the characteristic exponents of RP's incipient infinite clusters (IIC), which is why IP is believed to reproduce the emergent incipient infinite cluster which defines RP's connected state [29]. A threshold in IP effectively acts in the same way as the occupation probability for RP. This can be understood heuristically as follows: we assign lattice site strengths from a uniform distribution in the range [0,1] as is usual, but only invade sites if its strength is below some predetermined threshold. A cluster will terminate its growth once it exhausts all perimeter sites with strength less than the threshold. The threshold serves to separate independent realizations of clusters grown by the IP method, and these independent realizations will naturally lead to a distribution of cluster sizes. However, if the threshold is $r_{max} \geq p_c$ then it becomes possible that a cluster will grow indefinitely. The statistics of this process near the critical point will yield independent realization of RP's emergent IIC with cluster realization existing on all scales.

An alternative notion for a burst could rely instead on a "bulk to boundary" ratio. The idea is that critical clusters are described by a characteristic ratio where near p_c, the ratio between the perimeter of filled and unfilled sites was one. Using a similar strategy authors have argued that using a "bulk to boundary" ratio as a generalized way to determine the critical occupation probability [30], determining the ratio analytically using,

$$\lim_{N\to\infty} \frac{N}{B(N)} = T_c \tag{3.2}$$

but this leads to $T_c \to p_c$ as before. Since both mechanisms share the same critical point, its likely the cluster statistics are the same.

3.4 Critical Behavior

Since IP is believed to reproduce the critical aspects of RP [28], we would expect the critical exponents of IP to be the same as those belonging to RP. When IP was initially proposed [13], the critical behavior was believed to be described by the scaling of the acceptance profile, $B_1(n)$. This quantity, as described in the previous section, is a function of $p(r)$, the probability of invading a site/bond with strength, r. In the finite number N

limit the acceptance profile is defined as,

$$B_1(N) = \int_0^{p_c} [1 - p_N(r)]dr \tag{3.3}$$

where N is the number of invaded sites. Near a strength matching percolation's critical value, p_c, it was believed that the region deviating from the $p_N(r)$ defining $B_1(N)$, was described by a power-law as function of the number of invaded sites, N. That is, near the critical value $B_1(N)$ would scale according to $B_1(N) \sim N^{-1/\Delta}$ with the gap exponent $\Delta = \beta+\gamma$, and γ and β are usual exponents from regular percolation. However, exponents γ and β are determined as functions of the first and second moments of RP's finite size cluster size distribution. This is an important observation as Fisher's critical droplet model [12] distills criticality from the cluster distribution, and since there does not exist a cluster distribution native to IP, the source of IP's criticality becomes an open question. Perhaps this alone might not bring into question IP's criticality, if for example, it was also possible to discuss the characterization from the description of IP's order parameter, but as we will see, this too becomes problematic.

The absence of a cluster distribution prohibited the authors of [30] from utilizing IP to directly obtain something analogous to the Fisher exponent, τ, which in Fisher's formulation characterizes the distribution of non-interacting droplets near the critical point. It is only in trapping variants of IP where the notion of a defending fluid leads in a natural sense to a distribution of finite sized clusters. Still even in this case, studies of the scaling of these finite clusters show that they scale differently from RP finite clusters [13]. There are nonetheless valid reasons to suspect the appropriate relations between the criticality of RP and IP lies between IP's invasion cluster and RP's incipient infinite cluster [29].

In order to place the discussion of IP's criticality in a familiar setting we need to establish the existence of some critical distribution. A full critical description identifies a distribution of fluctuations that scale up and dominate all scales of the system, and a characterization of the criticality is born out of the characterization of this distribution [10]. In the previous section, we established the notion of a control parameter with a critical value. Because IP only produces a single infinite cluster, we can utilize the critical

threshold to define the critical distribution of fluctuations. The burst formulation of our model [20], produces a distribution of critical percolation clusters so long as the threshold, $T = p_c$. This allows a suitable definition of a Fisher exponent which generally follows the formulation,

$$n_s(T) = s^{-(\tau)} f\left[(T - T_c)\, s^{\sigma}\right] \tag{3.4}$$

with cluster size becoming scale invariant for $T \to T_c$ and following power-law $n_s \sim s^{-(\tau-1)}$. We note that we follow the conventional definition of n_s [31] and as such sn_s corresponds to the number of bursts of size s. This being the quantity we directly obtain, then has the shifted exponent, $\tau - 1$ that we report.

Because we seek to understand IP's criticality from the perspective of traditional percolation, we will briefly describe the framework from which we will derive our results. A particularly useful formalism comes from previous work which shows the mapping between the Ising thermal second order phase transition to that of the percolation transition [8–11]. Here one makes use of percolation's cluster distribution, n_s to define an analogous generating function suitable for percolation from which the order parameter and other essential quantities may be derived.

Fundamentally, this mapping is possible because the thermal fluctuations of the order parameter (magnetization) experience long range correlations that allow large, macroscopic clusters of similarly oriented spins to emerge. The correlation function describing the correlation between sites behaves similarly in both systems, and the emergence of macroscopic magnetization clusters is therefore similar to the emergence of large, connected percolation clusters. This behavior can be neatly summarized by characterizing the system's Fisher cluster distribution in addition to the behavior of its correlation length.

In much the same way that the free energy per spin behaves as the generating function for the Ising thermal critical transition, we define an analogous generating function from which we can derive RP's essential quantities. Beginning with the generating function,

	AIP (This Paper)	RP[31]	MFA[32]
D_f	1.902(3)	$91/48 \approx 1.896$	2
D_s	1.86(1)	$91/48 \approx 1.896$	2
τ	1.594(9)	$187/91 \approx 2.05$	3/2
σ	0.41(2)	$36/91 \approx 0.42$	1/2
α	0.10(5)	$-2/3$	-1
β	N/A	$5/36 \approx .014$	1
γ	0.971(5)	$43/18 \approx 2.4$	1
ν	1.301(2)	4/3	1/2

Table 3.1. A comparison of critical exponents from the Avalanche Burst Invasion Percolation (AIP) present in this paper and regular percolation (RP) and mean field approximation values (MFA).

$$G(n_s, h) = \int_{fc} ds \ \langle n_s \rangle \, e^{-hs} \tag{3.5}$$

where one introduces a ghost field, h, that allows every site to become connected. For $h = 0$ (the limit of the RP problem), the generating function becomes the mean number of finite sized clusters. A convenient feature of this formalism is that we can easily derive relations that define the order parameter, P, in terms of the first derivative of the generating function,

$$P = \left. \frac{dG(n_s, h)}{dh} \right|_{h=0} \propto \int_{fc} ds \ s \, \langle n_s \rangle \tag{3.6}$$

which is proportional to the probability a site belongs to an infinite cluster. The order parameter is also proportional to the density of sites, thus, fluctuations in the order parameter may be more intuitively understood as fluctuations in local site density.

Fluctuations in the order parameter can be calculated as the second derivative of the generating function. This would correspond to the second moment of the average cluster size distribution, $\langle n_s \rangle$, and coincidentally corresponds to the average cluster size, $\langle s \rangle$, with s sites.

$$\langle s \rangle = \left. \frac{d^2 G(n_s, h)}{dh^2} \right|_{h=0} \propto \int_{fc} ds \; s^2 \, \langle n_s \rangle \tag{3.7}$$

Next, the correlation length characterizes the spatial extent of system fluctuations. Traditionally, this is probed by the pair connectivity function,

$$C(r, p) \sim \frac{1}{r^{d-2+\eta}} e^{-r/\xi(p)} \tag{3.8}$$

which describes the likelihood two sites belong to the same cluster. It is dependent on the correlation length controlling when the sites begin to exhibit long range correlations such that for $p \to p_c$ the pair correlation function approaches power-law behavior described by $C(r, p_c) \sim r^{-(d-2+\eta)}$. The emergence of long-range connectivity is usually empirically motivated, and it is understood to be the consequence of the correlation length, ξ, diverging. The statement can actually be made more strongly and is known as the finite size scaling hypothesis [7]. The claim is that all singular behavior is a result of a diverging correlation length. If ξ becomes infinite, then the system lacks any intrinsic length scale and necessarily becomes scale invariant which is exactly the reason for the proliferation of power-law behavior describing all relevant variables.

In RP, we can calculate the mean linear dimension of clusters,

$$\langle \xi \rangle^2 = \frac{1}{\langle s \rangle} \int ds \;\; \langle R_s \rangle^2 \, s^2 \, \langle n_s \rangle \tag{3.9}$$

where $\langle R_s \rangle$ is the radius of gyration for a cluster with s sites. This is calculated for each cluster of size s using,

$$R_s = \frac{\int dr (r - r_{cm})^2}{s} \tag{3.10}$$

The average is performed over all clusters with s sites. Similarly, $\langle s \rangle$ is the average cluster size consisting of s sites.

The critical behavior of the system corresponds to when the system is near its critical threshold, p_c. Here, all quantities become scale invariant and in RP are described by the reduced critical parameter,

$$\epsilon_p = \frac{p - p_c}{p_c} \ll 1 \tag{3.11}$$

Thus, near the critical point we have,

$$G \sim \epsilon_p^{1-\alpha} \tag{3.12}$$

$$P \sim \epsilon_p^{\beta} \tag{3.13}$$

$$\langle s \rangle \sim \epsilon_p^{-\gamma} \tag{3.14}$$

$$\xi \sim \epsilon_p^{-\nu} \tag{3.15}$$

Having established the basic quantities characterizing critical behavior, we first set out in determining, G, the zeroth moment of the cluster distribution, n_s. The zeroth moment corresponds to the number of bursts making up the distribution. In practice, care is needed in determining the scaling of G, since the number of clusters is a function of the boundary/lattice constraints. In generating the clusters to determine G, one is naturally led to the relation $G \sim N_s / \langle S \rangle$ where N_s is the total number of sites grown in the lattice, and $\langle S \rangle$ is the average cluster size. Because we derive the statistics for different ϵ_T keeping N_s fixed, this ultimately means that our measures for G and $\langle S \rangle$ would be inversely proportional, leading to faulty measures. We therefore only determine G by keeping N_s constant but allow N_s to vary when determining $\langle S \rangle$. This leads to scaling of G with exponent $1 - \alpha = 0.90 \pm .05$.

Following this framework the order parameter for our AIP model should be a function of the first moment of n_s. Formally, the first moment corresponds to total number of sites making up the cluster distribution, however in RP we subtract the sites belonging to finite clusters in order to establish the notion of the strength of the "infinite" cluster. This quantity is also identical to the probability that there exists a percolating or "wrapping" cluster (a cluster that wraps or percolates across the lattice). Immediately, we encounter some difficulty here as RP's order parameter is defined to be the likelihood that a site will belong to the infinite cluster. Certainly, this does not generalize to our case, as there is not a notion of wrapping cluster. For $T \to T_c$ we are essentially simulating multiple

realizations of RP's infinite cluster condition, where in principle one can expect to observe a infinite cluster. To make this work in our case we reserve an infinite cluster to be the largest burst in the system, and P_∞ is understood to be the fraction of sites belonging to the largest burst. As was done with RP, we subtract the infinite contribution and therefore define the cluster distribution n_s to be the distribution of finite invaded bursts. This leads to an order parameter, P', defined as,

$$P' = \int ds\ sn_s - P_\infty \tag{3.16}$$

The results are shown in Figure 3.3 where behavior is similar to a step-function which quickly goes to zero for $T \sim T_c$. This result is similar to RP where P is zero except in the close vicinity of p_c. As with RP, we observe power-law scaling only very near T_c with $P' \sim \epsilon^0.66$.

Though we salvaged the notion of the infinite cluster, the strength of the infinite cluster given by P_∞ does not scale the same as P'. Further, as we will show, the scaling of the order parameter fluctuations does not describe the observed cluster distribution, n_s.

As is shown by Eq.3.7, we can calculate the second moment of n_s characterizing the fluctuations of burst distribution. Typically for critical systems the order parameter fluctuations dictate the observed clustering, and for RP this works out to a relation with the mean cluster/burst size. Following in this formalism, we calculate the scaling of the second moment which is of same form as Eq.3.14 and leads to exponent, $\beta = -1.0$. As was mentioned previously, we computed the mean cluster size while keeping the number of bursts fixed and allowed the total sum of sites to change.

Finally, we calculate the correlation length according to Eq.3.9. For each burst of size s we compute R_s and compute the weighted average according to Eq.3.9. This calculation along with the average burst size is the most straightforward quantity to determine, since its natural to characterize the spatial extent of bursts in this way. However, as with all the other exponents we find a scaling exponent, $\nu = 1.3$ which is different from RP given the statistical error bounds. Table 3.1 shows the values of the critical exponents as determined above. Next, we need to establish the significance of these critical exponents.

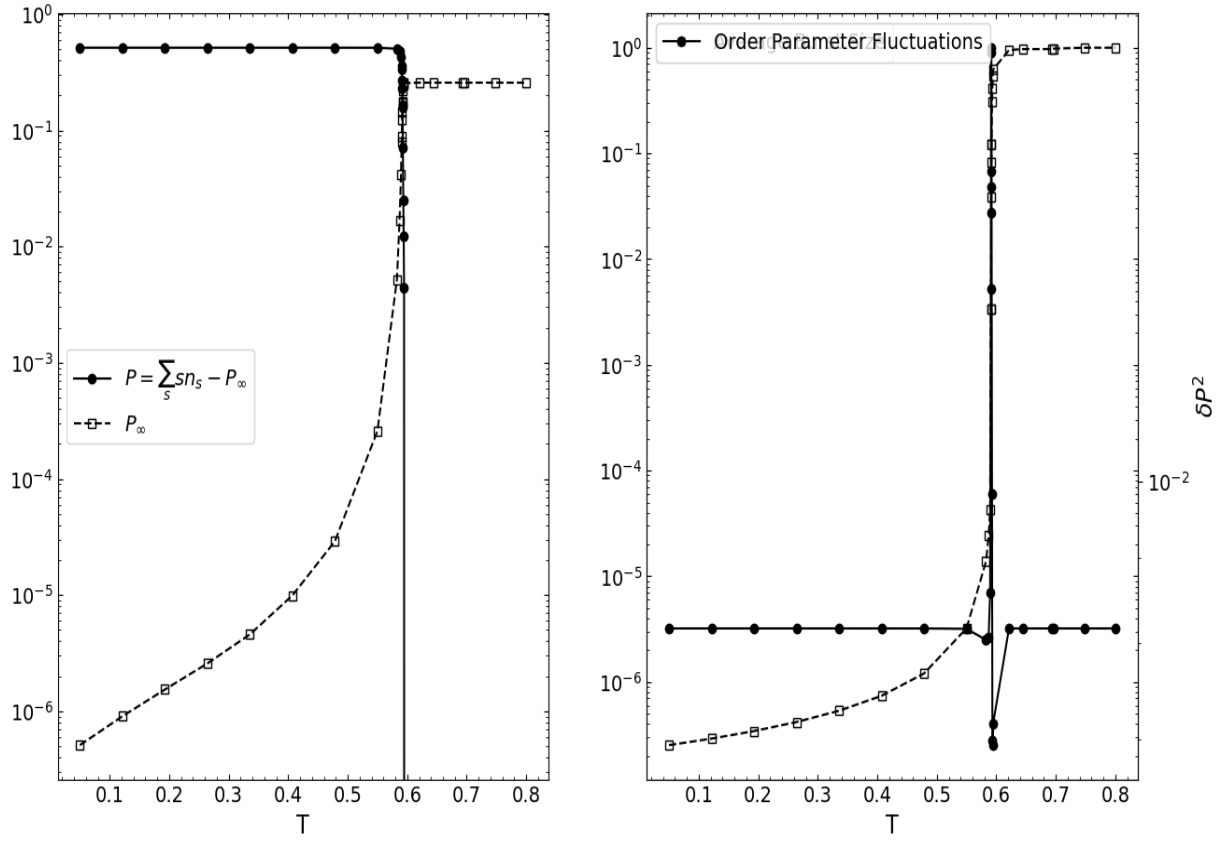

Figure 3.3. The critical behavior of the order parameter and infinite cluster (left) and the mean finite cluster size and order parameter fluctuations (right).

3.5 AIP Criticality Results

From relations 3.12-3.15, we can derive the scaling relations between burst distributions exponents and the characteristic quantities describing the AIP criticality. In addition to illustrating the central role of the burst distribution, the relations provide a consistency check for the results of the previous section. In order to establish these important relations we must first independently determine the two exponents of the cluster distribution, $n_s(\tau, \sigma)$ and the scaling burst size with its radius, R_s.

In our previous study [20] we determined the critical scaling of our burst distribution, τ, but we find this value to be sensitive to certain boundary and environment constraints. For example, $\tau - 1 \approx 1.52$ is found when one grows multiple connected bursts within a large lattice (10^4x10^4 for example) with FE boundaries. If each cluster is grown in isolation such that it grows until reaching threshold T and repeated to produce a distribution of

clusters, then one obtains a value $\tau - 1 \approx 1.0$. If instead, we implement periodic boundary conditions in the lattice we find a value of $\tau - 1 \approx 1.585$. In higher dimensions one would expect this value to approach the mean-field limit of $\tau - 1 = 1.5$. Variations in the cluster size distribution as a result of varying environment conditions was also found in [33]. Therefore, before establishing the requisite checks, we must ensure the cluster boundaries are suitably chosen to yield consistent results. Stated simply, the primary effect of the cluster boundary is to determine the extent of influence the current burst's extent has on future bursts extents since their spatial occupations are mutually exclusive. We find that if each burst grows without any preexisting burst, the scaling of $\tau \sim 1.0$, which reflects boundaries that foster the growth of large bursts. The PBC conditions allows preexisting bursts to strongly affect the growth of future bursts, and preferentially produces smaller bursts on average. The FE boundary is in between as is the mean-field limit, although the mean field limit is appropriate in high-dimensional lattices where sequential burst growth would not interfere with each other by virtue of high dimensionality keeping growth degrees of freedom accessible.

As was mentioned in Section 3.2, we explicitly developed PBC condition to develop relations in the infinite size limit, therefore, we proceed in characterizing the critical behavior with PBC conditions and use the $\tau - 1 \approx 1.59$ value. It is interesting that the FE boundary seems to be similar to the mean-field value and may have some interesting implications between the two regimes, but here, we chose the boundary that is most manifestly scale invariant.

Having established the value of τ with PBC conditions, we proceed in fully characterizing the critical behavior in RP by next determining the burst scaling exponent, σ shown in eq.3.4. From these, the scaling of the generating function, G, the order parameter, P, and average cluster size, $\langle s \rangle$, are the zeroth, first, and second moments respectively. Following the characterization of [31], the σ scaling exponent characterizes the behavior of the cutoff cluster size s_ξ which itself defines the cutoff burst size such that bursts with size $s > s_\xi$ become exponentially suppressed. As is usual, we would like to determine the scaling of s_ξ as we approach the critical point. To isolate the σ behavior, we can eliminate

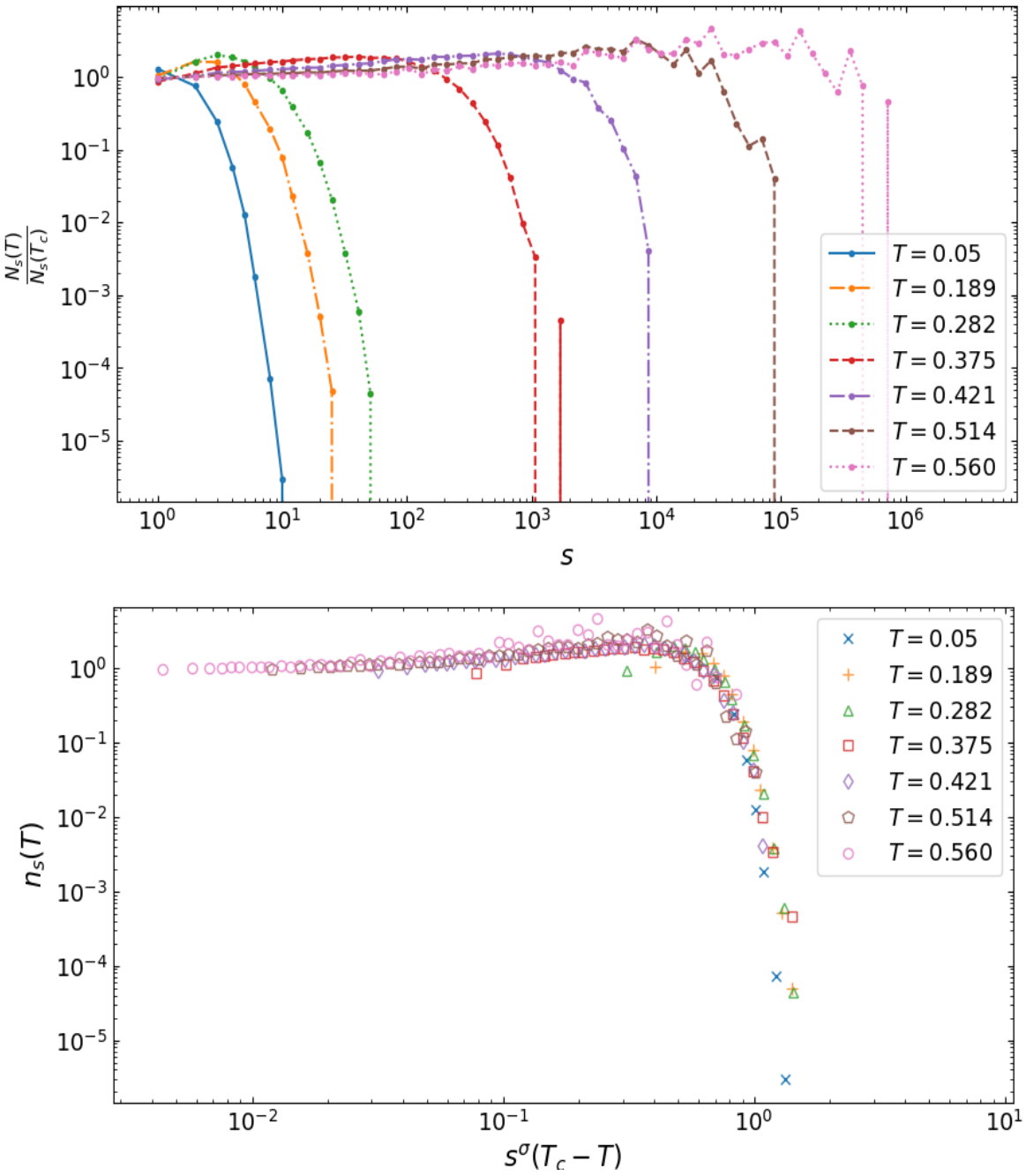

Figure 3.4. We show the behavior of the characteristic cutoff cluster size, s_ξ. (Top) The ratio $\frac{n_s(T)}{n_s(T_c)} \sim e^{-s/s_\xi}$ shows how bursts of size $s > s_\xi$ become exponentially suppressed for different thresholds, T. (Bottom) For $z \approx 1$, we establish the behavior of $s_\xi = (T_c - T)^{1/\sigma}$. For $z \ll 1$, the exponential term is a constant and corresponds to the regime where $s \ll s_\xi$.

the $\tau - 1$ dependence by considering the ratio:

$$\frac{n_s(T)}{n_s(T_c)} = \exp[-z] \tag{3.17}$$

where $z = (T_c - T)s^\sigma$. This leaves behind the exponential behavior of the cluster distribution. The two limits to consider is for $z \ll 1$ where the exponential becomes a constant, and in the large cluster limit where $z \gg 1$. In this limit, we observe the relation $s \gg (T_c - T)^{-1/\sigma}$. Thus, $s_\xi(T) = (T_c - T)^{-1/\sigma}$ behaves as the exponential cutoff cluster size for the cluster size distribution. By determining the scaling of $s_\xi(T)$ with T we can determine exponent σ, which for our cluster distribution is found to be $\sigma = 0.41 \pm 0.02$.

With sigma, one can work out the how the moments of size distribution n_s behave near the critical point, and derive relationships between the scaling of the generating function, average cluster size and order parameter in terms of τ and σ. These are:

$$2 - \alpha = \frac{(\tau - 1)}{\sigma} \tag{3.18}$$

$$\beta = \frac{(\tau - 1) - 1}{\sigma} \tag{3.19}$$

$$\gamma = \frac{2 - (\tau - 1)}{\sigma} \tag{3.20}$$

$$\nu = \frac{1}{\sigma D_s} \tag{3.21}$$

We shall briefly go through these relations individually and establish the appropriate conclusions. We begin with the generating function, G. In the previous section we reported $1 - \alpha \approx 0.9$. The scaling of the zeroth moment for RP is usually used to refer to the scaling of heat capacity for a typical thermal critical transition where the specific heat capacity is the second derivative of the free energy. As a result the exponent is shifted by two such that $c_v \sim \partial_T^2 f \sim \epsilon^{-\alpha}$. For RP this quantity becomes $\partial_s^2 G \sim \epsilon^{-\alpha}$. The situation is a bit further complicated because we work with the burst frequency distribution rather than the density distribution which normalizes each burst by burst

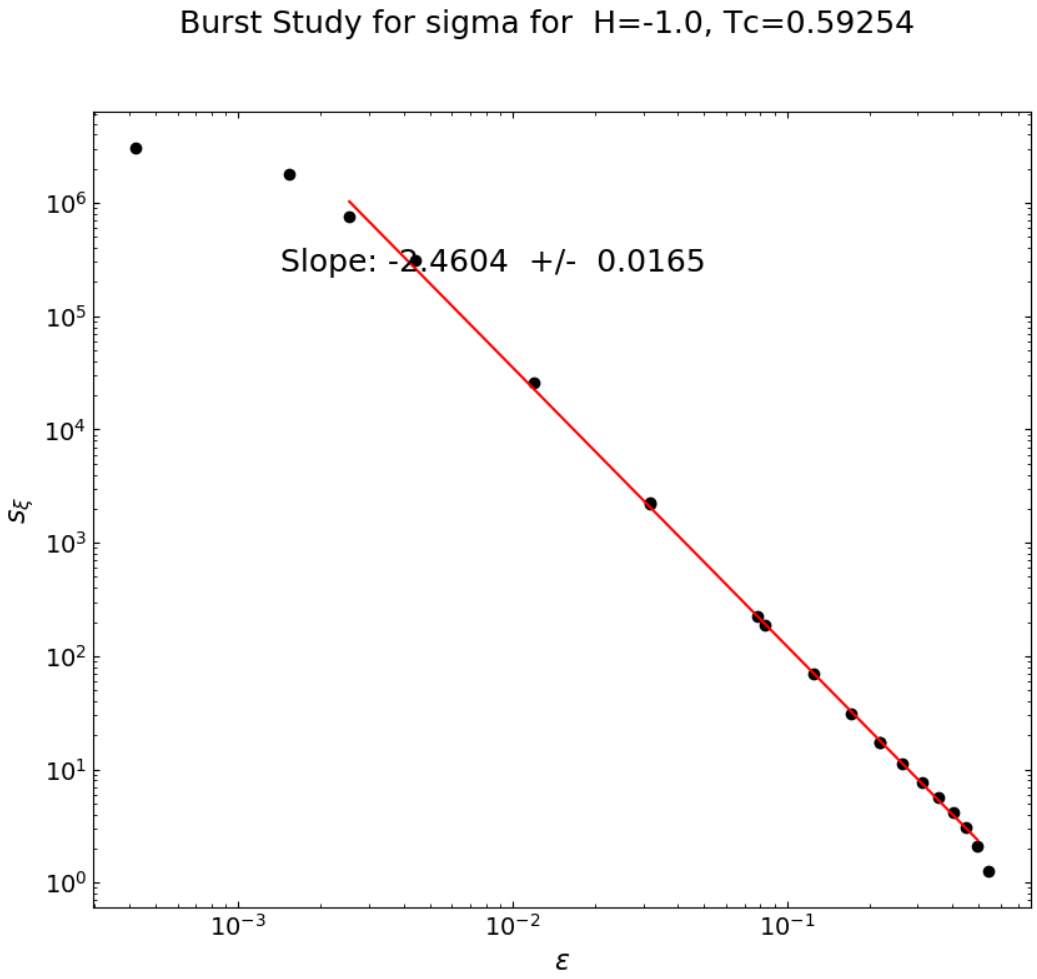

Figure 3.5. We show the LLS fit for burst size distribution exponent, σ. We fit $f(z)$ to an exponential to determine the decay constant, which corresponds to s_ξ. The log-log behavior of the cutoff burst size, s_ξ as a function of $\epsilon = (T_c - T)$. We find $1/\sigma \approx 0.41 \pm .02$.

size, s. The consequence is that we shift alpha by 1 rather than 2 in RP. We find $\alpha \approx 0.1$ which is somewhat curious. For RP, MF, and typical fluid or magnet thermal transitions give $\alpha = -2/3$, $\alpha = 0$, and $\alpha = 0 - 0.2$ [6]. There is some discrepancy reported in the literature with the percolation mean-field limit and the Ising mean-field limit, where $\alpha = -1, 0$ respectively, and may result from differences in distributions used to derive values.

The zeroth moment is also found with the burst distributions exponents as shown in Eq.3.18 which is the typical relation in RP. However, the situation is different for AIP, and undermines the relation's applicability. When analytically solving the moment integrals

we can represent the integrals as

$$M_k = \epsilon^{\frac{1+k-\tau}{\sigma}} \int_0^\infty dz\ z^{k-\tau} f[z] \tag{3.22}$$

where we must establish the convergence at the two limits. In the zero limit we can Taylor expand the integrand near zero which leads to $z^{1+k-\tau} f'[0]$. From this we can determine that for the integral to converge in the zero limit, we require $1 + k - \tau > 0$. Since $\tau \approx 1.6$, this leads to the condition $k > 0.6$. Thus, for the zeroth moment the integral fails to converge at the lower limit. In the upper limit the integrand is exponentially suppressed by function $f[z]$. We therefore conclude that the relation 3.18 does not hold for AIP. However, we can still determine the scaling of α as was done before.

Next, consider one of the most important quantities in characterizing the behavior of a phase transition, the order parameter. In RP we find that the order parameter is a function of the first moment and Eq3.19 establishes the relation between its exponents. We can check that the lower limit of integral converges since $k = 1 > 0.6$. However, there exists a problem of a different nature. Namely, in RP we find that the order parameter is proportional to the site density. Near the critical point we observe that the site density becomes scale invariant and is described by $\rho_c \sim L^{d-D_f}$. However, for AIP regardless of the threshold, T we find that the density is always described by ρ_c. Further, the first moment corresponds to the sum of all invaded sites. Again, this quantity is determined exactly by fractal dimension scaling, D_f and has no dependence on the control parameter. This undermines the existence of this type of order parameter.

Despite this we can still attempt to interpret the order parameter to be the fraction of sites belonging to the largest burst as was done in the previous section. From Figure 3.3 we can see the following relation $P \sim \epsilon_T^{0.66}$ which is only witnessed very close to the critical point, $\epsilon_T < 10^{-2}$. Coincidentally, this fails to match the expected relation given by Eq.3.19 $\frac{1.59-1}{0.41} \approx 1.46$. The reason is that when analyzing Eq3.16, the upper limit contribution is dominated by $P_\infty = \int dz\ z^{1-\tau} f[0]$ which converges if $\tau > 2$. This is a condition our τ fails to meet.

These inconsistencies highlight the key differences between RP and AIP models. In AIP all bursts are stochastic realizations of RP's incipient infinite cluster. Certainly, if we

looked at IP without any burst structure, we would only ever have a single infinite cluster growing indefinitely, so an invaded site has certainty of belonging to the infinite cluster and the wrapping probability is also unity. Moreover, an order parameter does not seem appropriate in IP because notions of distinct phases do not seem natural. It is not clear how one would define distinct phases such that at the critical point, IP is transitioning from one phase to the other through the critical formulation. Either the order parameter does not exist without further implementing behaviors to the model, or it is not obvious.

The deficiencies of the previous two quantities do not plague the third, the mean cluster size $\langle S \rangle$. The integral conditions for convergence all exist for the second moment. In the previous section we found that the mean clusters size scaled according to $\langle s \rangle \sim \epsilon_T^{-0.998 \pm .001}$. If we refer to Eq3.20 we get $\frac{2-1.59}{0.41} = 1.0$ which is exactly what we expect. However, we do find $\gamma \sim 1$ to be very different from RP ($\gamma_{RP} = 43/18 \approx 2.39$), which indicates that the burst distributions of RP and the distribution of AIP bursts to be different. Instead, we find a distribution whose mean cluster size is similar to the mean-field value.

More importantly, to establish the consistency of results we expect the susceptibility to diverge with the same exponent as the mean cluster size. We can calculate the susceptibility utilizing the fluctuation dissipation relation given by [7],

$$\chi \sim \frac{\beta}{V} \int_V d^d r \; C(r) \tag{3.23}$$

where $C(r)$ is the two-point correlation function as a function of distance between sites, r. Usually in thermal critical transitions, the susceptibility or the correlation function is itself a function of the order parameter fluctuations. In RP this also holds true except there is an additional term corresponding to the mean cluster size. This leads to the following relation:

$$\chi = \langle S \rangle + \delta P^2 \tag{3.24}$$

This offers yet another test for the order parameter as its fluctuations should contribute to the susceptibility divergence. In RP, it turns out that both terms diverge with the same exponent [34]. However, we find the order parameter fluctuations are only weakly consistent with the susceptibility since $\delta P^2 \sim \epsilon_T^{-0.89 \pm .05}$. When we evaluate the divergence of

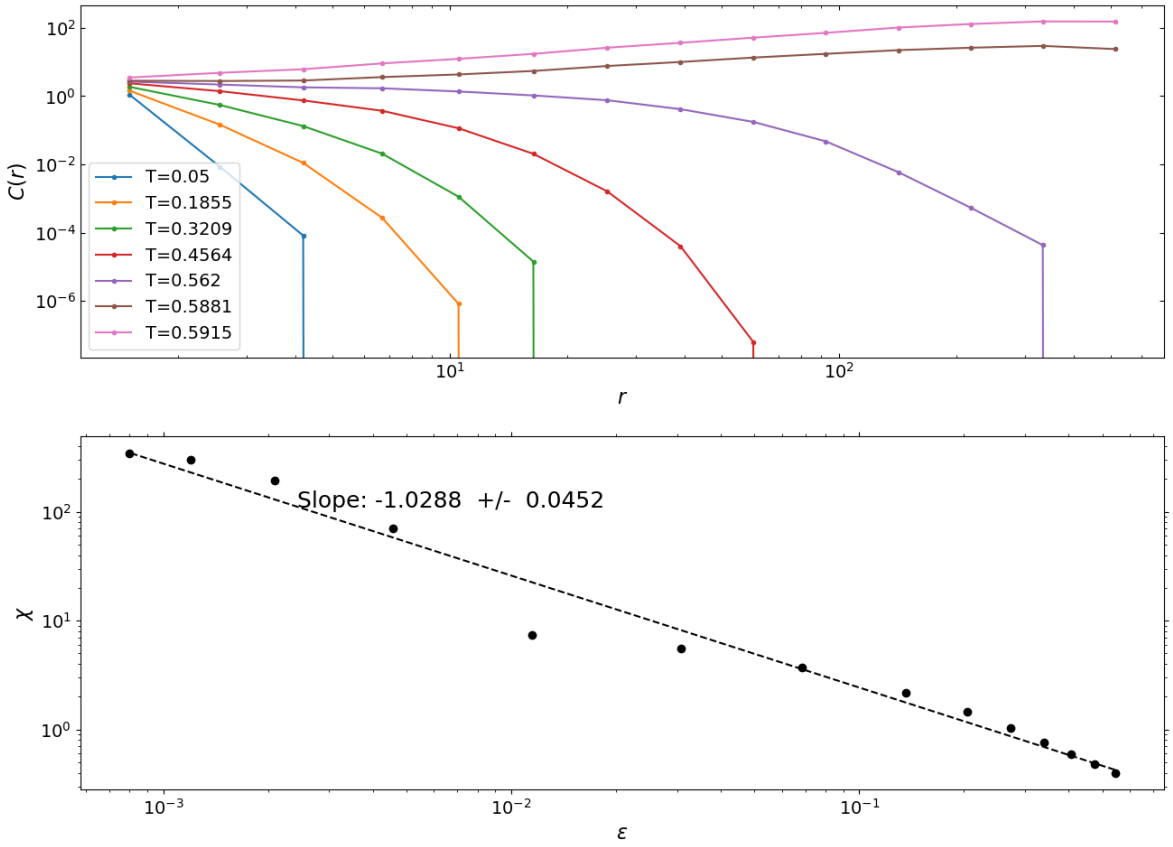

Figure 3.6. We show the results of the susceptibility divergence as a function of the pairwise correlation function. (Top) In the top plot we show the behavior of the pairwise correlation function $C(r,T)$ as a function of threshold, T and distance between sites r. We observe the expected general behavior $C(r,T) \sim r^{-\eta} f[-r/\xi(T)]$. (Bottom) We show the LLS fit of χ as a function of ϵ_T and find a scaling consistent with that of the mean burst size.

the susceptibility using Eq.3.23 we get an exponent $\gamma = 1.03 \pm .05$ which is consistent with our mean burst size scaling, but beyond the error bounds of δP^2. The larger magnitude of the exponent of $\langle S \rangle$ as compared to δP^2 means that $\langle S \rangle$ will dominate the behavior near the divergence.

The divergence of the susceptibility resulting from the pair-wise correlation function nicely leads us into the discussion of the correlation length, ξ, which also happens to be the final critical exponent relation we aim to discuss from the list, Eq.3.18-21. In some sense it might be more clear to begin with ξ, since after all, the behavior of the correlation length is the fundamental ingredient to explaining the emergence of scale invariance as posited by the finite size scaling hypothesis.

Since the characterization of ξ is so important, we will discuss it from two perspectives. First, we will discuss its natural relation to the correlation function previously discussed. Then, we will discuss how it relates to the characteristic spatial extent of each burst. Littered through these discussions will be checks with appropriate exponent scaling relations in order to ensure the results are consistent.

Again, the correlation function, $C(r)$, describes the probability that two sites separated some distance, r, are likely to belong to the same burst. To calculate $C(r)$, we first grow an ensemble of clusters (100) within a lattice of size $4096x4096$ with PBC conditions which is subsequently broken up into bursts as a function of threshold, T. For each burst we calculate $C(r)$ according to standard counting method [35], and average over all bursts to generate an average $\langle C(r)\rangle_b$ which is then averaged across the ensemble to produce an average for a given lattice size, $\langle\langle C(r)\rangle\rangle_L$. This is repeated for a range thresholds, T, in order to establish its behavior as we approach the critical value. We find that the behavior matches the expected behavior in 2D, $C(r) \sim r^{-\eta}e^{-r/\xi(T)}$ and based on the behavior very near the critical point we find $\eta = 0.23 \pm .02$.

The top plot in Figure 3.6 shows the effect of correlation length, ξ, which characterizes the length above which the likelihood of two sites to occupy the same burst becomes exponentially suppressed. As T increases so too does the correlation length such that near the critical point the length approaches the system size. This motivates the general relation that near the critical point, the correlation length behaves according to $\xi \sim \epsilon_T^{-\nu}$ which we will subsequently discuss, but first we discuss how the susceptibility diverges with the correlation length. Following the Eq.3.23, we can compute the integral in 2D using

$$\begin{aligned}\chi &\sim \int_0^{\xi} dr \frac{\langle\langle C(r)\rangle\rangle_L}{r} \\ &= \epsilon_T^{-\nu(1-\eta)}\end{aligned} \tag{3.25}$$

In the previous section we found exponent $\nu = 1.28$ using the typical RP definition of ξ defined by Eq.3.9. From the relation above we can check that $\gamma = 1.28(1 - 0.23) = 0.99$ and is very near the expected value of 1.

We can also assess the behavior of the correlation length by looking at the number of

sites contained in the largest burst. Since the density of sites is fixed the largest burst, s_∞, should scale according to the correlation volume, $\xi^2 = \epsilon_T^{-2\nu}$. From LLS fit of s_∞ vs ϵ_T we find $\xi \sim \epsilon_T^{-1.3\pm.03}$ which is within error bounds of our previous determination of ν.

As a final check we can utilize the burst size scaling with radius of gyrations given by $s \sim R_s^{D_s}$ to check relation 3.21. We find by LLS fit that $D_s = 1.859 \pm .002$ and as shown in the previous section $\sigma = 0.41 \pm .02$. This gives a value of $\nu = 1.31$ which is consistent within error bounds of the other results which all yield values in the vicinity of 1.3.

As a brief conclusion to this section, we found extrapolating from RP's behavior, we would expect mean square fluctuations in the order parameter coupled with the divergence of the correlation length to give rise to observed cluster structure of the model. However, we quickly ran into problems with the order parameter both in conceptually defining the notion of distinct states and formally deriving appropriate consistency relations between relevant quantities. Therefore, there was no consistent characterization of the order parameter, but we also found in characterizing the correlation length and mean cluster size that we were able to account for the critical divergence of susceptibility with these quantities alone. In RP the emergence of macroscopic connectivity is nicely characterized by the divergence of order parameter fluctuations, and it is a particularly nice conceptual feature that order parameter fluctuations and random site fluctuations should scale similarly. However, it does not seem necessary in describing the critical behavior of AIP (and perhaps more broadly applies to self-organizing critical behavior). What IP simulates is a growth mechanism, and if we introduce a threshold formulation to define distinct bursts, we find that we can define regimes of critical growth or subcritical growth depending on the threshold, T. This characterization better fits within the description of metastable nucleation of critical droplets.

3.6 Hyperscaling

We continue to delve into the critical behavior of AIP by analyzing whether hyperscaling is a feature of the model. While not an essential prerequisite for criticality its presence does highlight the existence of additional relations which simplify the quantities needed to

explain the observed behavior. Generally, systems with hyperscaling can be characterized by independently determining only 2 critical exponents. All others can be determined by the various relations including the additional hyperscaling relations. Still, compared to other notions we have discussed, the concept of hyperscaling is generally more loosely defined and essentially amounts to the criteria where their relations between exponents contain the dimensionality of the system. As an example, we will illustrate some of the more insightful of these relations and how it manifests itself in the system.

Perhaps the most significant quantity is the correlation length of the system, ξ. With ξ we can know the likelihood two sites are to be related to one another. In RP one would expect that this should be related to whether two sites belong to the same cluster, and in RP this statistically works out to be the case. We can see this with the following calculation. We consider a box with sides of length ξ. If we count the number of clusters contained in the box, we get some number that need not be 1. However, as we approach the critical point and the ξ increases and thereby the size of our correlation box, the clusters contained should scale proportionally such that number of clusters does not change.

To carry out this calculation, we can make use of G which is the zeroth moment of the cluster distribution and amounts to the number of clusters per site or the cluster density. If this quantity is multiplied by ξ^2 we should get the number of clusters in a correlation volume given by

$$N_\xi = G\ \xi^2 \sim \epsilon^{2-\alpha-2\nu} \sim constant \tag{3.26}$$

For RP $\alpha = -2/3$ and $\nu = -4/3$ which when plugged into the above yields an average cluster count which is constant. This is indeed what one would expect if the correlation length represented the spatial extent of observed clusters. Note, also that this leads to the following hyperscaling relation,

$$2 - \alpha = d\nu \tag{3.27}$$

Because we can also determine $2 - \alpha$ from the cluster distribution exponents, this also means that we can determine the scaling of the correlation length based entirely on the dimensionality of the system, a very powerful result. Similarly, because of all the other

relations between exponents, we can generate the complete set from the two exponents τ and σ.

Much of the same formalism can be applied directly to our AIP model, where we have characterized our own values for the critical exponents. First, we define the appropriate critical parameter ϵ_T as was shown in Section 4.6,

$$\epsilon_T = \frac{T - T_c}{Tc} \tag{3.28}$$

where T is the burst threshold and T_c is the critical burst threshold. The critical values of the scaling exponents are reported in Table 3.1. However, because n_s for us is a frequency distribution rather than a density distribution, we shift the exponent by 1. If we similarly calculate the number of bursts in correlation volume,

$$N'_\xi = G\xi^2 \sim \epsilon_T^{-0.6} \tag{3.29}$$

we find a scaling that diverges with value ≈ -0.6 in contrast with the RP case which remained constant.

This is another key difference between the apparent criticality present in this AIP model and RP, which suggests that because the bursts are not realizations of order parameter fluctuations as in RP, we do not observe similar behavior. Instead, there appears to be an excess of bursts contained within a correlation volume and scales according to N'_ξ. This observation introduces a new puzzle, but also establish the lack the hypersaling in our model, namely Eq.3.27. The absence of hyperscaling in IP models was also found by [14]. They found that the cluster distribution exponent τ could not be determined by spatial dimension d according to hyperscaling relation, $\tau = 1 + d/D_f$.

Further evidence comes from [36] who also observe the absence of hyperscaling in the mean-field regime of long-range bond percolation. They observe differences between scaling exponents, D_f and D_s (as defined here) and suggest that there are differences in cluster density for small versus large clusters. We can add to this line of inquiry by similarly noting a difference between exponents, D_f and D_s. (Though the differences are small, the differences are outside error bounds. Also, both measures are characterizations

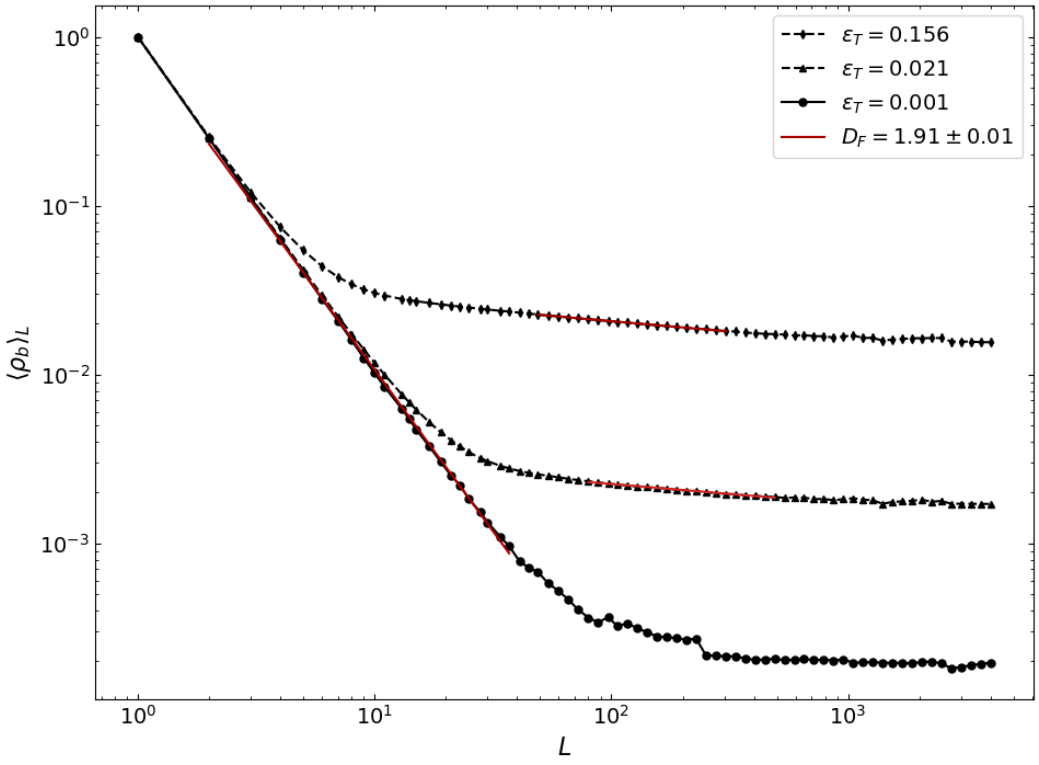

Figure 3.7. We show the results of the crossover behavior inherent to average burst epicenter density, $\langle \rho_b \rangle_L$ as a function of length scale, L. The correlation length defines the scale where we expect power-law behavior. Here we observer the average number of burst, $\langle N(L) \rangle$ in region size, L^2 scales according to the expected mass scaling of individual sites (as is expected from scale invariance), $N(L) \sim L^{D_f}$. On larger length scales, the scaling becomes uniform.

of many scales and consequently are rather insensitive measures, so any observed difference can have quite notable consequences) One possible explanation is that this suggests that there might be two competing correlation mechanisms. We can think about the density of sites versus the density of clusters. One correlation mechanism that is inherited from RP and is present in the IIC of the original IP cluster which would characterize the density of sites, given by $d - D_f$. The second correlation length comes about when we introduce the notion of bursts and burst density would therefore be characterized by $2 - D_s$. That these two are not the same is to say that site and burst density do not follow the same scaling.

We briefly provide evidence for this by computing the average density of burst epicen-

ters as function of length scale, l. For each burst we compute the epicenter as the burst center of mass. For each length scale, we can easily compute the average density according $\langle \rho_b \rangle_l = \langle N_b \rangle / l^2$, where N_b is the number of bursts contained in the box element, l^2. We can determine the correlation length by extrapolating where the power-law behavior intersects the homogeneous scaling regime. We can repeat this process for multiple values of critical scaling parameter ϵ_T to work out the correlation scaling for epicenters, $\xi_b \sim \epsilon_T^{-\nu_b}$ where ν_b defines the burst epicenter scaling. We find $\nu_b \approx 0.5$ which is the mean-field value, and the expected value if burst epicenters were distributed essentially according to a random walk. For length scales above ξ_b (nearly flat regions in upper curves of Figure 3.7) we observe scaling given $d - D = 0.127$, which yields a result consistent with D_s scaling.

We can also refer to [10] which built upon previous findings to understand a similar discrepancy when analyzing the behavior mean field clusters in the Potts 2D model. They found they could account for the excess of clusters in a correlation volume if instead cluster density was the result of a random walk distribution of clusters, and developed the notion of "fundamental clusters" which do have the property that their density matches that of their site density. In their analysis they found that the additional random walk element would contribute to number scaling by a factor of $\epsilon^{1/2}$, since the resulting spatial distribution is Gaussian whose width is given by $\sigma = \sqrt{N}$ where N scales as $G \sim \epsilon^1$. This is nearly of the same magnitude needed to account for our own excess.

3.7 Discussion

We find plenty of examples in the literature suggesting a connection between critical phenomena and seismicity. Naturally, one might ask: must we insist on the presence of a phase transition in order to describe the underlying mechanisms of seismicity? We found that our AIP model, a characteristic example of self-organized criticality (SOC), has many of the essential features of seismicity, except it does not inherit any phase transition mechanics (namely, no distinct phases and no notion of an order parameter). In characterizing our model, we found that all we needed is some notion of a critical

point where the correlation length of bursts diverges. This leads to the conclusion that in systems which are already described by the absence of a characteristic length scale, we need not discuss the transition of a state with finite correlation length (which may never have existed) to a state described by an infinite correlation length.

The absence of a phase transition is further supported because in AIP the site density remains constant, and is described as a feature of static network properties as shown in section 3.2. These static features arise independent to the pseudo-critical mechanisms we define here and in the previous sections, and are therefore, insensitive to the tuning of the critical parameter, T. This is in contrast to RP, where the phase transition is described by a mapping between the site density fluctuations and the observed cluster fluctuations, describing the emergence of global connectivity. This is understood from the observation that the pair distribution function is isomorphic to the pair connectedness function [10].

Nevertheless, the absence of the order parameter and its critical fluctuations does not prevent the system from exhibiting scale invariant structure. In fact, during seismicity where the system seems imbued with an infinite correlation length as is described by [37], and subsequent behavior exists atop underlying long range correlated behavior. AIP inherits IP's stochastic growth mechanism which grows without an intrinsic scale, perhaps akin to the Mandelbrot set being generated from a simple complex function. Or, it is perhaps appropriate to describe the system instead as a long-lived metastable state which we find in nucleation phenomena which also lead to characteristic critical droplets with the same structure as SOC avalanche models.

Therefore, rather than describing a phase transition we have only a stochastic growth mechanism with a notion of independent realizations that gives rise to a critical type burst distribution. The characterization of this distribution and the correlation length is adequate in defining the universality class of the model's inherent randomness and the growth mechanism by which the fluctuations grow to all scales.

Focusing on the growth mechanism, we notice in contrast to the general claim that SOC does not require a tuning parameter, our AIP is characterized by a critical distribution similar to Fisher's critical droplet distribution (or that near the Ising mean-field

spinodal). Thus, in order to produce scale invariant bursts (even atop the underlying fractal substrate) the control parameter must be near its critical value. However, it is possible to rescue the idea that AIP does not explicitly need to be fine tuned to be near its critical and reclaim one of the primary advantages believed to be a general feature of SOC. As [38] stress, nearly all SOC systems have some notion of a driving parameter, usually a ratio which characterizes the growth of the system. As was shown in Sec.4.6 Eq.3.2, we can recast the threshold as a bulk-to-boundary ratio which serves as the driving parameter describing burst growth. A system's equilibrium growth mechanics might then tend to the critical ratio.

Continuing in the characterization of the critical distribution, we can categorize the broader critical features, namely that it is near mean field, with exponents $\tau - 1 = 1.59 \pm .01$, $\sigma = 0.41 \pm .01$, where mean-field is given by 3/2 and 1/2 respectively. This naturally implies that AIP ought to belong to its own universality class since the exponents are all different from mean field as shown in Table3.1. Not only does the growth mechanism not belong to the same universality class as RP, but the correlation behavior is different as well. This is nicely illustrated by the feature that the number of bursts in a correlation volume, defined from the pairwise site correlation length, fails to remain constant. This fundamentally leads to absence of hyperscaling, which indicates the existence of multiple correlation lengths in the system. Stated differently, the density of sites (which is independent of any pseudo-critical phenomena) is different from the density of bursts, which near the critical value is consistent with a random walk.

Further, because the density which changed in proportion to the order parameter for RP does not for AIP, we find no natural notion suitable as the system's order parameter. We recall that in RP the order parameter is made to correspond to either the strength of the infinite cluster or the "wrapping" probability. Certainly, if we looked at IP without any burst structure, we would only ever have a single infinite cluster growing indefinitely, so, an invaded site has certainty of belonging to the infinite cluster and the wrapping probability is also unity.

In conclusion, the AIP model is a hybrid model with a Fisher type burst distribution

characterized with near mean-field exponents $\tau_{AIP} = 2.59$, $\sigma_{AIP} = 0.41$. Again, the normalized per site mean-field cluster distribution is characterized with exponents $\tau_{MF} = 5/2$ and $\sigma_{MF} = 1/2$ respectively. This naturally implies that AIP is similar to but distinct from mean-field and ought to belong to its own universality class, since the exponents are all different from mean field as shown in Table 3.1. Many of the static features are inherited from RP's IIC, and the addition of the avalanche burst mechanism introduces a correlation length for bursts that is consistent with mean-field, since $\nu \sim 1/2$. Despite the presence of multiple correlation lengths, the system maintains its fractal properties and is largely self-similar on all length scales. While the finite size scaling hypothesis does lead to manifestly scale invariant systems, in practice it is likely a constraint that need not be enforced, and instead more investigations should seek to understand how multiple correlation lengths lead to "effectively" scale invariance which may explain why it is so prevalent in so many complex systems.

Finally, because we inherit the long-range correlations present during the critical phase of RP, its fair to wonder how the behavior changes with different underlying correlation structure. This will be the subject of the next chapter where we consider the presence of long-range correlations present between sites described by $C(r) \sim r^{-H}$, where r is the distance between sites. This should yield distinct critical distributions, $n_s(T, \sigma, H)$, and thereby lead to a potential family of distributions with distinct burst scaling behavior. This is what we will seek to characterize in future work.

References

[1] J. B. Rundle, "Derivation of the complete Gutenberg-Richter magnitude-frequency relation using the principle of scale invariance," *Journal of Geophysical Research: Solid Earth*, vol. 94, no. B9, pp. 12337–12342, 1989.

[2] B. E. Shaw, "Generalized Omori law for aftershocks and foreshocks from a simple dynamics," *Geophysical research letters*, vol. 20, no. 10, pp. 907–910, 1993.

[3] Y. Y. Kagan, "Earthquake spatial distribution: the correlation dimension," *Geophysical Journal International*, vol. 168, no. 3, pp. 1175–1194, 2007.

[4] F. Ebrahimi, "Invasion percolation: A computational algorithm for complex phenomena," *Computing in Science & Engineering*, vol. 12, no. 02, pp. 84–93, 2010.

[5] J. Henderson, D. Barton, and G. Foulger, "Fractal clustering of induced seismicity in the Geysers geothermal area, California," *Geophysical Journal International*, vol. 139, no. 2, pp. 317–324, 1999.

[6] H. E. Stanley, *Phase transitions and critical phenomena*, vol. 7. Clarendon Press, Oxford, 1971.

[7] S.-K. Ma, *Modern theory of critical phenomena*. Routledge, 2018.

[8] K. Murata, "Hamiltonian formulation of site percolation in a lattice gas," *Journal of Physics A: Mathematical and General*, vol. 12, no. 1, p. 81, 1979.

[9] A. Coniglio and W. Klein, "Clusters and Ising critical droplets: a renormalisation group approach," *Journal of Physics A: Mathematical and General*, vol. 13, no. 8, p. 2775, 1980.

[10] W. Klein, H. Gould, N. Gulbahce, J. Rundle, and K. Tiampo, "Structure of fluctuations near mean-field critical points and spinodals and its implication for physical processes," *Physical Review E*, vol. 75, no. 3, p. 031114, 2007.

[11] P. Reynolds, H. Stanley, and W. Klein, "Ghost fields, pair connectedness, and scaling: exact results in one-dimensional percolation," *Journal of Physics A: Mathematical and General*, vol. 10, no. 11, p. L203, 1977.

[12] M. E. Fisher, "The theory of condensation and the critical point," *Physics Physique Fizika*, vol. 3, no. 5, p. 255, 1967.

[13] D. Wilkinson and J. F. Willemsen, "Invasion percolation: a new form of percolation theory," *Journal of Physics A: Mathematical and General*, vol. 16, no. 14, p. 3365, 1983.

[14] J. F. Willemsen, "Investigation on scaling and hyperscaling for invasion percolation," *Physical review letters*, vol. 52, no. 25, p. 2197, 1984.

[15] A. P. Sheppard, M. A. Knackstedt, W. V. Pinczewski, and M. Sahimi, "Invasion percolation: new algorithms and universality classes," *Journal of Physics A: Mathematical and General*, vol. 32, no. 49, p. L521, 1999.

[16] F. Ebrahimi, "The shape of invasion percolation clusters in random and correlated media," *Journal of Statistical Mechanics: Theory and Experiment*, vol. 2008, no. 04, p. P04005, 2008.

[17] M. A. Knackstedt, M. Sahimi, and A. P. Sheppard, "Invasion percolation with long-range correlations: First-order phase transition and nonuniversal scaling properties," *Physical Review E*, vol. 61, no. 5, p. 4920, 2000.

[18] A. M. Vidales, E. Miranda, M. Nazzarro, V. Mayagoitia, F. Rojas, and G. Zgrablich, "Invasion percolation in correlated porous media," *Europhysics Letters (EPL)*, vol. 36, pp. 259–264, nov 1996.

[19] S. Mertens and C. Moore, "Percolation thresholds and fisher exponents in hypercubic lattices," *Physical Review E*, vol. 98, no. 2, p. 022120, 2018.

[20] R. Ortez, J. B. Rundle, and D. L. Turcotte, "Universality class for loopless invasion percolation models and a percolation avalanche burst model for hydraulic fracturing," *Physical Review E*, vol. 103, no. 1, p. 012310, 2021.

[21] R. Kenna and B. Berche, "Universal finite-size scaling for percolation theory in high dimensions," *Journal of Physics A: Mathematical and Theoretical*, vol. 50, no. 23, p. 235001, 2017.

[22] R. M. Ziff, S. R. Finch, and V. S. Adamchik, "Universality of finite-size corrections to the number of critical percolation clusters," *Physical review letters*, vol. 79, no. 18, p. 3447, 1997.

[23] D. Heermann and D. Stauffer, "Influence of boundary conditions on square bond percolation nearp c," *Zeitschrift für Physik B Condensed Matter*, vol. 40, no. 1, pp. 133–136, 1980.

[24] G. Wagner, A. Birovljev, P. Meakin, J. Feder, and T. Jøssang, "Fragmentation and migration of invasion percolation clusters: Experiments and simulations," *Physical Review E*, vol. 55, no. 6, p. 7015, 1997.

[25] M. A. Knackstedt, M. Sahimi, and A. P. Sheppard, "Nonuniversality of invasion percolation in two-dimensional systems," *Physical Review E*, vol. 65, no. 3, p. 035101, 2002.

[26] M. S. Watanabe, "Percolation with a periodic boundary condition: The effect of system size for crystallization in molecular dynamics," *Physical Review E*, vol. 51, no. 5, p. 3945, 1995.

[27] M. Stephen, "Percolation problems and the Potts model," *Physics Letters A*, vol. 56, no. 3, pp. 149–150, 1976.

[28] J. T. Chayes, L. Chayes, and C. M. Newman, "The stochastic geometry of invasion percolation," *Communications in mathematical physics*, vol. 101, no. 3, pp. 383–407, 1985.

[29] A. A. Járai, "Invasion percolation and the incipient infinite cluster in 2D," *Communications in mathematical physics*, vol. 236, no. 2, pp. 311–334, 2003.

[30] S. Mertens and C. Moore, "Percolation thresholds in hyperbolic lattices," *Physical Review E*, vol. 96, no. 4, p. 042116, 2017.

[31] D. Stauffer and A. Aharony, *Introduction to Percolation Theory.(2nd edn), 1992*. London, Taylor and Francis., 1994.

[32] L. D. Landau and E. M. Lifshitz, *Statistical Physics: Volume 5*, vol. 5. Elsevier, 2013.

[33] A. Araújo, T. Vasconcelos, A. Moreira, L. Lucena, and J. Andrade Jr, "Invasion percolation between two sites," *Physical Review E*, vol. 72, no. 4, p. 041404, 2005.

[34] A. Coniglio and D. Stauffer, "Fluctuations of the infinite network in percolation theory," *Lettere al Nuovo Cimento*, vol. 28, no. 2, pp. 33–38, 1980.

[35] D. Turcotte, *Fractals and Chaos in Geology and Geophysics*. Fractals and Chaos in Geology and Geophysics, Cambridge University Press, 1997.

[36] T. Ray and W. Klein, "Crossover and the breakdown of hyperscaling in long-range bond percolation," *Journal of statistical physics*, vol. 53, no. 3, pp. 773–794, 1988.

[37] A. Sornette and D. Sornette, "Self-organized criticality and earthquakes," *EPL (Europhysics Letters)*, vol. 9, no. 3, p. 197, 1989.

[38] A. Gabrielli, G. Caldarelli, and L. Pietronero, "Invasion percolation with temperature and the nature of self-organized criticality in real systems," *Physical Review E*, vol. 62, no. 6, p. 7638, 2000.

Chapter 4

Correlated Avalanche Burst Invasion Percolation: Multifractal origins of self organized critiality

(Summary)

We extend our previous model, avalanche-burst invasion percolation (AIP) by introducing long-range correlations between sites described by fractional Brownian statistics. In our previous models with independent, random site strengths, we reproduced a unique set of power-laws consistent with some of the b-values observed during induced seismicity. We expand upon these models to produce a family of critical exponents which could be characterized by the local long-range correlations inherent to host sediment. Further, in previous correlated invasion percolation studies, fractal behavior was found in only a subset of the range of Hurst exponent, H. We find fractal behavior persists for the entire range of Hurst exponent. Additionally, we show how multiple cluster scaling power laws results from changing the generalized Hurst parameter controlling long-range site correlations, and gives rise to a truly multifractal system. This emergent multifractal behavior plays a central role in allowing us to extend our model to better account for variations in the observed Gutenber-Richter b-values of induced seismicity.

4.1 Introduction

One of the most interesting insights from random percolation (RP) is the emergence of long-range correlations from the inherently random process of independently occupying sites with probability, p on a lattice. As is characteristic with complex phenomena, we observe the emergence of characteristic features, namely, large scale connectivity that dominates behavior on all scales. Much of percolation's value comes from providing an extremely simple framework from which many puzzling features both can arise and can be understood.

Given the emergent nature of long-range connectivity, researchers naturally became curious of the effect of implicit long-range correlations imbedded in the lattice structure might have on the critical behavior[1–5]. This question is of interest not only from a formal perspective, but also, because long-range correlations (LRC) are described by fractal relations. These same fractal properties have been one of the most profound discoveries in the last few decades because of the explosion in number and diversity of fractal systems, and highlights the vast pervasiveness of fractal structures in nature. This was made famous by Mandelbrot[6], and grew into its own paradigm of inquiry.

In our previous paper [7], we characterized the critical behavior of our avalanche-burst invasion percolation (AIP) model, which produced a critical distribution of bursts, $n_s(T)$, as a function of strength threshold, T. These bursts existed on top of the random long-range correlations emergent to percolation near the critical point. We observed a unique burst distribution characterized by exponents, $\tau = 1.594 \pm .009$, $\sigma = 0.41 \pm .01$. These exponents are near but distinct from mean-field cluster scaling, $\tau_{MF} = 1.5, \sigma = 0.5$. This serves to define a distinct universality class of critical behavior, distinct even from RP.

Only a few studies have been done on LRC on IP [8, 9], and these studies only looked at the static network type scaling (D_f, D_{min}, D_b) properties which do little to provide insight into how the critical properties change. This is of course largely because the critical description of IP has been poorly understood, and had not been placed within the appropriate framework to assign it various critical properties. This was done with our AIP model, and now we are well positioned to address the topic of LRC's impact on

AIP's critical behavior.

In particular our AIP model lends itself to the description of induced seismicity as was shown in [10]. Invasion percolation simulates the infiltration of invading fluid into a defending substrate that is modeled as a lattice of sites with random and isotropic resistance. An invasion path following a principle of least resistance enforced at each time step will naturally select the subset of sites which exhibit long-range correlations between invaded sites. The additional burst mechanism allows us to identify the conditions which yield scale invariant bursts, and thus, allows us to speculate on the conditions that must exist to produce the observed scale invariant seismic distributions.

This study can be more accurate because studies of porous media find correlations between pore size in various sedimentary substrates. These studies indicate porous media sites are not independent and random, but rather, exhibit long-range correlations. In particular, fractional-Brownian statistics seem to well describe the porosity logs within many heterogeneous rock formations at large scales[11]. Similar findings for the permeability distribution have been found for oil reservoirs and aquifers [12]. Therefore, we now investigate how our AIP algorithms change in the presence of implicitly correlated lattice sites rather than a lattice of independent, random sites.

4.2 Long Range Correlations

One of the most profound realizations of the latter half of the 20th century is the widespread fractal nature describing many physical properties [6]. Perhaps the primary benefit is that these measures applied to a class of structures which were previously largely uncategorized. Their fractal characterization provided a new lens which allowed us to recognized commonalities shared among disparate systems.

As an illustrative example, we consider a region with mapped topographical elevation, h(x,y). Next, we consider height fluctuations as a function of distance, $r^2 = x^2 + y^2$, described by $\Delta h(r)$. A fractal dependence of the fluctuations is described by,

$$\Delta h(r) \sim r^{\alpha} \tag{4.1}$$

If the fluctuations are random then $\alpha = 1/2$, illustrating the random walk nature of

the fluctuations. Long-range correlations are described by a correlation function, $C(r)$, that is not exponentially bounded. This translates into Eq.4.1 as an α that will be non-integer and will also be different from 1/2. If we consider the autocorrelation function of heights, then the behavior of the integral of the autocorrelation function permits the understanding of different regimes of α [13]. For $\alpha < 0.5$ the correlations are antipersistent (anticorrelated) meaning nearby correlations will tend to be different, while for $\alpha > 0.5$ the correlation will be persistent meaning nearby values will become increasingly similar.

The literature has many examples of non-gaussian fractional statistics in addition to the permeability of different sediments previously mentioned. It is found that such statistics ought to arise whenever the correlation length, ξ becomes infinite. Again, this illustrates that there is no characteristic length scale to the system. This is the key property of scale invariant systems whose consequence is the power-law relation Eq.4.1.

Quite naturally it becomes a point of interest to understand how the critical properties of AIP change under these conditions, primarily because we understand that by virtue of the correlations power-law behavior must persist on all scales. Naively, one might fail to properly appreciate the unique impact of long-range correlations on critical behavior since one might well consider any other kind of change to the site lattice structure and consider its affects. However, as Harris [14] found in considering the effects of random defects on the critical temperature of the Ising model, the only defects that can have an effect are those whose correlation length, ξ_H is comparable to the correlation length of the unmodified lattice, ξ. Thus, since near the critical point ξ is described by a power-law, only those defects whose statistics similarly produce long-range correlations could have any effect on the critical behavior. Any short-range correlations would fail to meet this criterion. This reiterates the focal feature of critical behavior, where small scale interactions can eventually become renormalized, and only those that persist on all scales can contribute to its behavior.

Harris provided a powerful framework for anticipating the effect that changes in lattice structure could have on subsequent behavior [14]. Weinrib [1] extended Harris' formulation specifically to the percolation problem. We will cover the basic elements for the

framework necessary to understand how long-range correlations ought to affect the behavior of percolation systems.

We consider correlations that are sufficiently long-range while also convergent for all distances, and whose autocorrelation function is given by

$$C(r) \sim r^{-a} \tag{4.2}$$

where r is the distance between sites, and a is less than dimension d. Since this is the percolation problem, the autocorrelation function describes the correlations in site occupation, that is, the likelihood that two sites a distance r apart are occuppied. The long-range correlations are therefore an additional mechanism contributing to the site occupation probability other than the usual uniform occupation probability, p.

Specifically, we would like to know how distinct regions experience different effective occupation probabilities, p_l. To that end, we break up the lattice whose total linear dimension is L into regions of size, l. There will be $N_L = l^d$ such regions in the lattice. We will consider how the average occupation probability changes as a function of subregions size given by

$$\langle p_l \rangle_L = \frac{1}{N_L} \sum_{i \in N_L} p_i \tag{4.3}$$

where p_i is the occupation probability associated with the i-th lattice site, and the average is over the entire lattice. To understand how correlations in the fluctuations behave, we compute the variance in subregion occupation probability, p_l given by,

$$\langle \delta p_l^2 \rangle_L = \frac{1}{N_L^2} \sum_{i,y \in N_L} \langle p_i p_j \rangle \tag{4.4}$$

The function $\langle p_i p_j \rangle$ is exactly the auto-correlation function we seek to implement given by Eq.4.2, therefore we can integrate the correlation function up to the size of the correlation length ξ which define the extent of correlations. That is, we assume $L \sim \xi$

which gives the following integral:

$$\begin{aligned}\langle \delta p_l^2 \rangle_L &\sim \xi^{-d} \int_0^{\xi} dr\ C(r) r^{d-1} \\ &= \xi^{-d} \int_0^{\xi} dr\ r^{-a+d-1} \\ &\sim \xi^{-a}\end{aligned} \tag{4.5}$$

If the system is still to have a single uniform critical transition, then it should be the case that these fluctuations produce a correlation length less than that of unmodified transition. That is the fluctuations should be less than critical fluctuations leading to the condition

$$\begin{aligned}\frac{\langle \delta p_l^2 \rangle}{(p_c - p)^2} &\sim (p_c - p)^{a\nu - 2} \\ &\to 0\end{aligned} \tag{4.6}$$

where we made use of the relation $\xi \sim (p_c - p)^{-\nu}$ to expand the ratio. For the ratio to go to zero near the critical point we require the exponent to be greater than zero. This leads to the condition on a for the largest value of long-range correlations such that it will affect the critical transition while preserving a existence of a uniform transition. This is given by

$$a\nu - 2 > 0 \tag{4.7}$$

Thus, we can expect changes to the critical behavior if $a > 2/\nu$. For percolation where $\nu = 4/3$, we should expect that the minimum value requires $a > 3/2$.

We might naturally next ask, if a meets the minimum threshold, then how should we expect the behavior to change as function of a? As Weinrib points out [1], we can effectively understand the situation by considering competing long-range correlation mechanism in the correlation function as

$$C(r) = Ar^{-a} + Br^{-b} \tag{4.8}$$

To leading order the exponent with smallest magnitude will dominate on the largest scales. Thus, we would then expect that for $a > 3/2$ we should observe an effective correlation length scaling given by ν_a

$$\nu_a = 2/a \tag{4.9}$$

While percolation with long-range correlations has been studied in the past with interesting changes to network properties [2], and also applied to IP with [8], our AIP model is sufficiently different such that (with its looplessness and avalanche burst dynamics) it is necessary to understand how the critical and network aspects of our model change as a result.

4.3 Fourier Filter Correlation Method

It is common to parameterize such long-range scale invariant correlations using the Hurst exponent, where the (auto)correlation function, $C(r)$ defined as $C(r) = \langle u(r')u(r+r')\rangle$ has the following behavior:

$$C(r) \propto r^{2H} \tag{4.10}$$

Here, H is the Hurst exponent and in light of the results of the previous section, we find the correlations are antipersistent for $\alpha = 2H < 1/2$ and persistent for $2H > 1/2$. For $2H = 1/2$, the statistics follow fractional Gaussian noise, being neither persistent nor antipersistent.

There are a number of techniques for simulating fractional Brownian statistics [15]. We use the Fast Fourier transform (FFT) filter technique because of its computational efficiency. This technique relies on imprinting the desired correlations in the Fourier wave vector space, $\vec{k}$, and then applying an inverse FFT (IFFT) to create a lattice with correlated sites of form Eq.4.10. Formally, we will be working with 2 dimensional Fourier transforms, and it is well known that the Fourier transform of the autocorrelation function gives the Fourier power spectral density. That is, the correlation function, $\langle u(\vec{x})u(\vec{x}+r)\rangle$ and the power spectral density $S(\vec{k})$ are related according to:

$$\langle u(\vec{x})u(\vec{x}+r)\rangle = \int_{\mathcal{R}^n} S(\vec{k})e^{-i2\pi\vec{k}\cdot\vec{x}}d\vec{k} \tag{4.11}$$

We can make use that we are only concerned with the distance between two points. This leads to a suitable definition of a radial wave vector defined as $k_r = \sqrt{1+s^2+t^2}$ and with a switch of coordinates allows us to write it as a one dimensional Fourier transform:

$$C(r) = \int S(k_r)e^{-i2\pi k_r r}2\pi k_r dk_r \tag{4.12}$$

To create correlations of the form Eq.(4.10), our power spectral density should be made to follow the following power-law:

$$S(k_r) \propto \frac{1}{k_r^{\beta}} \tag{4.13}$$

To relate the exponents between Eq.4.10 and Eq.4.13 we can solve Eq.4.11 after substituting Eq.4.13 which gives the following integral to be solved:

$$C(r) = 2\pi \int k_r^{-\beta+1} e^{-2\pi i k_r r} dk_r \tag{4.14}$$

To solve the above integral we first make use of the following relation:

$$\frac{1}{k^{\beta}} = \frac{2\pi^{\beta/2}}{\Gamma(\beta/2)} \int_0^{\infty} \lambda^{\beta-1} e^{-\pi\lambda^2 k^2} d\lambda \tag{4.15}$$

The right side is easily Fourier transformed and upon switching the order of integration, we get:

$$\int_{\mathcal{R}} e^{-\pi\lambda^2|k|^2} e^{-2\pi i k r} dk = \lambda^{-1} e^{-\pi|r|^2/\lambda^2} \tag{4.16}$$

Then taking the 2D Fourier transform of both sides and plugging into Eq.4.15 gives:

$$\begin{aligned}
\int_{\mathcal{R}} k^{-\beta+1} e^{-i2\pi k_r r} dk_r &= \frac{2\pi^{\beta-1/2}}{\Gamma(\beta-1/2)} \int_0^{\infty} d\lambda \lambda^{\beta-2} \left[\lambda e^{-\pi|r|^2/\lambda^2}\right] \\
&= \frac{2\pi^{\beta-1/2}}{\Gamma(\beta-1/2)} \int_0^{\infty} d\lambda \lambda^{(\beta-2)-1} e^{-\pi|r|^2/\lambda^2} \\
&= \frac{2\pi^{\beta-1/2}}{\Gamma(\beta-1/2)} \frac{\Gamma((\beta-2)/2)}{2\pi^{1/2-\beta+1/2}} \frac{1}{|r|^{1-\beta+1}} \\
&\propto r^{\beta-2}
\end{aligned} \tag{4.17}$$

Setting the exponents equal between the final line of Eq.4.17 and Eq.4.10 gives:

$$2H = \beta - 2 \tag{4.18}$$

This gives our final relationship between the Hurst exponent and the appropriate Fourier power spectrum filter function exponent:

$$\beta = 2(H+1) \tag{4.19}$$

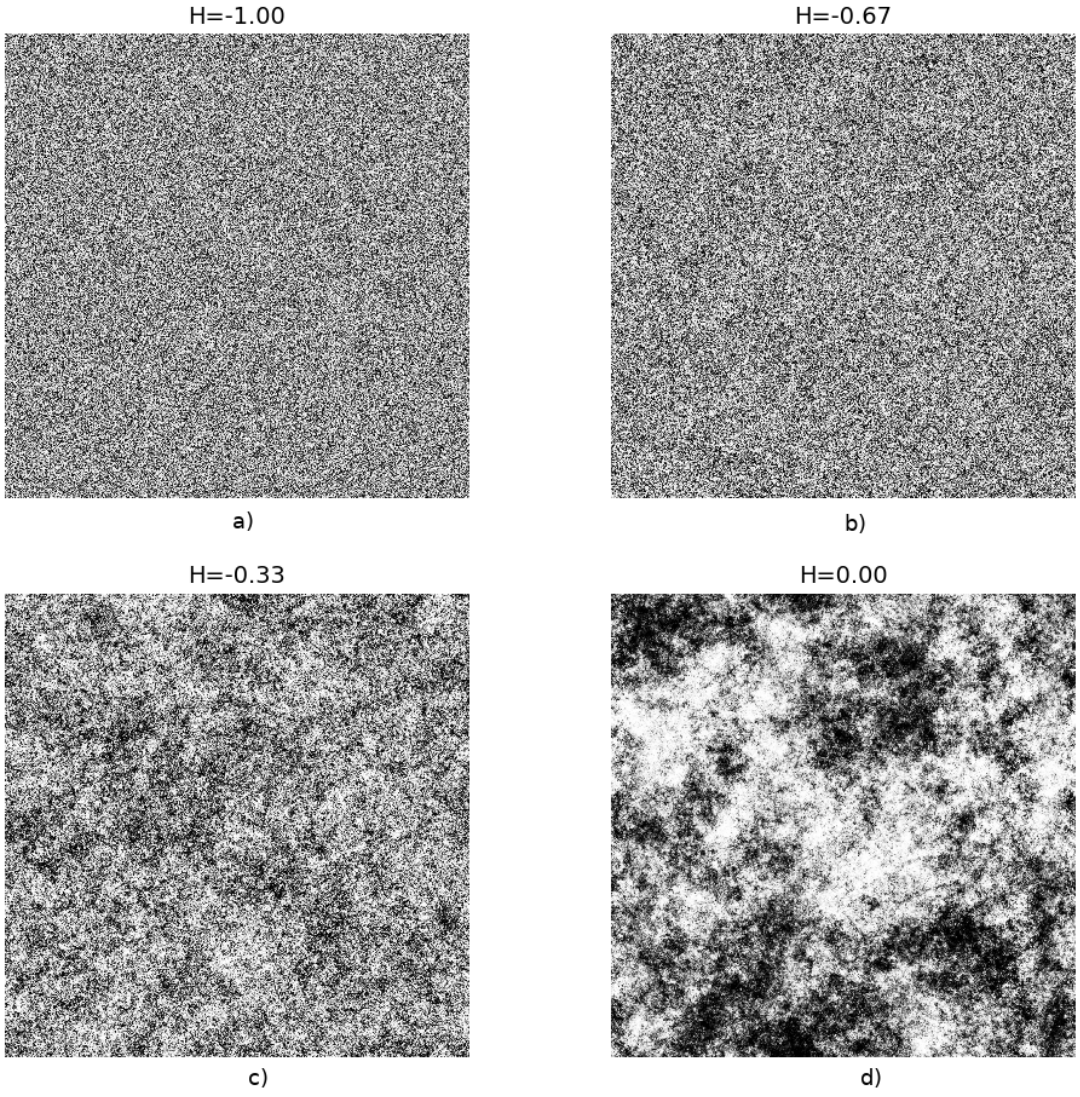

Figure 4.1. Sampling of lattices with increasing correlation. We show how the lattice sites become increasingly correlated as the generalized Hurst exponent increases from -1 to 0. a) $H = -1.0$ corresponds to the random case. b) $H = -0.67$ corresponds to antipersistent correlations c) $H = -0.33$ corresponds to persistent correlations d) $H = 0.0$ corresponds to increasingly large correlations where clustering of similar strengths is clearly observable.

Because the Hurst parameterization is typically 1D (given by Eq.4.10), but we rely on a 2D fourier transform parameterized in terms of β, whose value is shifted by 1 in 2D relative to 1D, we need to shift the value of the exponent of α by 1 as is show in Eq.4.19. Thus, if $\alpha = -1.0$ we get no long range correlations, and if $\alpha = 0$ we get Brownian long range correlations, whose power spectra behaves like k^{-2}. Since we construct the

correlated lattice by applying a Fourier filter characterized by $\beta = 2(\alpha + 1)$, we use α in range $[-1, 0]$.

More importantly, for these reasons we adopt a modified Hurst parameterization which shifts its values by -1. This comes at some risk since in much of the literature $\alpha = H$, and use the standard range, $[0, 1]$. We choose our parameterization in order to make explicit the need for a mapping between 1D and 2D Hurst characterizations. We suspect that this oversight may in part explain why previous authors report compact clusters for $H > 0.5$. Over the shifted range we preserve the fractal structure of our clusters. We find compact clusters begin forming for $H > 0.5$ which corresponds to an unshifted value of $3/2$. Such a value certainly would drive clusters to become compact. For the generalized Hurst exponent, we expect antipersistence for $H < -1/2$ and persistence for $H > 1/2$. For $H = -1/2$ we expect fractional Gaussian statistics.

4.4 Correlation Algorithm

We execute this Fourier filter technique using an FFT on a NxN dimensional array with complex coefficients [16]. The algorithm is outlined as follows:

1. We generate a NxN array with each value, h_{nm}, assigned a random value from a Guassian probability distribution.

2. We execute a 2D Fast Fourier Transform (FFT) giving an array of complex coefficients, H_{st}.

3. We define radial wave number k_r, which is non-zero for $s = t = 0$, as follows:

$$k_r = \sqrt{1 + s^2 + t^2} \tag{4.20}$$

4. Since $S(k_{st}) \propto |H_{st}|^2$ we define a new set of complex coefficients, H_{st}, multiplied by the appropriate filter function:

$$H'_{st} = H_{st}/k_r^{\beta/2} \tag{4.21}$$

5. Apply an inverse FFT (IFFT) on H'_{st} to produce a new NxN array with coefficients, h'_{st} with the desired correlations.

6. Apply the error function, $erf(h'_{st})$, to return a uniform correlated distribution with values in range [0,1].

We illustrate an example of the types of correlations produced by our algorithm in Figure 4.1.

4.5 Static Network Properties

IP was intended to simulate the quasi-static displacement of one fluid by another through capillary forces. The networks produced simulate long time expectations of systems eventually able to achieve equilibrium. These networks are frequently characterized by universality classes which in principle reflect symmetries in the lattice itself and are therefore insensitive to the distinct network growth mechanisms. However, the precise extent to which static network properties become insensitive to the growth mechanism is still an area of interest, so here we outline some of the static network properties and how these change as a result of the input long-range correlations.

In a previous study we characterized some of the essential network properties of our model [10]. This study utilized free edge boundary (FEB) conditions along both axes primarily due to ease of implementation. In a subsequent study we implemented periodic edge boundary (PEB) conditions in order to better establish the universality class of the exponents characterizing the model. We found PEB conditions reliably yielded the infinite lattice limit for the scaling exponents. Finally, a growth algorithm with PEB complements the implementation of site correlations as the Fourier filter technique described before also enforces periodic conditions in assigning site strengths to the lattice.

The first characteristic exponent is the scaling of occupied cluster sites, $M(L)$, with lattice size L. This scales with characteristic fractal dimension D_f according to:

$$M(L) = L^{D_f} \tag{4.22}$$

We can easily extract exponent D_f using the well-known box counting technique [16] and perform a linear fit using linear least squares (LLS) on a log-log plot.

Figure 4.2 shows the extracted D_f for different H. For the random case, $H = -1.0$, we reproduce the fractal dimension consistent with RP, $D_f = 1.895 \pm 0.016$. We find that

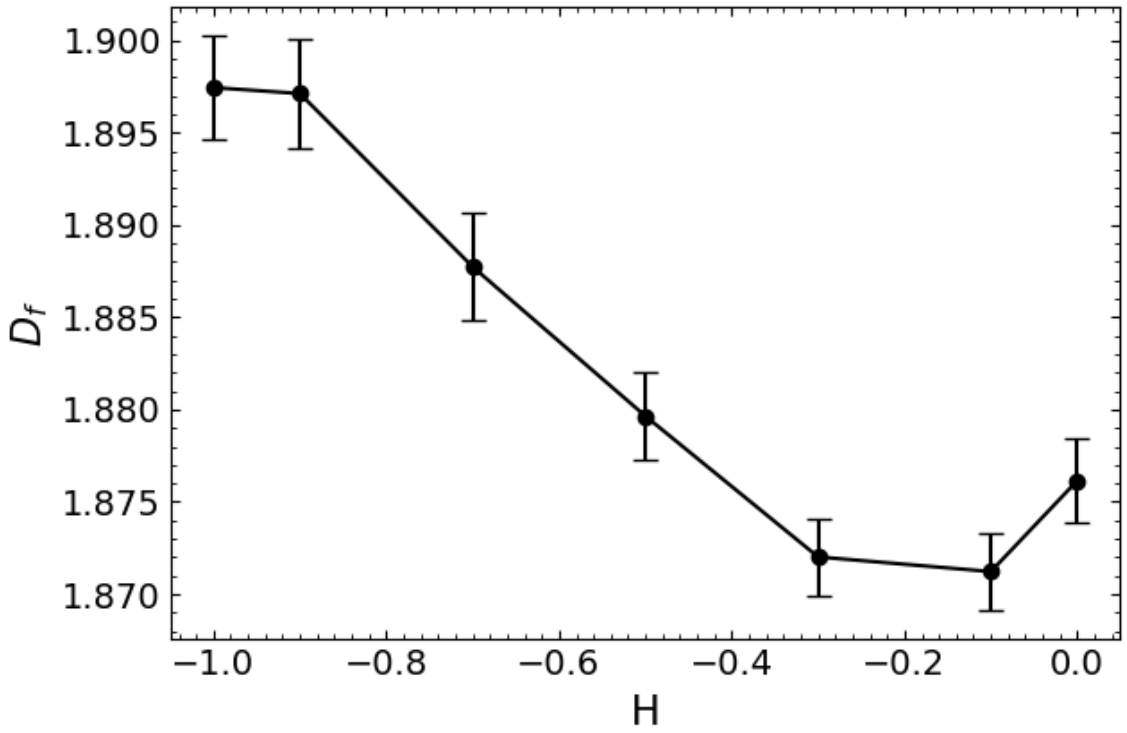

Figure 4.2. The fractal dimension, D_f for different H. For the random case, $D_f = 1.895 \pm 0.016$ which is similar to the expected value of RP. The values all seem to be consistent with one another and do not suggest much change as the correlation changes over the range of the study. For $H = 0.0$, $D_f = 1.939 \pm 0.028$, which is inconsistent at the 1σ from some of the other values.

input site correlations do not significantly affect the fractal dimension measure in the range of our study. This highlights the macro nature of this measure which is relatively insensitive to changes.

This is somewhat consistent with [3] which looked at RP with the same long-range correlations and found no change to D_f except for $H > -0.3$ and where the $D_f \to 1.95$ as $H \to 0$. The authors of [4] found similar behavior. Other authors report no detectable change in D_f [2] which considered equivalent H correlation in the range $[-1, 0]$. That we observe a change in D_f for $H > -0.9$ illustrates a difference between IP and RP growth mechanisms.

Perhaps more importantly is that we observe clear evidence that the site correlations change the density of the invaded sites, since site density is determined by, $\rho \sim L^{d-D_f}$. As observed in the Ising and percolation critical transition, changes in the order parameter

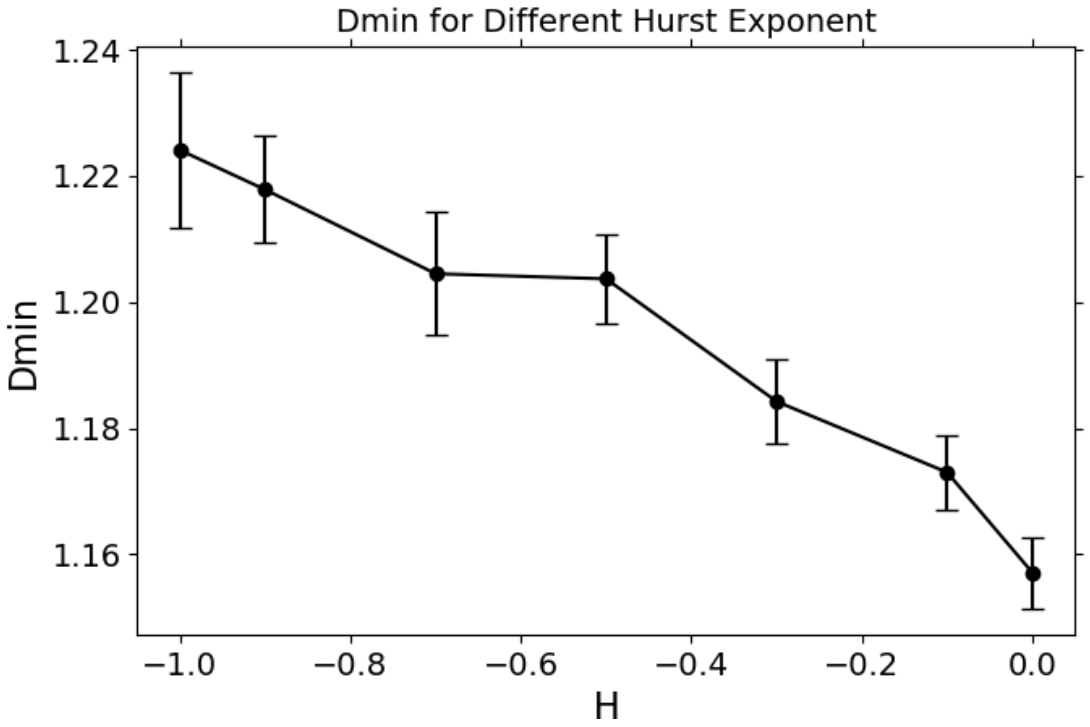

Figure 4.3. The scaling of distance between sites for different H. For the random case $D_{min} \approxeq 1.22$, this tends to decrease as H tends to 0. The loopless condition will prevent a cluster from becoming compact and D_{min} from becoming 1.

induce changes in the density. In our previous characterization of critical behavior of our model, we found that because ρ did not change, the notion of an order parameter seemed superfluous. However, now that this is no longer the case, we should expect the changing density to influence critical behavior of the model.

Previous studies on the trapping variant of long-range correlated IP in 2D found cluster behavior becomes non-fractal (compact) for $H > 0.5$ [17], though in this study they considered $0 \geq H \geq 1$. In another study the authors of [9] considered a non trapping variant similar to ours and found a minima as we did in the range of our study. While D_f for RP seems to remain unchanged at least for $H < -0.3$, for IP D_f decreases to a minima before likely increasing towards 2 as H increases above zero.

Though the effect of correlations on D_f is relatively small, we can better understand the effect of correlations on the resulting clusters by looking at the minimum distance between invaded sites. The basic formalism follows that outlined in Section 2.3. Where

D_{min} is the fractal dimension of the shortest path.

We find that as H increases, D_{min} tends to decrease. This behavior is reflected in Figure 4.3. We understand this behavior as follows: for the random case, we expect to find "holes" (trapped regions in IP cluster with loops) in the cluster which are also scale invariant. The paths and the distance between sites in the cluster will necessarily become circuitous. If site strengths are correlated such that similar strengths group together, and given that IP grows by breaking the weakest sites, the IP algorithm will naturally seek out connected regions of weaker sites. This means that fewer portions of the lattice will need to be sampled as the path between two connected sites becomes more direct since it is the result of correlations to create connected regions of weak site regions. Similarly, there will be larger regions devoid of any cluster growth as strong sites will likewise preferentially occupy these regions. This helps us understand the behavior of D_f which is related to the density exponent according to $D_f - 2$. The smaller D_f corresponds to a less dense cluster occupying the lattice, although locally in regions around the cluster, the cluster becomes more dense. This trend starts to reverse for $H > -0.1$, as the dense local cluster regions make up more of the lattice than the large voids filled with strong sites. Once again, the loopless condition will prevent D_{min} from becoming 1 because some paths will not be allowed in order to maintain the existence of only 1 path joining sites in the cluster.

This behavior is similarly summarized by looking at the backbone exponent D_{BB} as the authors of [2] did with RP. They found that as H increases D_{BB} approaches D_f, meaning that th majority of the cluster exists along the cluster backbone. This qualitatively has the effect of causing the cluster to become both more dendritic and compact as the Hurst exponent increases.

4.6 Critical Threshold

One of the most important features of percolation is its relation to critical phenomena [18]. In the previous section we looked at the static network properties of a percolation cluster, however, criticality is characterized by the structure of fluctuations near the critical point which grow to dominate all scales of the system. This then becomes much more a question

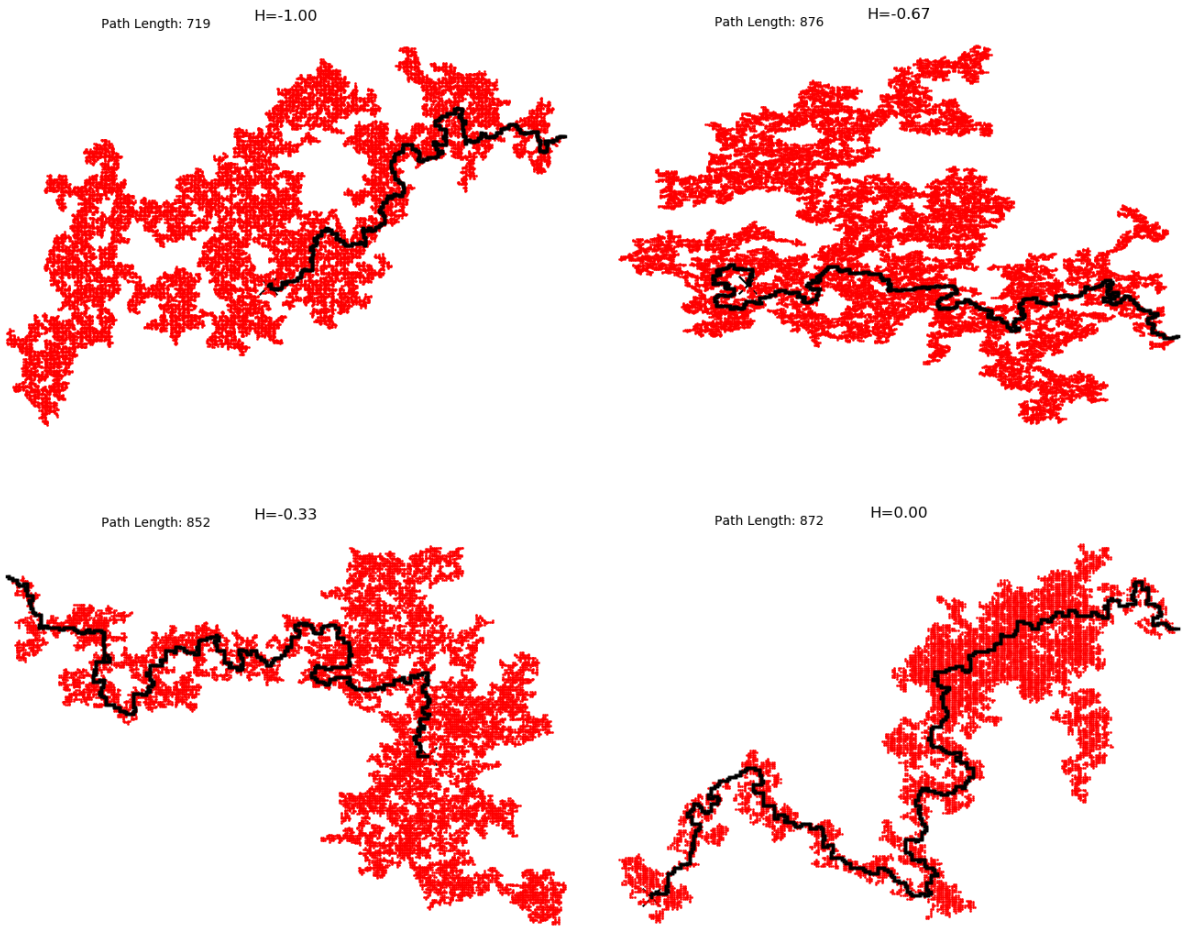

Figure 4.4. Comparison of clusters grown with different correlation exponent, H. As $H \to 0$ the clusters becomes more dendritic and compact.

of how the cluster grew to occupy its final form.

In RP the site occupation probability, p, serves as the control parameter for RP's second order phase transition. This phase transition is described by the emergence of global connectedness where the many isolated clusters existing in regime $p < p_c$ conglomerate into a single lattice spanning cluster for $p \sim p_c$. To better elicit the connection between RP and IP, it is instructive to understand how RP's critical point manifests itself in IP.

We begin by looking at the distribution of site strengths of the invaded cluster. In IP all lattice sites are randomly assigned values from a uniform distribution in the range [0,1], but when looking at the distribution of the strengths of invaded sites, we find the selection of strengths to be a regular subset of assigned strengths. In particular, in the limit where the number of invaded sites, N, becomes infinite, the invaded strength distribution is described by a step function:

$$\lim_{N\to\infty} p(r) = \begin{cases} k & 0 \geq r \geq r_{max} \\ 0 & r > r_{max} \end{cases}$$

where a random strength, r, has constant probability k, of being invaded up to some strength, r_{max}. These are related according to $1/k = r_{max}$, and it has been shown that $r_{max} = p_c$ where p_c is RP's critical occupation probability [19].

Without a threshold, a cluster grown by IP (random) will grow indefinitely, and reproduce many of the characteristic exponents of RP's incipient infinite clusters (IIC), which is why IP is believed to reproduce the emergent incipient infinite cluster which defines RP's connected state [20]. A threshold in IP effectively acts in the same way as the occupation probability for RP. This can be understood heuristically as follows: we assign lattice site strengths from a uniform distribution in the range [0,1] as is usual, but then only invade sites if its strength is below some predetermined threshold. A cluster will terminate its growth once it exhausts all perimeter sites with strength less than the threshold. However, if the threshold is $r_{max} \geq p_c$ then it becomes possible to grow a cluster infinitely. Thus growing a cluster with threshold equal to p_c will grow an independent realization of RP's emergent IIC.

However, to better understand the critical aspects of IP, we need to understand the

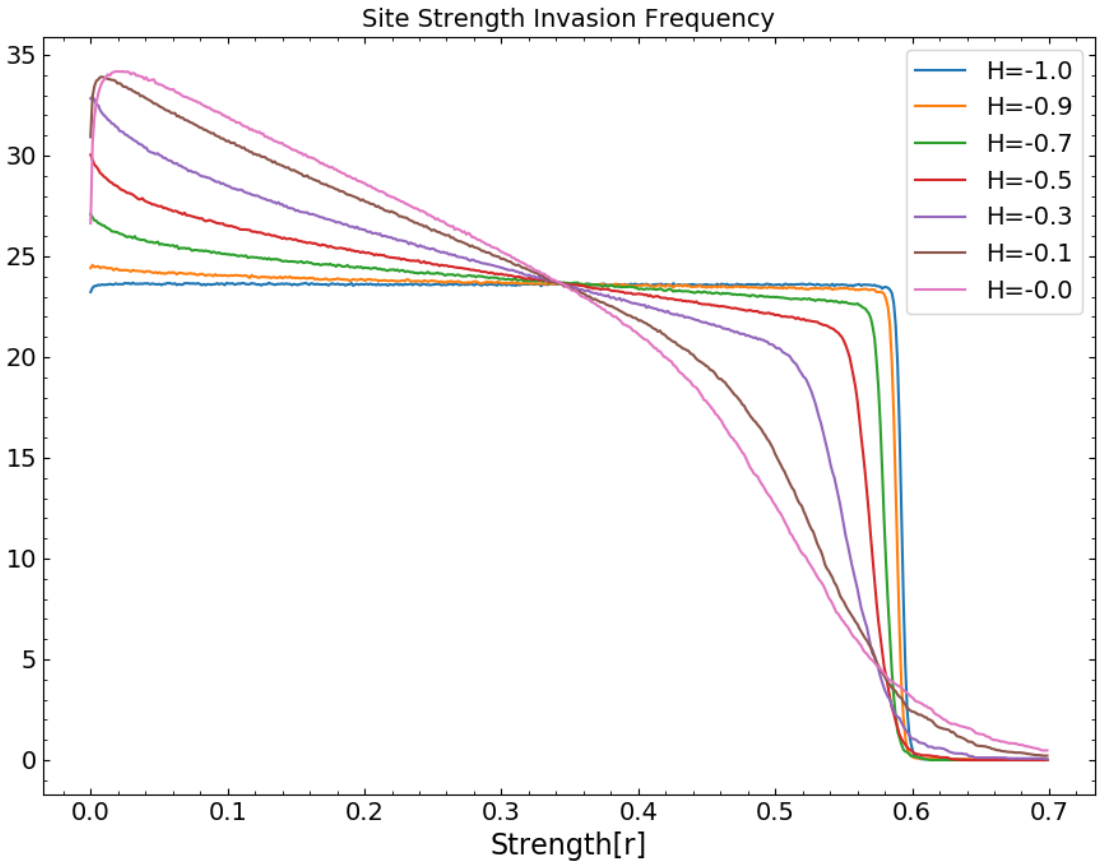

Figure 4.5. The changing distribution of invaded strengths for different correlation Hurst parameter, H. For the independent random case ($H = -1.0$) we recover an approximate step function reflecting constant probability of invading a particular site up to r_{max} anywhere in the cluster. As spatial correlations increase it becomes increasingly likely to sample weaker sites.

structure of fluctuations, and here the threshold seems to control the type of fluctuations which occur and will be discussed in detail in the next section. (This is the idea behind the notion of our burst mechanism presented in [10], and indeed we find that at the critical threshold the cluster size distribution is scale invariant.) Here we aim to understand how the critical threshold, which is r_{max} in the random case, changes under the application of long-range correlations to lattice site strengths.

A flat uniform distribution of invaded sites is evidence that regardless of where in the lattice the growth takes place, the likelihood of a particular strength to be invaded remains constant. If instead we could sample weaker sites with more regularity than stronger ones,

we would no longer observe a flat probability, and subsequently, the threshold would change depending on the local ratio of weak/strong bonds. This is precisely the scenario introduced when introducing long-range correlations into the assigned strengths. Fig4.5 shows how the distribution of invaded sites changes as a result of changing correlation exponent, H.

Previous studies with RP on long-range correlated lattices have shown that the p_c changes depending on the Hurst parameter, H [2]. Other authors have tried to use $p - p_c \sim L^{-1/\nu}$ relationship to determine p_c but this becomes problematic as ν changes as a result of long-range correlations in a non-trivial way [3] and as is shown in Section 4.2.

For our purposes we would like to generalize our AIP model which requires us to establish a burst threshold which serves to define distinct bursts grown from within a cluster. An important feature arises with the introduction of long-range correlations: this feature being that the local strength environments produces sufficiently different thresholds such that the notion of global lattice threshold breaks down.

Input correlations of type in Eq.4.19 will produce produce mean strength fluctuations defined as are described by described by:

$$< u(r')u(r'+r) >= \left\langle \delta s^2 \right\rangle - \left\langle \delta s \right\rangle^2 \tag{4.23}$$

where $\delta s = u_i - x$ and u_i is strength of the ith site and x is the random non-correlated component of the strength. We find the mean strength fluctuations are also described by:

$$\left\langle \delta s^2 \right\rangle - \left\langle \delta s \right\rangle^2 \sim r^{-2H} \tag{4.24}$$

which we recognize as also describing the second moment of the strength distribution, which will have well-defined mean for $2H > 2$ and well-defined variance for $2H > 3$. Thus by construction the variance of average strengths is poorly defined since the tail events are not exponentially bounded. This results in infinite variance. Moreover, even average values for quantities resulting from averaging over distinct regions will not be well behaved. Thus, any averaged macroscopic quantity will be poorly behaved.

An alternative notion for a burst could rely instead on a "bulk to boundary" ratio, r_{BB}. The authors in [2] used a similar argument to determine p_c with long-range correlations

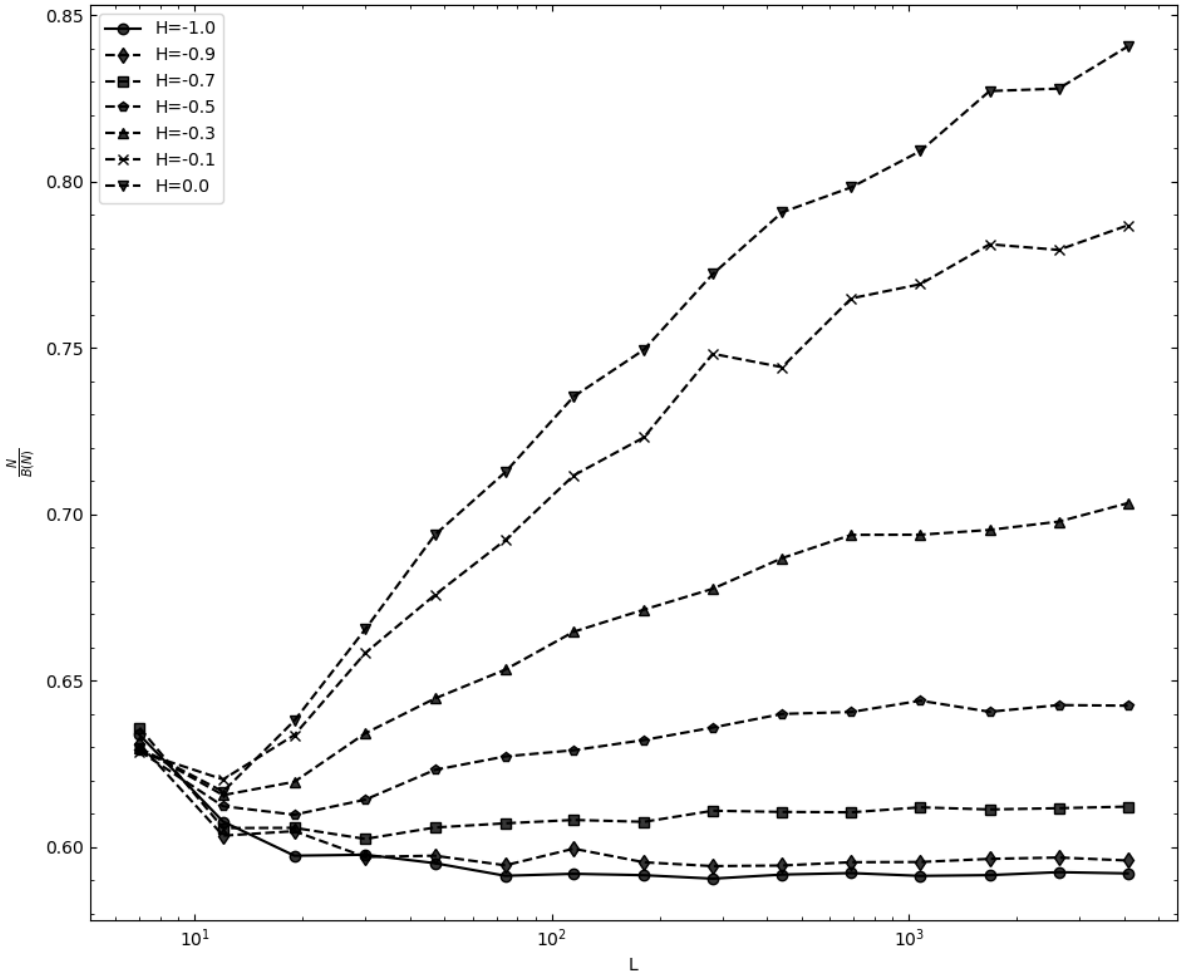

Figure 4.6. Here we show how the "bulk to boundary" ratio changes as a function of Hurst correlation exponent H. For random case ($H = -1.0$) we see the ratio approach $p_c = T_c$, but for $H > -0.5$ the ratio fails to asymptote to a known value.

where they determined p_c by noting which p_{occ} produced a ratio of one between the perimeter of filled and unfilled sites. Using a similar strategy authors have argued that using a "bulk to boundary" ratio as a generalized way to determine the critical occupation probability [21]. However, determining the ratio analytically using:

$$\lim_{N\to\infty} \frac{N}{B(N)} = T_c \tag{4.25}$$

leads to slightly different results since $T_c \to p_c$ in the random case. In Leath's original paper [22] the expression for the probability of finite clusters of size n with b empty perimeter sites assumed sites with independent random probabilities. One must instead empirically determine the ratio needed to produce scale invariant distribution of bursts.

We empirically determined the ratio, r_{BB} for our clusters for different H. We found that the behavior of r_{BB} did not universalize in any way to allow us to preserve the notion of a collective critical point. Not only do the values of stable ratios change, but we find that for $H > -0.5$, r_{BB} fails to asymptote to a fixed value. These results are shown in Fig4.6.

With random IP we were able to establish the existence of a critical threshold, but with long-range correlations, these relationships no longer hold. In the next section we discuss how the phase transition is smoothed such that there is no longer a power-law divergence with the control parameter as $T \to T_c$. The notion of criticality itself begins to break down, but its worth asking whether we have the correct notion of the critical control parameter such that we observe universal critical behavior in the presence of long-range correlations.

4.7 Correlated Critical Behavior

In this section we explore how the Hurst long-range correlations affect AIP's growth mechanism, and in particular, we would like to establish how site correlations impact the system's critical behavior. Of course, since criticality is inherently scale free, it is most sensible to extend AIP's behavior subject to PBC. In the previous study[7], we characterized AIP's critical Fisher type burst distribution, $n_s(\tau, \sigma)$, subject to PBC. This distribution, in conjunction with the correlation length scaling exponent, ν_I, produces a distinct universality class, though, only as a pseudo critical system due to the absence of a natural order parameter (and perhaps suggests the suitable way of categorizing all SOC systems). AIP's underlying growth mechanism utilizes the emergent long-range correlations of RP near the critical occupation probability. This property is derived from the behavior of fluctuations in average site occupation which scale according to $\delta\langle p_{occ}\rangle \sim L^{-1/\nu_R}$ (where ν_R is the RP correlation length scaling exponent). This is the emergent structure that allows scale invariant connected burst sequences to form. However, this inherited behavior from RP is altered in AIP because we switch from RP to IP growth dynamics by instead assigning strengths between [0,1] sampled from a uniform random

distribution. AIP then follows a simple path of least resistance algorithm to form a connected self-avoiding sequence of the weakest sites. The set of invaded sites and their associated strengths will form a subset of strengths in the range $[0,\ T_c]$ (where $T_c = p_c$) with characteristic length L^{-1/ν_I} ($\nu_I = 1.3$ slightly different from RP's $\nu_R = 4/3$). Bursts grown at T_c reproduce RP's incipient infinite cluster (IIC), and importantly do so without producing the adjoining distribution of finite clusters. This is the primary reason the two models differ. In AIP bursts grown near T_c, we continually sample IICs subject to an environment of already populated and grown with previous iterations of IICs. If we now input additional correlations that yield fluctuations in strength according to $\delta\langle h\rangle \sim L^{-H}$, this alters the mechanism responsible for the emergent structure, and we expect these to affect the effective correlation length and burst size distribution. If these quantities are altered then the overall critical behavior of the system must necessarily change.

To that end, we begin with a discussion of the correlation length scaling where we refer back to the fundamental finite size scaling hypothesis, the bedrock of criticality. We begin by addressing the question of how site strength correlations affect the correlation length, ξ.

For lattice systems, the notion of correlation length is generally understood by the correlation function (pairwise correlation function) which empirically has been established to behave according to

$$C(r) \sim r^{d-2+\eta} e^{-r/\xi} \tag{4.26}$$

Therefore, the correlation length, ξ, characterizes when random correlations become exponentially suppressed as a function of distance, r. If $\xi \sim L_{sys}$, then the correlations display long-range behavior described by a power law $C(r) \sim r^{2-d+\eta}$.

As before, the correlation length defines the statistical spatial extent of bursts, that is, the likelihood two sites a distance r apart are likely to belong to the same burst. Despite the effect of increasingly dominant Hurst correlations, burst characteristics still greatly depend on the burst threshold, and thus, we expect the correlation length to similarly depend on the burst threshold.

Though the characterization of $C(r)$ provides a rather simple, intuitive understanding,

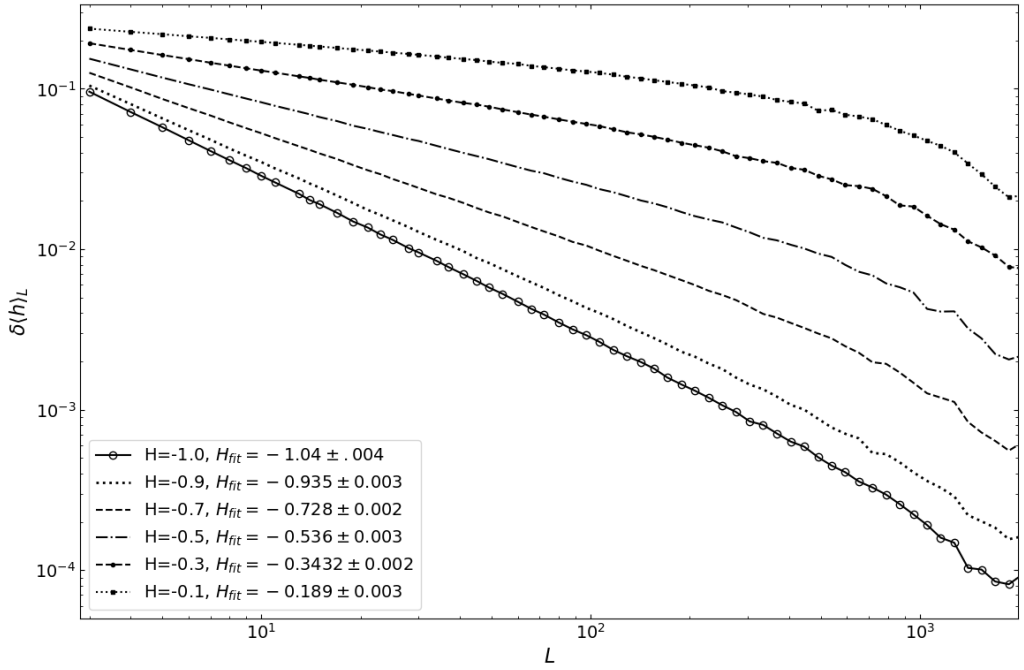

Figure 4.7. Mean site strength fluctuations. We show the expected scaling of lattice site strength fluctuations, $\delta\langle h\rangle_L \sim L^{-H}$.

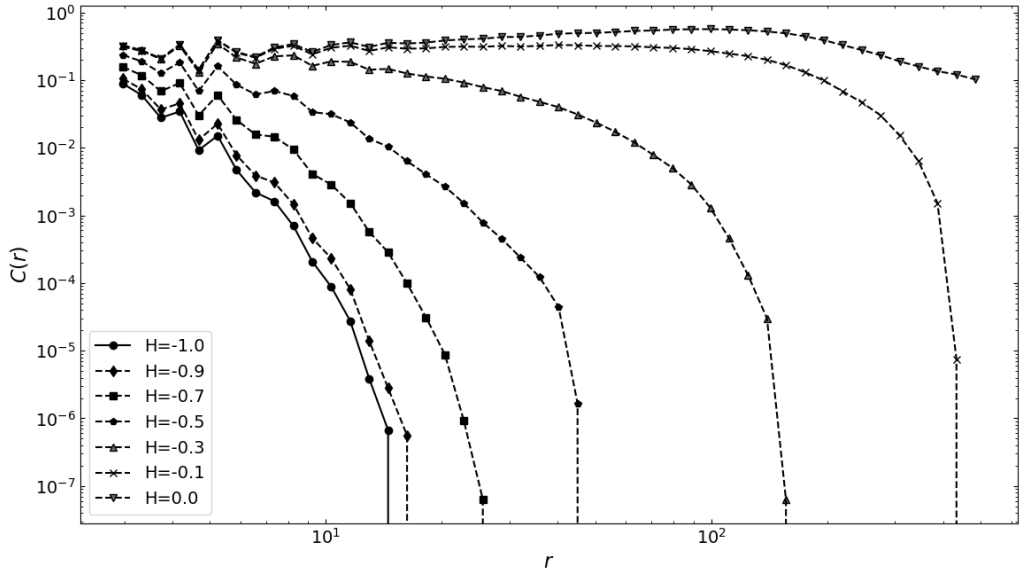

Figure 4.8. Here we show how the correlation function for different Hurst correlation values, H, changes. We fix the threshold to be $T = 0.25$ for all H, and we observe how the exponential decay constant, ξ varies from ~ 1 in the random case to $\sim L$ in the maximally correlated case.

it is seldom used in the literature since the pairwise correlation function is often very cumbersome to calculate. Its computations scale according to $O(N^2)$ with N sites/particle. Given an individual cluster ensemble contains 10^7 sites, of which we use $10^2 - 10^3$ ensemble elements to obtain reliable statistics, acquiring the requisite statistics quickly becomes computationally prohibitive. Fortunately, we were able to rely on a highly optimized and parallelized implementation to efficiently compute, $C(r)$ [23] which gave good results.

We find that the effect of long-range correlations on burst formation is to change the required threshold that is likely to produce an infinite sized burst (when $R_{gyr} \sim \xi$). The effect of H on correlation function, $C(r)$ is shown in Fig.4.8. In order to isolate the H dependence, we keep ϵ_T fixed for all curves and vary H. In the random case, we observe the usual $\xi(T)$ that becomes exponentially suppressed for burst of order 2, but with correlations we observe the additional H dependence, $\xi(T, H)$ which can greatly extend the correlation length despite keeping ϵ_T fixed. In fact, we can nearly reproduce the $C(r)$ near the critical value by merely changing H. One can work out that the expected relation is

$$\xi(T, H) \sim \epsilon_T^{1/H} \tag{4.27}$$

which agrees with the empirical results of Fig4.8. In our formulation, the random case corresponds to $H = -1.0$ which yields a correlation length of order $1/\epsilon_T$, while the maximally correlated case, $H = 0$, yields a strongly diverging correlation length and becomes strongly limited by the system lattice size, L_{sys}.

This effect shows how Hurst site correlations become increasingly dominant as correlations increase ($H \to 0$). We even find that the correlation length can be more dependent on Hurst correlations parameter, H, than the burst threshold used to define distinct bursts. This leads us to consider different regimes where the burst behavior is better described by Hurst site correlations and those regimes better described by typical critical parameter. As is common practice, we define a characteristic lengths, ξ_H and ξ_I to correspond to these respective length scales.

For length scales much smaller than the system lattice size, $l \ll L_{sys}$ we recover the typical description of critical behavior characterized by the scaling of the critical

parameter, and in the random AIP we found suitable scaling behavior for $\epsilon_T = (T_c - T)/T_c$. This characterization describes how the correlation length scales according to $\xi_I \sim \epsilon_T^{-\nu_I}$. This scaling is preserved for all length scales subject to the condition, $l < \xi_I$. For larger length scales we observe crossover phenomena driven by the affects of Hurst correlations on scales, $\xi_I < l < \xi_H$.

Briefly, we can anticipate this crossover behavior by recalling the arguments of the extended Harris condition which led to Eq.4.9. These results ought to describe the changes in correlation scaling under the condition that the global lattice correlation length uniformly diverges. As we will show, the divergences become increasingly smeared as Hurst correlations become increasingly dominant. This follows what was shown in the previous Section (4.6) which shows the critical point itself being spread out over a range. Also, Fig.4.10 shows the burst threshold likely to produce scale invariant bursts as a function of H. Not only does the required threshold drop, suggesting fewer range of strengths need to be sampled to grow arbitrarily large bursts, but also, the typical characterization relying on ϵ_T breaks down as the critical burst threshold becomes degenerate.

Despite the Hurst correlations becoming dominant on the largest of scales and near the critical point, we can still see evidence of more traditional critical behavior described by burst threshold parameter, ϵ_T, away from the critical point. By looking at the zeroth and first moments (number of bursts and average burst size) of the burst distribution, we can observe qualitative differences associated with changing H. One way to quantify the onset of crossover behavior is by recognizing that the width of the critical transition region scale with ξ_H^{-H}. That is, the fluctuations become dominated by the Hurst correlations. However, so long as $\epsilon_T > \xi_H^{-H}$ the scaling should be dominated by the usual scaling dependent on ϵ_T.

We can observe this regime in Fig4.9, where we can see similar behavior of the moments up until the vicinity of the critical point where the behavior radically departs. This is evidence for crossover phenomena where for $l < \xi_I$ we get behavior largely characterized by ϵ_T, and a departure from this behavior for $l > \xi_I$. Further, we can notice that the curves of different H do not lie on top of each other, indicating that the scaling exponents

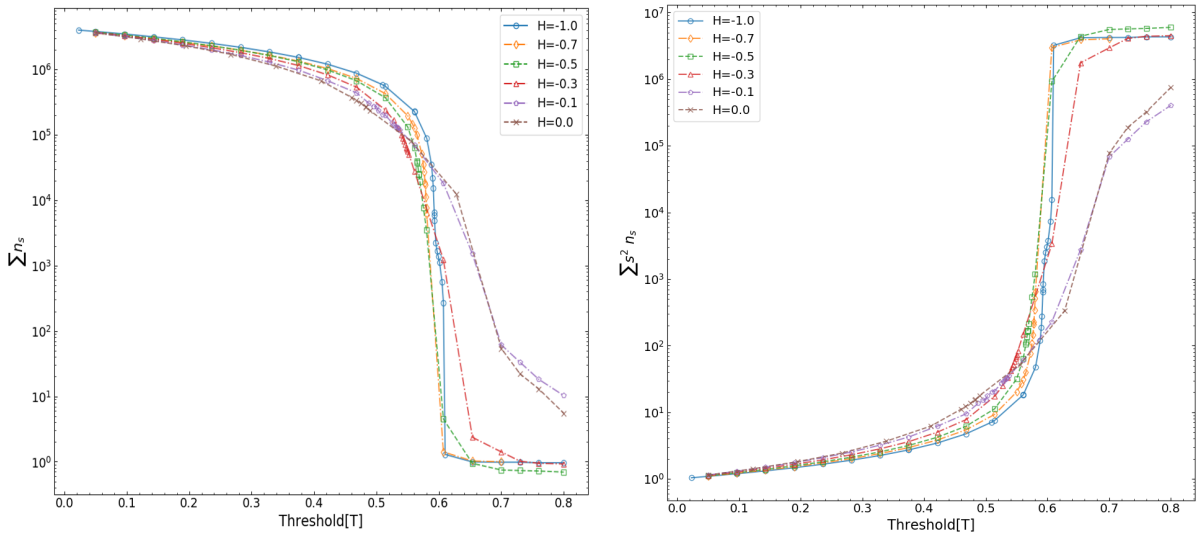

Figure 4.9. Here we show how the cluster distribution moments fail to diverge, except for the random case ($H = -1.0$). The transition region becomes increasingly broadened as the Hurst correlation parameter increases. (left) This plot represents the zeroth moment and corresponds to the number of bursts as a function of threshold, T. (right) The behavior of the second moment corresponding to the average burst size as function of threshold, T.

ought to be different. In this case, the zeroth and second moments are given by α, γ and we do find changes with these scaling exponents as H changes.

The essential bit of evidence for critical behavior is the existence of Fisher type burst distributions, and we observe the existence of scale free burst distributions for all ranges of H we considered. As we showed previously, we were largely able to define the critical behavior by characterizing the burst distribution, namely, $n_s(\tau, \sigma)$. This strongly suggests that a similar description should be appropriate here where we begin with the description of a critical threshold, T_c.

As was suggested by Fig.4.10, there exist distinct critical thresholds which give rise to distinct cluster/burst distributions for different H. So long as $\epsilon_T > \xi_I^{-1/\nu_H}$, we expect there to exist a scale invariant distribution of bursts up to some scale ξ_I. Our task is to understand precisely how the critical behavior changes with H in this regime. To that end, we might expect a precise relationship governing $\tau(H)$, since from Fig.4.11 we can see an increasing magnitude of τ as H increases. An increase in the magnitude of τ translates to the general trend that prefers cluster growth by smaller bursts rather than larger ones. However, Fig.4.9 shows average burst size decreasing only very near the critical point and

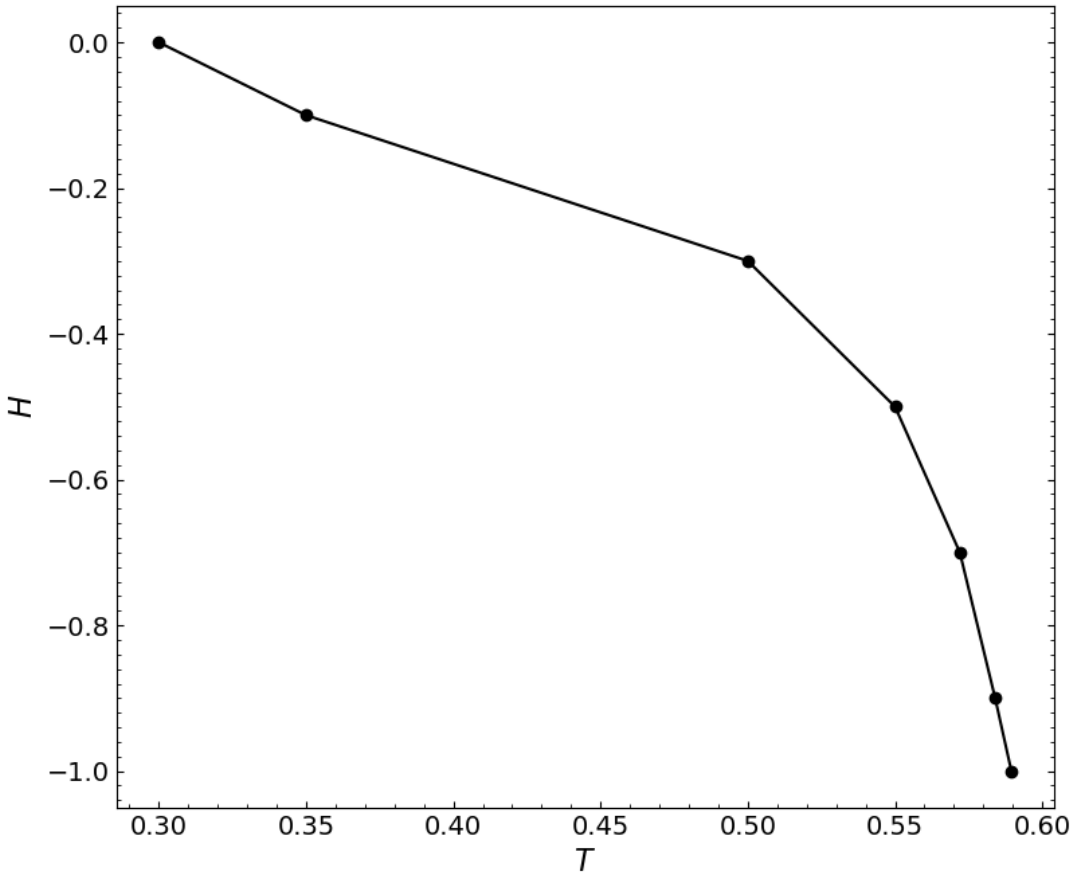

Figure 4.10. Here we show how the value of thresholds, T, changes with H. It is $\xi(T, H) \sim L_{sys}$ that gives rise to scale invariant burst distribution.

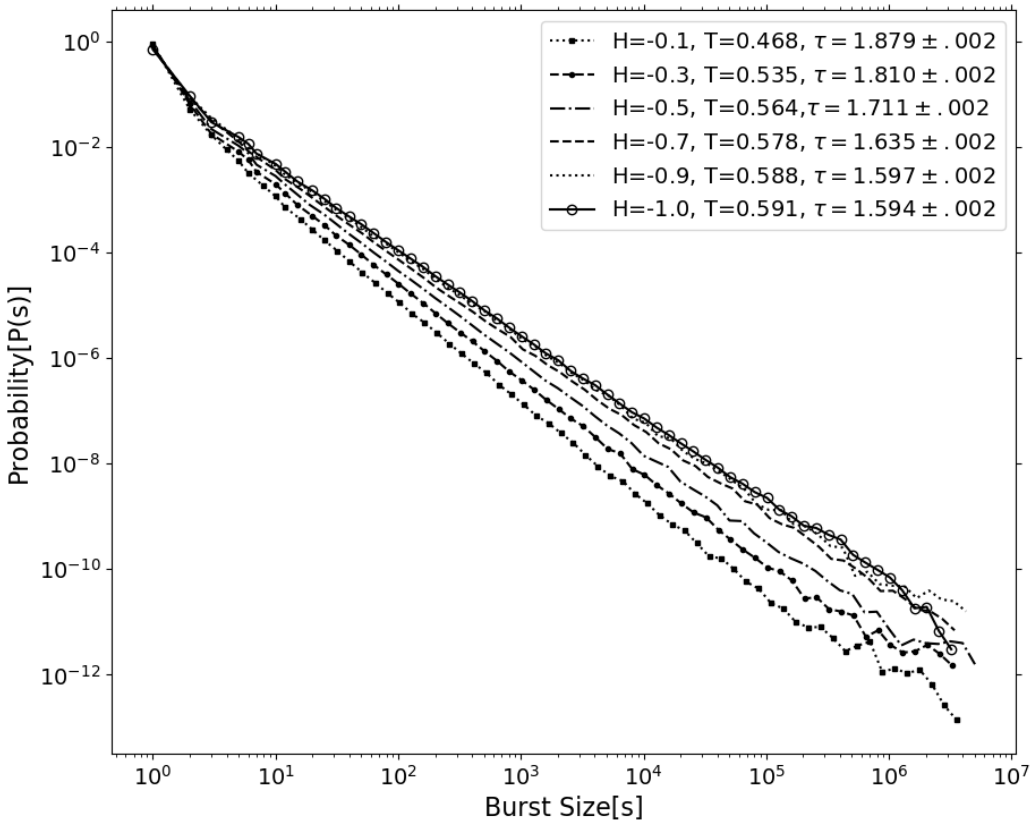

Figure 4.11. The burst size frequency-magnitude scaling for different Hurst correlations, H. We observe a spectrum of τ exponents [1.59, 1.90] characterizing the burst size distribution as H changes. As Hurst correlations increase $\tau \to 2$ which indicates a preference for smaller burst sizes.

above. Below the transition value, the tendency is for cluster growth to occur via larger average burst sizes as Hurst correlations increase. This is further evidence of a crossover type of phenomena near the transition regime. Still, we will want to be able to account for this somewhat contradictory behavior in our description.

Of course, one of the nice features of working with the burst distribution is that we can directly calculate the expected behavior of the average burst size scaling. This is done

with the usual moment calculation,

$$M_k = \epsilon_T^{\frac{1+k-\tau}{\sigma}} \int_0^1 dz\ z^{k-\tau} f[z] \tag{4.28}$$

where here $k = 2$, $z = (T_c - T)s^\sigma$, and in the upper limit, we observe the relation $s \gg (T_c - T)^{-1/\sigma}$. Thus, $s_\xi(T) = (T_c - T)^{-1/\sigma}$ behaves as the exponential cutoff cluster size for the cluster size distribution. Since the integrand evaluates to a constant, we once again get the familiar γ exponent relationship

$$\gamma = \frac{2 - \tau}{\sigma} \tag{4.29}$$

However, we must characterize the burst cutoff size s_ξ. This is done with the relation $s_\xi = \xi^{D_s}$ from Eq.4.22 and leads to the exponent relation

$$\frac{1}{\sigma} = D_s \nu \tag{4.30}$$

There is a slight distinction between $D_s \approx 1.865$ and $D_f \approx 1.896$ in the random case, which does not significantly affect the critical behavior, and these differences decrease for increasing Hurst correlations since $D_s \sim D_F$. As was discussed previously and found in Section 4.5, these fundamental mass-length scalings change very little for changing Hurst correlations, therefore, this leads to the important behavior of ν which we introduced in Section 4.2.

By plugging Eq.4.30 into Eq.4.29 we establish the following relation:

$$\gamma = (2 - \tau) D_s \nu \tag{4.31}$$

which will allow us to determine how the average burst size ought to behave as a function of exponents τ, ν. We expect from the extended Harris criteria that the site strength correlations become relevant when their associated correlation scaling becomes larger than that of the random case, $\nu_H = 1/H > -4/3$. While we do see some minor effects for $H = -0.9$ on the correlation length scaling, we generally observe behavior consistent with the extended Harris criteria, which tells us that for $H > -3/4$ the correlation exponent ν_H is given by

$$\nu_H = 1/H \tag{4.32}$$

	D_f	D_s	$1-\eta$
$H=-1.0$	1.897 ± 0.003	$1.860 \pm .002$	$1.804 \pm .009$
$H=-0.9$	1.894 ± 0.003	$1.857 \pm .002$	$1.79 \pm .01$
$H=-0.7$	1.888 ± 0.003	1.863 ± 0.002	$1.79 \pm .01$
$H=-0.5$	1.880 ± 0.002	1.867 ± 0.001	1.794 ± 0.007
$H=-0.3$	1.872 ± 0.002	1.855 ± 0.002	1.78 ± 0.01
$H=-0.1$	1.871 ± 0.002	1.850 ± 0.002	1.77 ± 0.01

Table 4.1. Static scaling exponents.

	T_c	τ	ν	γ_{obs}	γ_{th}
$H=-1.0$	0.5926(5)	1.594(2)	1.301(2)	0.971(5)	0.9825
$H=-0.9$	0.590(1)	1.597(2)	1.359(2)	1.025(3)	1.017
$H=-0.7$	0.580(5)	1.635(2)	1.47(2)	1.041(5)	1.00
$H=-0.5$	0.570(5)	1.711(2)	1.95(2)	1.066(3)	1.052
$H=-0.3$	0.54(1)	1.810(2)	3.1(1)	1.10(2)	1.09
$H=-0.1$	0.48(9)	1.90(5)	7.6(5)	1.18(1)	1.4

Table 4.2. Critical scaling exponents. This shows a comparison of scaling exponents for AIP model with different Hurst correlations H, where $H=-1.0$ is the random case ($H=0$ in the usual formulation) and Hurst correlations increase with increasing H. We used a 4096x4096 lattice with PBC to generate statistics. In order to account for any remaining finite size affects, we set the burst size threshold to be 10^6. We used at least $10^6 - 10^9$ bursts for all statistics, depending on the proximity to the critical point. The error represented in parenthesis of the final digit is the error in the LLS fit. We find that critical relations start breaking down as $H \to 0$, indicating critical processes no longer govern behavior.

We confirm this behavior by calculating ξ_H in the standard way [7, 24]. The obtained scaling is reported in Table 4.2.

As we observed previously, it is somewhat unexpected that the average burst size should increase with decreasing, τ. Eq.4.31 neatly provides an explanation for why the average burst size increases despite the burst distribution preferring smaller clusters. The

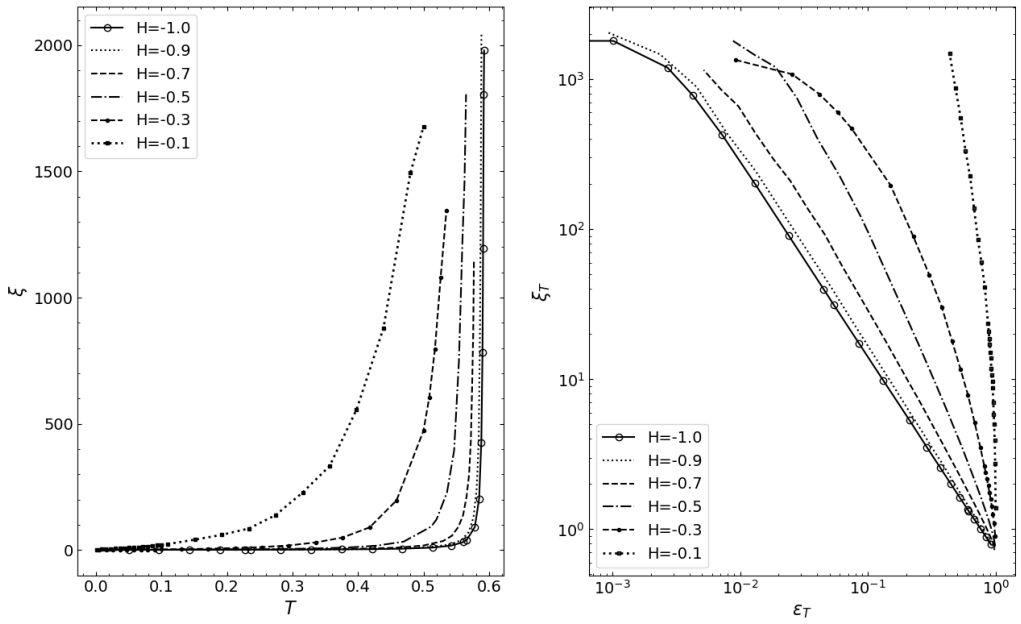

Figure 4.12. Correlation length comparison for different Hurst correlations, H. This is generated from the statistics of over 10^7 bursts grown with PBC on lattice of size 4096x4096. (left) We plot the correlation ξ_T vs burst threshold, T. (right) We plot the burst critical scaling with critical parameter, ϵ_T. For the random case with $H = -1.0$, we get correlation length scaling exponent, $\nu = 1.30$, which is nearly similar to the RP value. Also, we can confirm that for $H > -3/4$ we get correlation length scaling exponent given approximately by $\nu_H \sim 1/H$.

necessary condition is for ν_H to increase more drastically with H than the decrease of τ. Since ν_H largely follows the extended Harris relation, we can see that this condition is satisfied, and the result is increasing magnitude of the γ exponent. We verify Eq.4.31 by numerical average burst size calculations.

We summarize the behavior of the system for length scales, $l < \xi_b$, as being primarily critical in nature since we observe a correlation length governed by $\xi_l \sim \epsilon_T^{-\nu_H}$. This correlation length scaling forms the basis for a family of interdependent critical exponents and most importantly the existence of a scale invariant burst distributions characterized by exponents, τ, $\sigma(\nu)$. Some exponents change very little $(D_f, D_s, 1-\eta)$, while others change quite noticeably (τ, ν). These family of exponents potentially give rise to a whole host of distinct universality classes if these properties are extrapolated to the entirety of a system, but we are careful to note that these relations only hold up to a certain

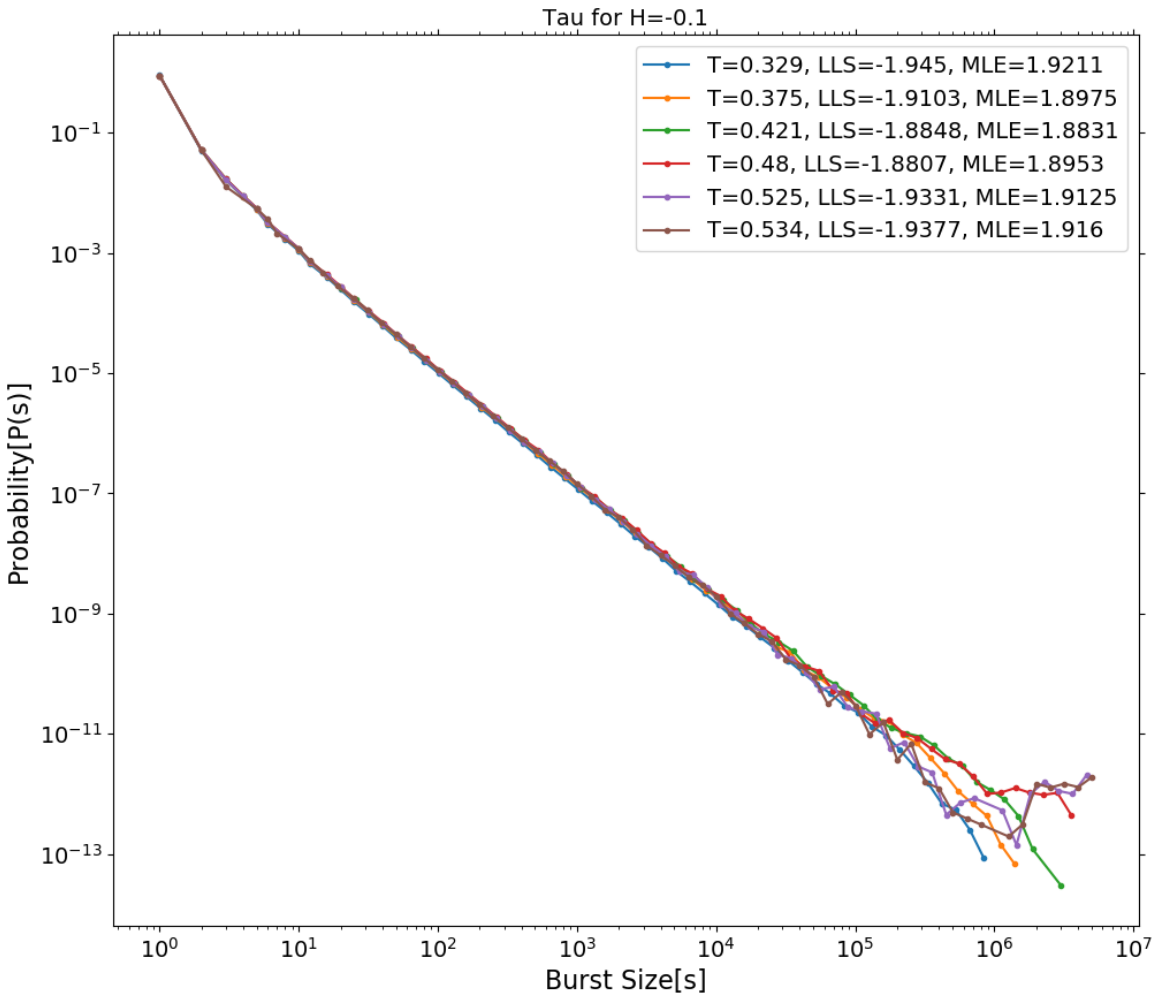

Figure 4.13. Burst scaling for correlated case, $H = -0.10$. Each curve represents the burst statistics for different burst thresholds, T. Also shown are the linear fits to each curve represented by LLS and by MLE methods. The threshold becomes degenerate as a wide range of thresholds lead to similar burst scaling statistics. We see a family of power-laws for thresholds in the range $[0.329, 0.534]$ which produce scaling exponents τ in the range $[1.88, 1.92]$

length scale, namely, for $\xi < \xi_H$. In fact, our system more importantly displays crossover phenomena where the critical point gives way to new behavior governed by the Hurst correlations.

The reason for crossover phenomena stems from the requirement of the extended Harris criteria which relied on the existence of a global, uniform lattice transition. Should this condition exist, we would fail to observe crossover phenomena, but this condition fails precisely because the transition is smeared over a range of thresholds. The effect of

Hurst correlations is to produce distinct regions of site strengths which alter the threshold required to grow scale invariant bursts within these pockets. This range of thresholds is given by $\xi_H^{-1/H}$ and therefore quickly increase as $H \to 0$. Further, these correlated regions themselves are scale invariant by construction which is what effectively permits a range of threshold to produce the same scale invariant bursts. We can see primary evidence of this for $\xi > \xi_H$ by looking at the Fisher burst distributions, $n_s(T)$ for different T. Fig4.13 gives an example of the degeneracy of burst distributions for different thresholds for $H = -0.1$. We observe a wide range of thresholds produce nearly the same scaling. This suggests that the burst distribution scaling is governed primarily by the correlated scale invariant pockets of site strengths rather than the avalanche burst threshold mechanism. This fundamentally alters the mechanism generating the critical Fisher distribution from the avalanche burst type to Hurst correlations, and importantly admits mechanisms that are non critical in origin (at least not governed by $\xi \sim \epsilon_T^{-\nu}$) to produce a scale invariant burst distribution. This last point is particularly important since the presence and characterization of the Fisher distribution has largely been adequate in motivating and confirming critical behavior. Here, we have an example of such a distribution absent the usual mechanisms that drive a critical transition; one where the ϵ characterization fails to describe scaling behavior. Still, the correlation length of the system is a power law, but it does not diverge as a function of the proximity to the critical point, and therefore fails to satisfy the requirements of second order phase transition mechanics.

For behavior with length scales, $l > \xi_I$ we observe crossover behavior where the dominant length scale becomes the Hurst correlation length scale, ξ_H. On this length scale we expect fluctuations to be governed by $\xi_H^{-1/H}$ and general property scaling of a function to be given by $f(l, \xi) = \xi_H^a f(l/\xi_H)$.

We can find an interesting way this crossover behavior manifests itself within the general framework characterizing our system. Returning to the correlation function, if $\xi(T, H) \to \infty$, then we get power-law scaling of the correlation function given by $C(r) \sim r^{2-\eta}$ since the exponential term goes to one. Of course, since we simulate finite sized clusters, the condition of an infinite correlation length is when $\xi > L_{sys}$. This insures that

there is very little deviation from power-law over the calculable range of r. In practice, this is done by choosing a burst threshold suitably large ($T > T_c$) so as to observe power-law behavior for r up to L_{sys}. In this limit we find very little difference between the η exponent for different H and it remains very near the random uncorrelated case.

A complementary technique for calculating the average burst size comes from the fundamental, fluctuation dissipation theorem [25] which relates the susceptibility to average site strength correlations. In the language of percolation this becomes a relation between the pairwise correlation function mentioned previously, $C(r)$, and the average burst size, $\langle s \rangle$ [24, 26]. The relationship is given by

$$\langle s \rangle = 1/V \int dV C(r) \tag{4.33}$$

where V is typically taken to be the correlation volume given by, ξ^d. Again, we compute $C(r)$ using [23] with good results. With $C(r)$ given by Eq.4.26 we can rewrite Eq.4.33 as

$$\begin{aligned} \langle s \rangle &= \xi^{-2} \int dr \; r^{2-\eta} \exp^{-r/\xi} \\ &= \xi^{-2} \xi^{3-\eta} \int_0^\infty dz \; z^{3-\eta} \exp^{-z} \\ &\sim \xi^{1-\eta} \\ &\sim \epsilon_T^{\nu(1-\eta)} \end{aligned} \tag{4.34}$$

where $z = r/\xi$ and the integrand yields a constant. The last line also makes use of the usual critical scaling relation $\xi \sim \epsilon_T^{-\nu}$ which we know is valid on smaller length scales. This gives another relation,

$$1 - \eta = (2 - \tau) D_s \tag{4.35}$$

by plugging into Eq.4.31. Since $1 - \eta$ and D_s are nearly constant for changing H, we would similarly expect τ to be nearly constant, but this of course is not true as is shown in Fig4.11. Solving the above equation for τ gives a value near 1.59, which is the burst distribution scaling for the random case and for $\gamma \sim 1$.

This contradictory result indicates the dominant fluctuations and average cluster size no longer scale in the same way. Knowing that there exist multiple correlation lengths in the system, it is problematic to integrate over all length scales without distinguishing

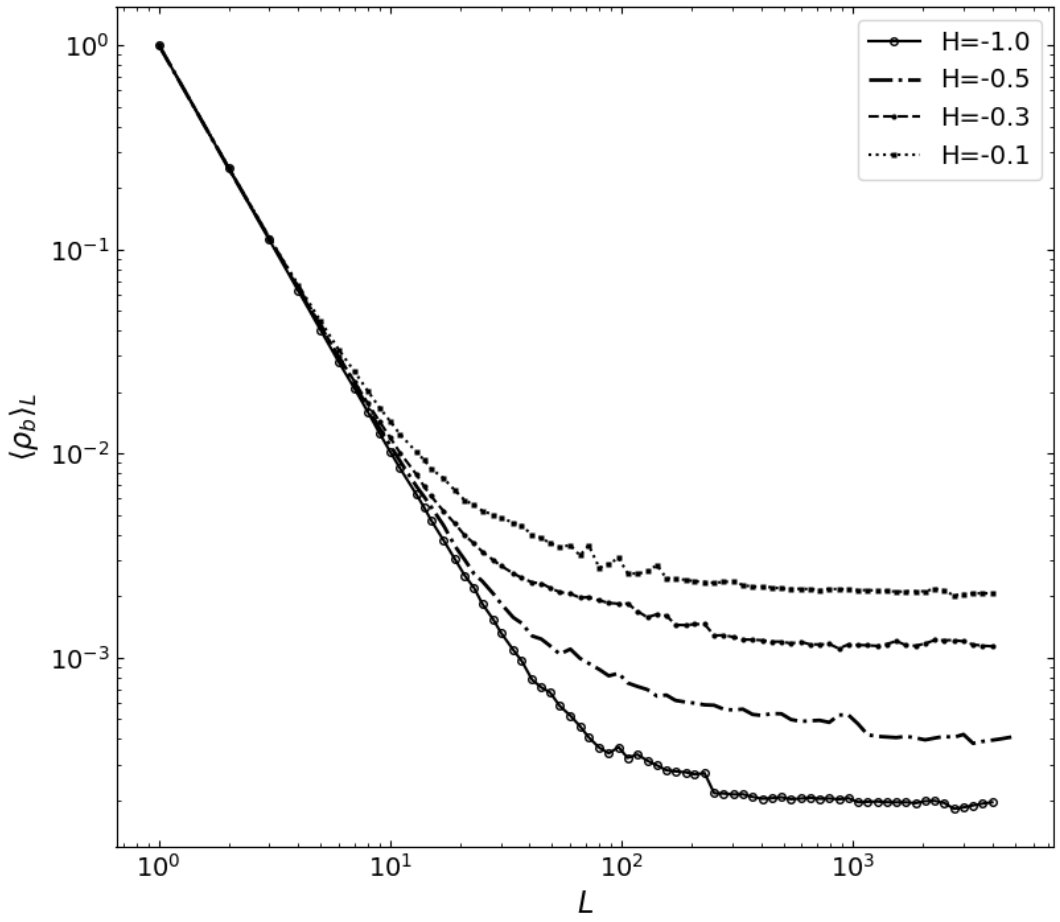

Figure 4.14. We show the crossover behavior inherent to AIP subject to different H. We find that average burst epicenter density follows correlation length determined by $\xi_I \sim \epsilon_T^{-1/2}$ for small scales and ξ_H^{-H} at the crossover.

length regimes. If we consider the scaling of larger bursts, then we find an average burst size that scales according $(1-\eta)/H$, where this relation predicts a much more dramatic increase in cluster sizes as H increases. For example, for $H = -0.3$ we expect $\gamma \sim 2.5$, in contrast to the 1.1 we observe for scales up to ξ_I. The failure of the fluctuation dissipation theorem as originally defined provides further evidence that behavior departs from the usual critical fluctuation scaling dominating percolation transitions, which is entirely interrupted by Hurst correlation effects.

Finally, in our previous work [7], we found the burst epicenter scaling differed from

the general site mass scaling. This result is significant because it suggests the existence of multiple correlation lengths. One correlation length is associated with the likelihood of sites to occupy different burst clusters, and the other correlation length is associated with the likely distance between burst centers. By looking at the scaling of average burst epicenters density, $\langle \rho_b \rangle$ as a function of length scale, we found the expected crossover behavior where for lengths less than ξ_I we get scale invariant $\langle \rho_b \rangle$ and nearly homogenous $\langle \rho_b \rangle$ for length scales greater. The scaling of ξ_I as function of burst threshold also was found to behave with mean-field correlation exponent, $\xi_I \sim \epsilon_T^{-1/2}$, suggesting that burst epicenters were distributed as a random walk about the lattice.

With the addition of Hurst correlations, there is yet another correlation length to factor, and we find scale invariant $\langle \rho_b \rangle$ on smaller length scales, but the crossover length scales for different H follow ξ_H^{-H} dependence. However, the threshold dependence still follows a random walk characterization. Fig4.14 shows how the crossover length of $\langle \rho_b \rangle$ changes for different H. Namely, we can see that this length follows ξ_H^{-H} as it gets shorter as $H \to 0$.

The behavior of $\langle \rho_b \rangle$ provides an instructive way to understand why the generalized burst scaling breaks down. The crossover length above which $\langle \rho_b \rangle$ becomes uniform, indicates that burst with characteristic length above this must uniformly spaced. A burst with a much larger characteristic length would necessarily cause a great void, and thus because burst centers are distributed according a random walk, this will necessarily limit the maximum size a burst can grow. Since this happens at a smaller length scale for larger correlations, we expect to see a preference for smaller bursts which is what we find since $\tau \to 2$ for $H \to 0$.

4.8 Discussion

In our previous study [27], we found that the AIP model was not the usual critical system. Rather, it was built upon the inherent scale invariance of RP and AIP's growth mechanism, which largely preserved scale invariance while altering the generalized critical scaling behavior in non-trivial ways. Absent an order parameter, it is not appropriately

described as the transition of the system from one phase to another, rather, it seems to describe the growth mechanism of the meta-stable spinodal state, since it still produced a characteristic critical Fisher type distribution. In this study, we include the addition of long-range order input from site-strength Hurst correlations. The result is that the clustering behavior of sites into bursts is changed, and therefore alters the resulting critical Fisher distribution. Up to length scale, $l < \xi_I$, we get descriptions of different classes of meta-stable spinodal type growth governed by H, but more importantly, we find that the existence of $n_s(\tau, \sigma)$ is preserved even when the underlying burst mechanism was not critical in nature (ie is not governed by critical parameter, ϵ_T). In this regime, the long-range order of the background correlated lattice of site strengths could preserve scale invariant bursts over a wide range of length scales regardless of burst threshold.

With these additions, we have been able to distance the behavior of correlated AIP from traditional critical mechanisms. This offers some interesting possibilities. First, because the existence of critical systems required the system to be at a rather finely tuned point between small scale order and large scale disorder, namely near the critical point, it is fair to wonder whether traditional critical theory can appropriately describe all forms of emergent long-range order (a potentially rare event, since we would necessarily have to rely on a single point in all of phase space). SOC systems offered the advantage in that they do not require systems to be finely tuned to a particular value of phase space, rather, a small external driving mechanism allowed the system to form meta-stable growth dynamics which results in the system innately growing in the critical regime. In many ways SOC growth dynamics seem to describe the potentially long-lived meta-stable states describing droplet nucleation and spinodal states. Authors have noted the similarity between SOC variants of tradition critical systems. For example, [28] shows how in SOC singularities arise not from order parameters but instead from control parameters which have a critical value. Also, [29] argues for the existence of characteristic ratio driving the behavior of SOC systems.

While our findings support these claims, here we also show how scale invariant behavior resulting from the competition of correlation mechanisms allows us to consider an even

wider range of possibilities. Ever since Fisher showed that much of critical behavior could be characterized from characterization of a critical distribution, $n_s(\tau, \sigma)$ [30], it has been widely assumed that the existence of Fisher type of distribution demonstrated critical behavior. In this study, we find this not to be true. We find a Fisher distribution even when the driving mechanism is not near its critical value. That is, the Fisher distribution exists largely independent of its proximity to the critical value (in our case the critical value is the burst threshold). Thus, not only do we escape needing to apply artificial phase transition mechanics, but also the need to argue for a self-organization about some general critical point. Thus, in systems with implicit long-range correlations, the correlation length of the dynamics is strongly determined by the long-range correlations, and done in such a way that preserves dynamic scale invariant properties (ie burst/cluster formation).

The generality of this result applies directly to broad extremal SOC type systems (of which AIP and CAIP belong), and can naturally be applied to stochastic energy minimization systems like interface motion in disordered media leading to domain walls [31], minimum spanning trees describing strongly disordered spin-glass models [32], abrupt species morphology changes through gradual changes in biologic fitness [33], and optimal neural topologies [34].

However, as much of our work is focused on the feature of the IP process which is best known as a drainage process of fluid infiltration [35–38], we focus on CAIP's application to fracture mechanics and induced seismicity[10, 27, 39, 40].

In [41], the authors argued for SOC description of tectonic seismicity producing rupture events with $b \sim 0.4$. This follows the work of [42, 43] among others that comparison of model event scalings should be made independent of the 3/2 energy scaling factor implicit in G-R scaling values. Tectonic seimicity is described by $b \sim 2/3$, which is closer to many mean-field models $b = 1/2$ and our random AIP model, $b \sim 0.6$. However, with correlations, we can obtain b-values in the range $[0.6, 1.0]$ depending on the H. This can in part account for the larger b-values associated with induced seismicity, $[0.8, 1.3]$.

However, given the wide range of observed induced seimic event scalings, it is likely necessary to account for the inherently 3D injection activity that only in some cases can

be constrained to be 2D. [44] shows how even within the same shale, the dimension of the injection activity can greatly differ. A previous study[45] attempted to parameterize 1D and 2D growth through an anisotropic preference for growth along one of the axes. In the limit where growth was strongly directed and along one axis, the burst scaling changed from $\tau(2D) = 1.52 \rightarrow \tau(1D) = 1.45$. This represents a change far too small to account for the diversity of b-values associated with induced seismicity if only the dimension is allowed to change. An instructive way to understand why increasing the dimension only has a small effect on burst scaling is to understand that all burst sizes are nearly equally likely to increase in size as a result of a new degree of freedom. Further, above the critical dimension (D=6) we expect all scaling to be mean field making this notion exact.

This problem is potentially side-stepped if we extend Hurst site correlations to 3D as well. We find burst epicenters to exhibit interesting behavior, being primarily distributed according to typical percolation process on small length scales, but exhibits crossover behavior for length scales greater than ξ_b where the burst centers are distributed according to a random walk. This means that clusters larger than ξ_b will not follow percolation type scaling, but tend to uniform density. This necessarily limits the probability of larger clusters.

In 2D we have already found that larger Hurst correlations prefer growth by smaller bursts, and when we allow this preference to be amplified by an additional degree of freedom, its likely that we will observe an even more dramatic change in burst scaling. We know that the random walk nature of bursting behavior is essentially preserved with the introduction of H, and permits a higher density of bursts then would be allowed if it were entirely a percolation system. This can account for event densities which are essentially uniform on large scales, and have mass scaling that is given by the usual non-fractal dimension scaling, d. Thus, by extending our model along with Hurst correlations into 3D we expect to reproduce a greater range of b-values.

Finally, the primary feature inherited by traditional critical (second order phase transition) phenomena is a single correlation length diverging with power-law behavior. In many real physical complex system, there may exist multiple correlation lengths domi-

nating behavior within their respective regimes. We have shown that depending on the growth dynamics long-range order can subsequently be modified through the competition of correlation mechanisms and alter the scale invariant behavior in non-trivial ways. Contrary to criticality requirements, we find the existence of multiple correlation lengths to be consistent with power-law behavior and indicative of SOC type processes where the critical nature is fundamentally changed. We still preserve many essential features, namely, the ability of a stochastic process to manifest itself across a wide range of scales, but the interference of competing correlation mechanisms alters the resulting behavior. Understood across all length scales, the correct approach is perhaps a multifractal one where the characteristic distributions behave with moment description, $M_k(L) \sim L^{y(k)}$, with the key additional understanding that for many of the scales of interest scale invariance is essentially preserved.

The multifractal framework [46] understood through the lens of the hierarchy of correlation lengths would have a set of fractal scalings describing the dominant singular behavior associated with each length scale. Briefly, in the case of a single length scale, which in addition give rise to hyperscaling, yields moment distributions in terms of correlation lengths according to

$$M_k(l, \xi) \sim \xi^{d-kD_f} f(l/\xi) \tag{4.36}$$

where k represents the k-th moment, D_f the characteristic mass scaling, and $f(l/\xi) \to 1$ for $l \ll \xi$. The essential behavior is that exponents of successive moments are equally spaced according kD_f, since k is an integer. Should we have $\xi_1 > \xi_2$ where ξ_1, ξ_2 are the respective characteristic length scaling regimes, with scaling exponents, D_1, D_2 then we would expect, for lengths $l > \xi_1$ to behave according to $\xi_2^{d-kD_2} \sim (l^{d-kD_1})^{d-kD_2} f(l/\xi_2)$ Then we expect moment dependence to have quadratic dependence on k rather than linearly, and thus for its successive moments to depend on $y(k^2)$. The inherently multifractal behavior of our model provides an excellent case study for developing and better understanding current multifractal analysis techniques.

4.9 Acknowledgements

The research of RAO and JBR has been supported by a grant from the US Department of Energy to the University of California, Davis DOE Grant No. DE-SC0017324.

References

[1] A. Weinrib, "Long-range correlated percolation," *Physical Review B*, vol. 29, no. 1, p. 387, 1984.

[2] S. Prakash, S. Havlin, M. Schwartz, and H. E. Stanley, "Structural and dynamical properties of long-range correlated percolation," *Physical Review A*, vol. 46, no. 4, p. R1724, 1992.

[3] K. Schrenk, N. Posé, J. Kranz, L. Van Kessenich, N. Araújo, and H. Herrmann, "Percolation with long-range correlated disorder," *Physical Review E*, vol. 88, no. 5, p. 052102, 2013.

[4] M. Sahimi and S. Mukhopadhyay, "Scaling properties of a percolation model with long-range correlations," *Physical Review E*, vol. 54, no. 4, p. 3870, 1996.

[5] H. A. Makse, S. Havlin, M. Schwartz, and H. E. Stanley, "Method for generating long-range correlations for large systems," *Physical Review E*, vol. 53, no. 5, p. 5445, 1996.

[6] B. B. Mandelbrot and B. B. Mandelbrot, *The fractal geometry of nature*, vol. 1. WH freeman New York, 1982.

[7] R. Ortez and J. B. Rundle, "Critical description of the avalanche burst invasion percolation mode," 2022.

[8] M. A. Knackstedt, M. Sahimi, and A. P. Sheppard, "Invasion percolation with long-range correlations: First-order phase transition and nonuniversal scaling properties," *Physical Review E*, vol. 61, no. 5, p. 4920, 2000.

[9] A. M. Vidales, E. Miranda, M. Nazzarro, V. Mayagoitia, F. Rojas, and G. Zgrablich, "Invasion percolation in correlated porous media," *Europhysics Letters (EPL)*, vol. 36, pp. 259–264, nov 1996.

[10] R. Ortez, J. B. Rundle, and D. L. Turcotte, "Universality class for loopless invasion percolation models and a percolation avalanche burst model for hydraulic fracturing," *Physical Review E*, vol. 103, no. 1, p. 012310, 2021.

[11] M. A. Knackstedt, A. P. Sheppard, and W. Pinczewski, "Simulation of mercury porosimetry on correlated grids: Evidence for extended correlated heterogeneity at the pore scale in rocks," *Physical review E*, vol. 58, no. 6, p. R6923, 1998.

[12] P. Leary and F. Al-Kindy, "Power-law scaling of spatially correlated porosity and log (permeability) sequences from north-central North Sea Brae oilfield well core," *Geophysical Journal International*, vol. 148, no. 3, pp. 426–442, 2002.

[13] H. Qian, "Fractional brownian motion and fractional gaussian noise," in *Processes with Long-Range Correlations*, pp. 22–33, Springer, 2003.

[14] A. B. Harris, "Effect of random defects on the critical behaviour of Ising models," *Journal of Physics C: Solid State Physics*, vol. 7, no. 9, p. 1671, 1974.

[15] Y. Fisher, M. McGuire, R. F. Voss, M. F. Barnsley, R. L. Devaney, and B. B. Mandelbrot, *The science of fractal images*. Springer Science & Business Media, 2012.

[16] D. Turcotte, *Fractals and Chaos in Geology and Geophysics*. Fractals and Chaos in Geology and Geophysics, Cambridge University Press, 1997.

[17] M. A. Knackstedt, M. Sahimi, and A. P. Sheppard, "Nonuniversality of invasion percolation in two-dimensional systems," *Physical Review E*, vol. 65, no. 3, p. 035101, 2002.

[18] M. Stephen, "Percolation problems and the Potts model," *Physics Letters A*, vol. 56, no. 3, pp. 149–150, 1976.

[19] J. T. Chayes, L. Chayes, and C. M. Newman, "The stochastic geometry of invasion percolation," *Communications in mathematical physics*, vol. 101, no. 3, pp. 383–407, 1985.

[20] A. A. Járai, "Invasion percolation and the incipient infinite cluster in 2d," *Communications in mathematical physics*, vol. 236, no. 2, pp. 311–334, 2003.

[21] S. Mertens and C. Moore, "Percolation thresholds in hyperbolic lattices," *Physical Review E*, vol. 96, no. 4, p. 042116, 2017.

[22] P. Leath, "Cluster shape and critical exponents near percolation threshold," *Physical Review Letters*, vol. 36, no. 16, p. 921, 1976.

[23] M. Sinha and L. H. Garrison, "CORRFUNC - a suite of blazing fast correlation functions on the CPU," *mnras*, vol. 491, pp. 3022–3041, Jan 2020.

[24] D. Stauffer and A. Aharony, *Introduction to Percolation Theory.(2nd edn), 1992*. London, Taylor and Francis., 1994.

[25] S.-K. Ma, *Modern theory of critical phenomena*. Routledge, 2018.

[26] A. Coniglio, "Cluster size and shape in random and correlated percolation," *Journal of Physics A: Mathematical and General*, vol. 12, no. 4, p. 545, 1979.

[27] R. Ortez and J. B. Rundle, "Avalanche burst invasion percolation model: Emergent scale invariance on a pseudo-critical system," *Physical Review E*, To Be Published.

[28] P. Grassberger and Y.-C. Zhang, "self-organized formulation of standard percolation phenomena," *Physica A: Statistical Mechanics and its Applications*, vol. 224, no. 1-2, pp. 169–179, 1996.

[29] A. Gabrielli, G. Caldarelli, and L. Pietronero, "Invasion percolation with temperature and the nature of self-organized criticality in real systems," *Physical Review E*, vol. 62, no. 6, p. 7638, 2000.

[30] M. E. Fisher, "The theory of condensation and the critical point," *Physics Physique Fizika*, vol. 3, no. 5, p. 255, 1967.

[31] M. Cieplak, A. Maritan, and J. R. Banavar, "Optimal paths and domain walls in the strong disorder limit," *Physical review letters*, vol. 72, no. 15, p. 2320, 1994.

[32] T. Jackson and N. Read, "Theory of minimum spanning trees. I. Mean-field theory and strongly disordered spin-glass model," *Physical Review E*, vol. 81, no. 2, p. 021130, 2010.

[33] K. Sneppen, P. Bak, H. Flyvbjerg, and M. H. Jensen, "Evolution as a self-organized critical phenomenon.," *Proceedings of the National Academy of Sciences*, vol. 92, no. 11, pp. 5209–5213, 1995.

[34] S. Bornholdt and T. Rohlf, "Topological evolution of dynamical networks: Global criticality from local dynamics," *Physical Review Letters*, vol. 84, no. 26, p. 6114, 2000.

[35] C. P. Stark, "An invasion percolation model of drainage network evolution," *Nature*, vol. 352, no. 6334, p. 423, 1991.

[36] D. Sornette, *Critical phenomena in natural sciences: chaos, fractals, selforganization and disorder: concepts and tools*. Springer Science & Business Media, 2006.

[37] M. Knackstedt and L. Paterson, "Invasion percolation," *Complex Media and Percolation Theory*, pp. 175–190, 2021.

[38] W. Klein, H. Gould, N. Gulbahce, J. Rundle, and K. Tiampo, "Structure of fluctuations near mean-field critical points and spinodals and its implication for physical processes," *Physical Review E*, vol. 75, no. 3, p. 031114, 2007.

[39] J. Q. Norris, D. L. Turcotte, and J. B. Rundle, "Loopless nontrapping invasion-percolation model for fracking," *Physical Review E*, vol. 89, no. 2, p. 022119, 2014.

[40] J. B. Rundle, R. Ortez, J. Kønigslieb, and D. L. Turcotte, "Constrained invasion percolation model: Growth via leath bursts and the origin of seismic b-value," *Physical Review Letters*, vol. 124, no. 6, p. 068501, 2020.

[41] K. Chen, P. Bak, and S. Obukhov, "Self-organized criticality in a crack-propagation model of earthquakes," *Physical Review A*, vol. 43, no. 2, p. 625, 1991.

[42] D. Vere-Jones, "A branching model for crack propagation," *pure and applied geophysics*, vol. 114, pp. 711–725, 1976.

[43] M. Bebbington, D. Vere-Jones, and X. Zheng, "Percolation theory: a model for rock fracture?," *Geophysical Journal International*, vol. 100, no. 2, pp. 215–220, 1990.

[44] S. Maxwell, "Microseismic hydraulic fracture imaging: The path toward optimizing shale gas production," *The Leading Edge*, vol. 30, no. 3, pp. 340–346, 2011.

[45] J. Q. Norris, D. L. Turcotte, and J. B. Rundle, "Anisotropy in fracking: a percolation model for observed microseismicity," *Pure and Applied Geophysics*, vol. 172, pp. 7–21, 2015.

[46] T. C. Halsey, M. H. Jensen, L. P. Kadanoff, I. Procaccia, and B. I. Shraiman, "Fractal measures and their singularities: The characterization of strange sets," *Physical review A*, vol. 33, no. 2, p. 1141, 1986.

Chapter 5

Conclusion

While the study of complex systems has seemingly progressed at a modest pace, some of the major insights have been to reveal the shortcomings of traditional analytical approaches. In particular, the Lorenz system, a characteristic example of chaos, revealed a class of phenomena which despite being entirely deterministic, becomes analytically intractable due to the system's non-linearities [1]. Computational approaches have shown that the system is reproducible only with exact knowledge of the initial conditions and with the ability to compute solutions to arbitrary precision [2] . More importantly, the limits of computer precision lead to the conclusion that phase space trajectories are not reproducible even when accounting for the errors associated with precision. This frustrates traditional approaches which rely on the tremendously successful strategy of finding perturbative approaches to capture the essential features and leaves complications as higher order corrections to the underlying phenomena. This potentially leads to the conclusion that the failure to find useful analytical solutions does not represent a lack of wit or cleverness, but rather a far larger shortcoming that invalidates linear approaches altogether. That these strategies are not universal in scope, is one of the most important insights to emerge from the study of complex systems.

This is echoed in early studies with cellular automata that showed very simple systems could create chaotic, unpredictable behavior [3]. One might think that these are special, pathological examples of nature, but the innate fractal structure of cellular automata and the fractal structure of the Lorenz phase space are evidence that where there are fractal

characteristics there is likely to exist these pathologies. Further, we have found that nature seems to be imbued with many examples of fractal and repeating structures which strongly indicate that the non-linearities present in these systems are much more the norm rather than the exception [4]. Thus, the development for entirely new approaches to these disparate classes of problems has come to describe the amalgamation which is the study of complex systems as a formal field. Computational and information theoretic models have made good progress in recent years. The approach outlined here follows in these steps where the goal is the development of computational models that capture the fractal characteristics that have come to define distinct complex systems. Since the governing differential equations are frequently too difficult to solve, their insights become limited, and it becomes more sensible to merely have an algorithm or set of rules to generate the system, and to rely on a statistical approach to characterize its fractal properties.

The study of critical phenomena parallels these developments where intrinsically random models coupled with scale invariant correlation lengths lead to fractal descriptions. Formally, critical systems describe a phase change in a substance where small scale interactions with a small correlation length define the stable equilibrium phase. During the phase change, the stable equilibrium state gives way to the system's intrinsic fluctuations with infinite correlation length and leads to the observed critical properties. This apparent dichotomy between finite/infinite correlation lengths seems to nicely capture when fractal characteristics are likely to proliferate. However, if we follow this model explicitly, we would expect some notion of a stable equilibrium state with finite correlation length to give way to fractal behavior and for many examples, this does not seem to be the case. For example, deposition is not described by the existence of stable equilibrium states with a finite correlation length that then gives way to scale invariant behavior. Therefore, it is incumbent to study alternative descriptions. As IP is a variant to RP, we propose a variant description where fluctuations and an infinite correlation lengths do not emerge during a transition of phase. Rather, the fractal characteristics are emergent results of slowly driven non-equilibrium dynamics. It is still the case that we aim to characterize distinct fractal systems with their appropriate universality class, but as we have loosened

the constraint of requiring the notion of distinct phases, we can explore a broader set of universality classes. With this approach, we seek to find mappings between universality classes and the fractal statistics of natural phenomena. A particularly effective method is to utilize the prominence of Fisher type distributions and their utility in characterizing distinct universality classes.

With these generalizations, we explore a broader framework of models that produce fractal statistics. For example, the scaling hypothesis suggests that a single scale invariant correlation length leads to fractal statistics, but with our AIP model, we show that we can relax this constraint and produce "effective" scale invariance which preserves scale invariance over greater than 4 scales. Further, our AIP model preserves the existence of a critical Fisher distribution that defines the associated universality class. Not only can we do away with phase transition mechanics by not needing to define distinct phases, but we also do not need to enforce a single scale invariant correlation length. This leaves hyperscaling as the only essential property which emerges from second order phase transitions. Should natural systems have fractal statistics consistent with hyperscaling relations, then it's likely that some underlying phase transition mechanics are applicable. However, as we have shown fractal statistics emerge in all manner of cases and without any explicit notion of phases.

As our primary aim is to find a suitable universality class for induced seismicity, and because our AIP model produced a critical Fisher distribution (despite its two scale invariant correlation lengths), it however, failed to produce the desired magnitude scaling of events. While AIP more aptly described the behavior of slowly driven non-equilibrium systems, it produced only a single magnitude scaling (near but distinct from mean-field scaling), while induced seismicity is consistent with a range of magnitude scalings.

By incorporating inherent long-range correlations between sites into AIP, we produce a range of magnitude scalings, some of which are consistent with induced seismicity. Additionally, the long-range correlations introduce yet another scale invariant correlation length into the system and rather than eliminating scale invariant behavior, we find that it persists. Not only do we preserve a critical Fisher distribution, but we also eliminate

the need for the system to be near a critical value in order to produce it. Thus, not only do we eliminate the need for distinct equilibrium states, but we also eliminate the need for the system to self organize around a special value. This introduces a multifractal description where different scale invariant phenomena emerges depending on the dominant correlation length. "Effective" scale invariance can persist across many length scales, but can experience crossover phenomena described by different scalings when another correlation length becomes dominant. Alternative, some scale invariant features can be unaffected by other correlation mechanisms. We find this to be the case with the Fisher distribution, which persists without any observable crossover behavior.

This introduces a new paradigm for understanding the emergent fractal properties. This strategy seeks to identify the multiple correlation lengths that govern the dynamics. The realization of multifractal analysis seeks both to identify and disentangle how the distinct scale invariant correlation lengths interact to produce observed fractal properties. These models also provide an excellent framework for formulating approaches that map a multifractal spectrum to the underlying correlation mechanisms.

The introduction of multiple scale invariant correlation lengths resolves another problem inherent to percolation type models. We approximate the fracture network of induced seismicity by a 2D network. This is partly justified by the observation that in fracking, the fluid is injected into tight shales which are well described as being planar with a non zero thickness. Given the perils of simplifying assumptions, it is necessary to understand the full 3D description with restricted growth along one axis. For percolation models as the dimension increases, it is known that models approach a mean-field description. Applied to the results of our AIP model, it would make the magnitude scaling even less compatible with observation. However, for AIP with long-range correlations, this need not be the case. Full 3D correlation with growth restricted along one axis will likely favor growth by smaller scaling events. This allows us to explain why induced seismicity has a characteristically small magnitude scaling ($b = -2$ where for tectonic $b = -1$ and 2D mean-field would produce $b = 0.75$). Thus, extension to a 3D description becomes a promising next stage of study.

5.1 Acknowledgements

The research of RAO and JBR has been supported by a grant from the US Department of Energy to the University of California, Davis DOE Grant No. DE-SC0017324.

References

[1] E. N. Lorenz, "Deterministic nonperiodic flow," *Journal of atmospheric sciences*, vol. 20, no. 2, pp. 130–141, 1963.

[2] E. N. Lorenz, "Computational chaos-a prelude to computational instability," *Physica D: Nonlinear Phenomena*, vol. 35, no. 3, pp. 299–317, 1989.

[3] S. Wolfram, "Cellular automata as models of complexity," *Nature*, vol. 311, no. 5985, pp. 419–424, 1984.

[4] A. Bunde and S. Havlin, *Fractals in science*. Springer, 2013.